ΤΜΗΜΑ ΙΑΤΡΙΚΗΣ
FACULTY OF MEDICINE

ΠΑΝΕΠΙΣΤΗΜΙΟ ΚΡΗΤΗΣ
UNIVERSITY OF CRETE

Διδακτορική Διατριβή

Ο ΡΟΛΟΣ ΤΟΥ ΑΝΟΣΟΠΟΙΗΤΙΚΟΥ ΣΥΣΤΗΜΑΤΟΣ ΣΤΗ ΔΙΑΤΡΟΦΙΚΗΣ ΑΙΤΙΟΛΟΓΙΑ ΛΙΠΩΔΗ ΔΙΗΘΗΣΗ ΤΟΥ ΗΠΑΤΟΣ

ΜΩΥΣΙΔΟΥ ΜΑΡΙΑ

Ηράκλειο, Μάιος 2018

ΤΜΗΜΑ ΙΑΤΡΙΚΗΣ
FACULTY OF MEDICINE

ΠΑΝΕΠΙΣΤΗΜΙΟ ΚΡΗΤΗΣ
UNIVERSITY OF CRETE

Διδακτορική Διατριβή

Ο ΡΟΛΟΣ ΤΟΥ ΑΝΟΣΟΠΟΙΗΤΙΚΟΥ ΣΥΣΤΗΜΑΤΟΣ ΣΤΗ ΔΙΑΤΡΟΦΙΚΗΣ ΑΙΤΙΟΛΟΓΙΑ ΛΙΠΩΔΗ ΔΙΗΘΗΣΗ ΤΟΥ ΗΠΑΤΟΣ

ΜΩΥΣΙΔΟΥ ΜΑΡΙΑ

Τριμελής επιτροπή

ΒΕΝΥΧΑΚΗ ΜΑΡΙΑ
ΚΑΡΑΛΗ ΑΙΚΑΤΕΡΙΝΗ
ΜΑΡΓΙΩΡΗΣ ΑΝΔΡΕΑΣ

Ηράκλειο, Μάιος 2018

Acknowledgements

This work was carried out in the laboratory of Katia Karalis in the department of Clinical Experimental Surgery & Translational Research in Biomedical Research Foundation Academy of Athens (BRFAA). The work was supported by a PhD grant from a Greek National fund through the Operational Program "Education and Lifelong Learning" of the National Strategic Reference Framework-Research Funding Program: Hrakletus II, taken by the Medical School of University of Crete, and the European Union 7th Framework Programme, Regpot activity grant 245928 (TRANSMED).

First and foremost, I would like to thank my professor & mentor Dr. Katia Karalis, for her guidance and support in pursuing my interests and encouragement. Katia had always an open door for to bring up any kind of discussion and had the ability to always give valuable feedback and inspiration when needed it the most. I would also thank her for giving me the opportunity to travel to USA and Canada for the attendance and presentation of my work in international conferences, and visit her in Boston for the attendance of a practical course in Wyss Institute at Harvard Medical School and training in experimental techniques at the Harvard School of Public Health.

I would also like to thank past and present members of Dr. Katia Karalis group for their contribution and support via scientific input, technical help and sharing of motivation during the course of my PhD years. Special thanks to Dr. Sevasti Karaliota for her time, guidance, patience and invaluable daily discussions, advice and encouragement particularly during the periods I was pregnant. Dr.Maria Salagianni that kindly shared her expertise in flow

cytometry. Dr.Yassemi Koutmani that shared her expertise in a range of techniques throughout my graduate studies as well as her friendship and support. Dr.Triantafyllos Chavakis for his involvement in the experimental approaches involving immune cells transfer and data discussions. Furthermore, I would like to thank the members of my dissertation committee for their time, commitment and valuable insights.

To the end, I would like to thank my parents and my whole family, for their support and patience during these years. Special thanks to my two children, Panos and Thodora, their coming in the world brings me a lot of happiness and make me stand and complete my PhD thesis.

Contents

1.Περίληψη

1.1. Σύντομη περίληψη

Ο ανοσομεταβολισμός «Immunometabolism” είναι ένα καινούργιο ερευνητικό πεδίο που μελετά τις αλληλεπιδράσεις του ανοσοποιητικού συστήματος και της μεταβολικής δραστηριότητας και τη συμμετοχή τους στην εξέλιξη διάφορων νόσων. Ένα καλά μελετημένο παράδειγμα αφορά τη συσσώρευση των ανοσοκυττάρων στο λευκό λιπώδη ιστό που διαμεσολαβεί στην ανάπτυξη αντίστασης στην ινσουλίνη και τη συνεπακόλουθη συστημική μεταβολική δυσλειτουργία που χαρακτηρίζει την παχυσαρκία αλλά και άλλες χρόνιες παθήσεις. Παρόλο που ο ρόλος των κυττάρων της φυσικής ανοσίας και των κυτοκινών που εκκρίνουν, όπως οι TNFα, IL1 και IL6, στη λειτουργία του λιπώδους ιστού έχει χαρακτηρισθεί και πιστοποιηθεί από πολλές πειραματικές και κλινικές μελέτες, ο ρόλος των λεμφοκυττάρων στη ρύθμιση της ενεργειακής ομοιοστασίας δεν είναι ακόμα σαφής. Σε αυτή τη μελέτη χρησιμοποιήσαμε *Rag1*$^{-/-}$ μυs, που έχουν ένδεια ανοσίας εξαιτίας γενετικής αιτιολογίας διαταραχής στη λειτουργική ωρίμανση των Τ και Β λεμφοκύτταρων τους, για να χαρακτηρίσουμε την επίδραση των Τ λεμφοκυττάρων στη μεταβολική ομοιοστασία όπως καθορίζεται από τον λευκό λιπώδη ιστό και το ήπαρ. Ανάλυση της μεταβολικής δραστηριότητας των *Rag1*$^{-/-}$ μυών αποκάλυψε αυξημένη 24ωρη μεταβολική δραστηριότητα και συγκεκριμένα αυξημένη χρησιμοποίηση λιπιδίων χωρίς σημαντικές διαφορές είτε στην πρόσληψη τροφής ή στην κινητικότητα μεταξύ *Rag1*$^{-/-}$ και μυών αγρίου τύπου (WT). Έγχυση λειτουργικών λεμφοκυττάρων σε *Rag1*$^{-/-}$ μύες αποκάλυψε ότι η έλλειψη των Τ, και συγκεκριμένα των CD8^{+} Τ λεμφοκυττάρων, ήταν ο κύριος λόγος της αυξημένης μεταβολικής τους δραστηριότητας. Συγκεκριμένα η

έλλειψη αυτού του λεμφοκυτταρικού πληθυσμού οδηγεί σε αυξημένη οξείδωση των λιπαρών οξέων και δημιουργία λιποκυττάρων με μεγάλη περιεκτικότητα σε μιτοχόνδρια (μπεζ λιπώδης ιστός) εντός του υποδόριου λευκού λιπώδους ιστού. Αυξημένη κατεχολαμινεργική δραστηριότητα στο υποδόριο λίπος και η συνεπακόλουθη τροποποίηση της περιεκτικότητας του σε κύτταρα φυσικής ανοσίας, όπως τα ηωσινόφιλα και τα πρόσφατα ταυτοποιημένα κύτταρα φυσικής ανοσίας (innate lymphoid cells-ILCs), υπέδειξαν συγκεκριμένους μηχανισμούς που συνδέονται με την ενεργοποίηση του μπεζ λιπώδους ιστικού αποθέματος. Μεταμόσχευση $CD8^+$ Τ λεμφοκυττάρων επανέφερε τη μεταβολική λειτουργία, καθώς και τους ανωτέρω δείκτες, των *Rag1*$^{-/-}$ μυών στα επίπεδα των WT μυών. Η ανασταλτική δράση των $CD8^+$ Τ λεμφοκυττάρων αναιρέθηκε μετά από παρεμπόδιση της δράσης της IFNγ με χορήγηση ειδικού αντισώματος. Σε συμφωνία με αυτά τα ευρήματα, δείξαμε επίσης αυξημένη μπεζ λιπογένεση στον υποδόριο ιστό των *CD8*$^{-/-}$ μυών. Μελέτη της μεταβολικής λειτουργίας του ήπατος των *Rag1*$^{-/-}$ μυών έδειξε επίσης αυξημένη οξείδωση των λιπαρών οξέων αλλά και του μεταβολισμού των υδατανθράκων, όπως καταδεικνύεται από τη μειωμένη αποθήκευση γλυκαγόνου. Αυξημένη γονιδιακή έκφραση των παραγόντων που διαμεσολαβούν την ενεργοποίηση της μεταβολικής δραστηριότητας υποστηρίζει τα ανωτέρω ευρήματα στους *Rag1*$^{-/-}$ μυς . Η σημαντικότητα των $CD8^+$ Τ λεμφοκυττάρων στη συγκεκριμένη διεργασία επιβεβαιώθηκε με λεπτομερείς πειραματικούς χειρισμούς. Συμπερασματικά οι μελέτες μας περιγράφουν ένα νέο ρόλο των $CD8^+$ Τ λεμφοκυττάρων στη ρύθμιση της ενεργειακής ομοιοστασίας μέσω ενεργοποίησης πολλαπλών ειδικών παραγόντων στο φυσιολογικό λιπώδη ιστό και καταδεικνύουν τους

πιθανούς μηχανισμούς που εμπλέκονται. Τα αποτελέσματα μας προσφέρουν μία πιθανή εξήγηση για τη μεταβολική δυσλειτουργία σε χρόνιες παθήσεις που χαρακτηρίζονται από μεγάλες διαταραχές είτε στην κατανάλωση ενέργειας, με χαρακτηριστική την καχεξία, ή στην αποθήκευση της, όπως στην παχυσαρκία. Τα ευρήματά μας οδηγούν στην υπόθεση ότι τα $CD8^+$ Τ κύτταρα θα μπορούσαν να στοχευθούν για την καταπολέμηση ασθενειών που χαρακτηρίζονται από αλλαγές της ενεργειακής ομοιόστασης όπως ο διαβήτης τύπου 2, αλλά και χρόνιες λοιμώδεις νόσοι, διάφορες μορφές καρκίνου με έντονη καταβολική δραστηριότητα αλλά και οι ανεπιθύμητες ενέργειες διαφόρων φαρμάκων.

1.2. Εκτεταμένη Περίληψη

Ο ανοσομεταβολισμός «Immunometabolism" είναι ένα καινούργιο ερευνητικό πεδίο που αναφέρεται στο ρόλο της αλληλεπίδρασης του ανοσοποιητικού συστήματος με τη μεταβολική δραστηριότητα στην φυσική ιστορία διαφόρων ανθρώπινων παθήσεων. Το επίκεντρο αυτής της εργασίας ήταν να διερευνηθεί η συμβολή, και τελικά η σημασία, της επίκτητης ανοσίας στη ρύθμιση της ενεργειακής ομοιοστασίας στο λιπώδη ιστό και στο ήπαρ. Αυτές οι διαδικασίες είναι σημαντικές για την παχυσαρκία και το διαβήτη τύπου 2 αλλά και για ασθένειες που σχετίζονται με την αδυναμία διατήρησης της ενεργειακής ισορροπίας και χαρακτηρίζονται από σημαντική απώλεια βάρους (1). Στα πειράματά μας χρησιμοποιήσαμε *Rag1*$^{-/-}$ μύες που έχουν ένδεια επίκτητης ανοσίας.

Αρχικά μετρήσαμε διάφορες μεταβολικές παραμέτρους σε φυσιολογικούς (WT) και *Rag1*$^{-/-}$ μύες χρησιμοποιώντας ένα σύστημα παρακολούθησης της

μεταβολικής τους δραστηριότητας (CLAMS-comprehensive laboratory animal monitoring system). Τα ευρήματά μας δείχνουν ότι οι *Rag1*$^{-/-}$ μύες έχουν αυξημένη μεταβολική δραστηριότητα, και μειωμένη χρησιμοποίηση υδατανθράκων έναντι των λιπιδίων, παρά το γεγονός ότι η κατανάλωση τροφής και η κινητική δραστηριότητα δε διέφερε ανάμεσα στους δυο γονότυπους. Αυτά τα αποτελέσματα δείχνουν ότι η επίκτητη ανοσία συνεισφέρει στη διατήρηση της ενεργειακής ομοιόστασης.

Καθώς ένα από τα μεγαλύτερα παγκόσμια προβλήματα υγείας της σημερινής εποχής είναι η παχυσαρκία και ο διαβήτης τύπου 2, επικεντρωθήκαμε να αποσαφηνίσουμε τη σημασία της έλλειψης λεμφοκυττάρων στη ρύθμιση της ενεργειακής ομοιόστασης στο λευκό λιπώδη ιστό αρχικά σε βασικές συνθήκες. Έχει περιγραφεί ότι τα λεμφοκύτταρα συνεισφέρουν στην ανάπτυξη αντίστασης στην ινσουλίνη και τη φλεγμονή που συνοδεύουν την παχυσαρκία. Η σημασία της αλληλεπίδρασης των Τ κυττάρων με τα λιποκύτταρα στη ρύθμιση της ενεργειακής ομοιόστασης και το μεταβολισμό των λιπιδίων παραμένουν ακόμα ασαφείς (2, 3).

Πρόσφατα, έχει ταυτοποιηθεί ένας νέος τύπος λιπώδους ιστού, που ονομάσθηκε «beige» λιπώδης ιστός, ιδιαίτερα σημαντικός για τη ρύθμιση της ενεργειακής ομοιοστασίας μέσω κατανάλωσης ενέργειας (4-6). Τα “beige” κύτταρα εντοπίζονται κυρίως μέσα στον υποδόριο λευκό λιπώδη ιστό (subcutaneous white adipose tissue-scWAT) και χαρακτηρίζονται από αυξημένο αριθμό μιτοχονδρίων και, συνεπακόλουθα, έκφρασης της μιτοχονδριακής διαζευκτικής πρωτεΐνης 1 (Ucp1-uncoupling protein 1)(7). Ο ρόλος της φυσικής ανοσίας στην ανάπτυξη μπεζ λιπώδους ιστού μέσα στο scWAT έχει χαρακτηρισθεί πρόσφατα (8-10), όπως και η πιθανότητα ο

υποδόριος ιστός να αποτελέσει στόχο στις προσπάθειες που γίνονται για την καταπολέμηση της παχυσαρκίας.

Πράγματι, στους *Rag1*$^{-/-}$ μυς που βρήκαμε αυξημένη μεταβολική δραστηριότητα, ιστολογική ανάλυση του υποδόριου ιστού έδειξε σημαντικά αυξημένο σχηματισμό μπεζ κυττάρων σε σύγκριση με τους WT μύες. Επιπλέον, χρώσεις με ανοσοφθορισμό έναντι του κυρίαρχου θερμογενετικού παράγοντα, Ucp1, αλλά και μέτρηση της έκφρασης άλλων συναφών γονιδίων όπως τα *Cidea, Prdm16* και *Dio2* υποστηρίζουν την αυξημένη μεταβολική δραστηριότητα στους *Rag1*$^{-/-}$ μύες. Αρχικά εξετάσαμε αν η μεταφορά σπληνοκυττάρων, πληθυσμού κυττάρων πλούσιου σε Τ και Β λεμφοκύτταρα, που απομονωθήκαν από φυσιολογικούς μύες, θα μπορούσε να αναστρέψει το φαινότυπο των *Rag1*$^{-/-}$ μυών. Πράγματι μετά την έγχυση σπληνοκυττάρων ο σχηματισμός μπεζ λιποκυττάρων όπως και η έκφραση σχετικών γονιδίων ήταν μειωμένα στους *Rag1*$^{-/-}$ μύες. Προκειμένου να κατανοήσουμε το μηχανισμό που χρησιμοποιούν τα λεμφοκύτταρα για να αναστείλουν το σχηματισμό μπεζ λιπώδους ιστού, αξιολογήσαμε τη δραστηριότητα πρόσφατα χαρακτηρισμένων σηματοδοτικών μονοπατιών με συμβολή στη ρύθμιση της θερμογένεσης, όπως είναι η παρεμπόδιση της αδρενεργικής δράσης. Οι *Rag1*$^{-/-}$ μύες παρουσιάζουν αυξημένη έκφραση των αδρενεργικών υποδοχέων (4, 5) στο scWAT και θετική χρώση της υδροξυλάσης της τυροσίνης, ενός δείκτη ειδικού για τους κατεχολαμινεργικούς νευρώνες (11). Μεταμόσχευση WT σπληνοκυττάρων στους *Rag1*$^{-/-}$ μύες ανέστρεψε αυτό το φαινότυπο. Ενώ χορήγηση πραζοσίνης, ενός αναστολέα των α-αδρενεργικών υποδοχέων, μείωσε τόσο τις περιοχές με τα μπεζ κύτταρα στον υποδόριο ιστό των *Rag1*$^{-/-}$ μυών όσο και την έκφραση των θερμογενετικών γονιδίων.

Στη συνέχεια εξετάσαμε την απόκριση των *Rag1*$^{-/-}$ μυών σε φυσιολογικά ερεθίσματα, όπως είναι οι αλλαγές στη θερμοκρασία, που αναστέλλουν την έκφραση (12) ή επάγουν την έκφραση της Ucp1 (7). Για την αναστολή της έκφρασης της Ucp1, WT και *Rag1*$^{-/-}$ μύες εγκλιματίστηκαν στους 30^{o}C για 20 ημέρες, που οδήγησε σε μείωση των διαφορών στο σχηματισμό των μπεζ λιποκυττάρων στο scWAT . Για την επαγωγή της έκφρασης της Ucp1 και το σχηματισμό μπεζ λιποκυττάρων, WT και *Rag1*$^{-/-}$ μύες εγκλιματιστήκαν στους 4^{o}C για 2 ημέρες. Το αξιοσημείωτο είναι ότι οι *Rag1*$^{-/-}$ μύες διατήρησαν τη θερμοκρασία του σώματος τους σε πιο υψηλά επίπεδα από τους WT μύες, δείχνοντας πως η ικανότητα των *Rag1*$^{-/-}$ μυών να επάγουν το σχηματισμό του μπεζ λίπους στο scWAT δεν έχει εξαντληθεί . Η μείωση της θερμοκρασίας είναι ένας φυσιολογικός χειρισμός για να αυξηθεί η θερμογένεση και ο σχηματισμός μπεζ λίπους. Για να προσδιορίσουμε ποιος είναι ο σημαντικός υποπληθυσμός των λεμφοκυττάρων που διαμεσολαβεί στη διατήρηση της μπεζ λιπογένεσης σε χαμηλά επίπεδα στους WT μύες, χρησιμοποιήσαμε κυτταρομετρία ροής και συγκρίναμε τον αριθμό των CD4^{+}, CD8^{+} και Τ ρυθμιστικών κυττάρων στο scWAT WT μυών που εκτεθήκαν σε φυσιολογική και χαμηλή θερμοκρασία περιβάλλοντος. Η ανάλυση αυτή έδειξε ότι ο υποπληθυσμός που είναι ιδιαίτερα μειωμένος στην έκθεση σε κρύο είναι τα CD8^{+} Τ κύτταρα. Προηγούμενες μελέτες έδειξαν εκλεκτική άθροιση CD8^{+} Τ κύτταρων στο scWAT σε παχυσαρκία, που προηγήθηκε αυτής των μακροφάγων. Τα ευρήματά μας αναφέρονται για πρώτη φορά δεδομένου ότι ενώ η μεταφορά CD8^{+} Τ κυττάρων σε *CD8*$^{-/-}$ μυς χειροτερεύει σημαντικά τη φλεγμονή στο λιπώδη ιστό (2), δεν υπάρχει βιβλιογραφία για το ρόλο των

$CD8^+$ Τ κυττάρων στη διαφοροποίηση του λευκού λιπώδη ιστού και πιο συγκεκριμένα στο σχηματισμό μπεζ λιποκυττάρων.

Στη συνέχεια προχωρήσαμε με μία σειρά πειραμάτων για να διαλευκάνουμε τον ακριβή ρόλο των $CD8^+$ Τ κυττάρων στο σχηματισμό μπεζ λιποκυττάρων και την ταυτοποίηση των μηχανισμών που εμπλέκονται. Μεταφορά $CD8^+$ Τ κυττάρων σε *Rag1*$^{-/-}$ μύες μείωσε σημαντικά το σχηματισμό μπεζ λιποκυττάρων και οδήγησε σε μείωση της έκφρασης των γονιδίων της θερμογένεσης και του καταβολισμού των λιπιδίων μετά από έκθεση σε θερμοκρασία περιβάλλοντος αλλά και σε μειωμένη θερμοκρασία. Σε συμφωνία με την υπόθεσή μας, αναπλήρωση του ελλείμματος σε $CD8^+$ Τ κύτταρα ανέστρεψε την αυξημένη έκφραση της υδροξυλάσης της τυροσίνης στους *Rag1*$^{-/-}$ μύες, χαρακτηριστική της κατεχολαμινεργικής δραστηριότητας που συνιστά μέρος ενός από τους πιθανούς μηχανισμούς λιπογένεσης που επηρεάζονται από τα $CD8^+$ Τ κύτταρα. Επιπλέον μελέτη του μεταβολικού προφίλ των *CD8*$^{-/-}$ σε αντιπαραβολή με αυτό των WT μυών, έδειξε αυξημένη μπεζ λιπογένεση στο scWAT σε απουσία των $CD8^+$ Τ κυττάρων σε συμφωνία με τον ανασταλτικό ρόλο αυτών των κυττάρων στην μεταβολική ομοιόσταση.

Πρόσφατες μελέτες έδειξαν ότι η επαγωγή θερμογένεσης απαιτεί τη συμμετοχή δύο κυτταροκινών : (α) της IL-4 που προέρχεται από τα ηωσινόφιλα και δρα μέσω της επαγωγής των M2 μακροφάγων, που ευοδώνουν την ενεργοποίηση της μπεζ λιπογένεσης κινητοποιώντας και την αυξημένη έκκριση κατεχολαμινών (7) και (β) της IL-13 ή/και IL-5 που προέρχονται από τα κύτταρα της φυσικής ανοσίας τύπου 2 (Type 2 Innate lymphoid cells-ILC2s) που επάγουν την ανάπτυξη του μπεζ λίπους μέσω αύξησης της διαθέσιμης IL-4 (13). Επιπλέον αυτές οι μελέτες έδειξαν ότι

απομάκρυνση αυτών των κυτοκινών, ή των κυττάρων που επάγουν την παραγωγή τους ή των μακροφάγων, που είναι ο στόχος αυτών των κυτοκινών, μπλοκάρουν την επαγωγή μπεζ λιπογένεσης. Για να διαλευκάνουμε τους μηχανισμούς που χρησιμοποιούν οι *Rag1*$^{-/-}$ μύες για την επαγωγή της μπεζ λιπογένεσης, και τη σχέση τους με τα υπάρχοντα δημοσιεύματα, αναλύσαμε τη σχετική περιεκτικότητα αυτών των κυττάρων και των αντίστοιχων κυτταροκινών που εκκρίνουν στον υποδόριο λιπώδη ιστό. Αρχικά εξετάσαμε τον πληθυσμό των ηωσινοφίλων και των κυττάρων της φυσικής ανοσίας (ILCs) στον υποδόριο ιστό σε WT και *Rag1*$^{-/-}$ μύες τόσο σε φυσιολογικές συνθήκες όσο και σε κρύο περιβάλλον (4^{o}C), και δείξαμε ότι απουσία λεμφοκυττάρων οδηγεί σε ιδιαίτερα αυξημένα ποσοστά αυτών των κυττάρων, ενώ η παρουσία των CD8^{+} Τ κυττάρων οδήγησε σε σημαντική μείωση του αριθμού τους. Αυτά τα ευρήματα συμφωνούν με τη βιβλιογραφία ότι τα ηωσινόφιλα και τα ILC2 κύτταρα ευοδώνουν τη μπεζ λιπογένεση και την επακόλουθη θερμογένεση και επιβεβαιώνει και στο μοντέλο μας ότι τα CD8^{+} Τ κύτταρα συμμετέχουν στη μείωση των μπεζ λιποκυττάρων στον υποδόριο ιστό. Επιπλέον υποδεικνύουν τη σημασία των ηωσινοφίλων και των ILCs σε αυτή τη διαδικασία. Αντίστοιχες ήταν και οι διαφορές στα επίπεδα των IL-4, IL-5 και IL-13 κυττοκινών που εκκρίνονται από τα παραπάνω κύτταρα στο scWAT των WT, *Rag1*$^{-/-}$ και *Rag1*$^{-/-}$ μυών που τους χορηγήθηκαν CD8^{+} Τ κύτταρα. Για παράδειγμα, τα αποτελέσματά μας καταδεικνύουν εξαιρετικά αυξημένη έκφραση αυτών των κυτοκινών στους *Rag1*$^{-/-}$ μύες, ενώ η χορήγηση CD8^{+} Τ κυττάρων επανέφερε τις τιμές τους σε παρόμοια επίπεδα με αυτά που ανιχνεύθηκαν στους φυσιολογικούς μύες. Αυτό το εύρημα υποδεικνύει ένα ενδιάμεσο μηχανισμό που κινητοποιείται από τα CD8^{+} Τ κύτταρα για τη

ρύθμιση της μπεζ λιποgένεσης και εμπλέκει την αλλαγή του αριθμού των κυττάρων της φυσικής ανοσίας και των αντίστοιχων κυτταροκινών που επάγονται από αυτά.

Περαιτέρω, υποβάλαμε το ερώτημα αν τα ίδια τα $CD8^+$ Τ κύτταρα εκκρίνουν κάποιο παράγοντα μέσω του οποίου αναστέλλουν την αυξημένη θερμογένεση στον υποδόριο ιστό. Τα πειράματά μας έδειξαν μεταφορά $CD8^+$ Τ κύτταρων που δεν εκκρίνουν IFNγ, μία κυτοκίνη που εκκρίνεται σε μεγάλες ποσότητες από τα $CD8^+$ Τ κύτταρα, οδήγησε σε απώλεια της ικανότητας αναστολής του σχηματισμού μπεζ λιπώδους ιστού. Επιπλέον σύγκριση *IFNγ*$^{-/-}$ και WT μυών, έδειξε ότι σε απουσία της IFNγ οι μύες παρουσιάζουν ιδιαίτερα αυξημένη μπεζ λιποgένεση και αυξημένα επίπεδα ηωσινοφίλων, γεγονός που υποδεικνύει την IFNγ ως σημαντικό παράγοντα του μηχανισμού δράσης των $CD8^+$ Τ κυττάρων στη διαφοροποίηση του λιπώδους ιστού και τη ρύθμιση της ενεργειακής ομοιοστασίας.

Το επόμενο μας βήμα ήταν να διασαφηνίσουμε αν η έλλειψη της επίκτητης ανοσίας είχε παρόμοιες επιδράσεις στο μεταβολισμό και την αποθήκευση λιπιδίων στο ήπαρ μυών που λαμβάνουν δίαιτα χαμηλής θερμιδικής αξίας, το οποίο γνωρίζουμε ότι τουλάχιστον στα πρώτα στάδια είναι ένα δυνατό ερέθισμα για την αυξημένη αποθήκευση λιπιδίων στο ήπαρ. Σχεδιάσαμε τα πειράματα μας με την υπόθεση ότι σε απουσία των κυττάρων της επίκτητης ανοσίας, όπως έχουμε στους *Rag1*$^{-/-}$ μύες, αυξημένη κατανάλωση ενέργειας έναντι αποθήκευσης λιπιδίων, θα συμβαίνει και στο ήπαρ,. Ο πειραματικός χειρισμός που χρησιμοποιήσαμε για πρόκληση αποθήκευσης λιπιδίων στο ήπαρ ήταν η 24ωρη στέρηση τροφής (14, 15) σε *Rag1*$^{-/-}$ μύες, . Χρώση ηπατικών δειγμάτων με Oil Red O (ORO) έδειξε μειωμένη αποθήκευση

λιπιδίων στους *Rag1*$^{-/-}$ μύες έναντι των WT μυών μετά από ασιτία, ενώ το μονοπάτι της οξείδωσης των λιπαρών οξέων είναι ιδιαίτερα ενεργοποιημένο στους *Rag1*$^{-/-}$ μύες. Επιπρόσθετα, για να αξιολογήσουμε συνολικά τη συνεισφορά των κυττάρων που απουσιάζουν στην αυξημένη αποθήκευση λιπιδίων στους *Rag1*$^{-/-}$ μύες, πραγματοποιήσαμε μεταφορά σπληνοκυττάρων, που απομονώθηκαν από υγιείς WT μύες, σε *Rag1*$^{-/-}$ μύες. Η μεταφορά σπληνοκυττάρων ανέστρεψε το φαινότυπο που περιγράψαμε στους *Rag1*$^{-/-}$ μύες έχοντας σαν αποτέλεσμα την αυξημένη αποθήκευση λιπιδίων και τη μείωση της οξείδωσης των λιπαρών οξέων σε επίπεδα παρόμοια αυτών των WT μυών. Το επόμενο βήμα ήταν να αξιολογήσουμε την επίδραση συγκεκριμένων υποπληθυσμών Τ κυττάρων όπως τα CD8^{+} Τ κύτταρα στη διαδικασία αυτή. Η μεταφορά CD8^{+} Τ κυττάρων είχε ως αποτέλεσμα την αύξηση της αποθήκευσης λιπιδίων στο ήπαρ, την αναστολή της οξείδωσης των λιπαρών οξέων και το μπλοκάρισμα της σύνθεσης της γλυκόζης στο ήπαρ των *Rag1*$^{-/-}$ μυών, αναστέλλοντας το φαινότυπο όπως και η χορήγηση του μικτού πληθυσμού λεμφοκυττάρων (σπληνοκύτταρα).

Συνοπτικά, η μελέτη μας αποδεικνύει για πρώτη φορά πως τα CD8^{+} Τ κύτταρα είναι ένας ισχυρός ανασταλτικός παράγοντας στο σχηματισμό του μπεζ λιπώδους ιστού και της κατανάλωσης ενέργειας στο λευκό λιπώδη ιστό και στο ήπαρ. Αυτά τα αποτελέσματα συνεισφέρουν στην έρευνα των μηχανισμών που εμπλέκονται στη διατήρηση της ενεργειακής ομοιόστασης και έχουν πιθανές εφαρμογές στη θεραπεία μεταβολικών νοσημάτων μέσω κυτταροθεραπειών.

1.3. Short abstract

Accumulation of lymphocytes in the white adipose tissue (WAT) in obesity is linked to insulin resistance and the associated chronic inflammatory state, whereas the role of this cell population in the coordinated regulation of the overall energy homeostasis remains unclear. Here, we demonstrate enhanced energy dissipation in *Rag1*$^{-/-}$ mice that was “normalized” to the levels detected in the WT mice by adoptive transfer of lymphocytes. Recapitulation of this effect by CD8^{+} T cells alone provided evidence that the CD8^{+} T cell deficiency of the *Rag1*$^{-/-}$ mice is the primary reason behind their enhanced energy utilization reflected primarily to their profoundly increased beige fat depot within the subcutaneous white adipose tissue (scWAT). Consistently, *CD8*$^{-/-}$ mice also presented with enhanced beige adipogenesis. The reversal of beige adipogenesis in the *Rag1*$^{-/-}$ mice reconstituted with CD8^{+} T cells was inhibited by blockade of IFNγ, a main secretory product of the CD8^{+} T cells in the adipose tissue. Our findings identify a novel effect of CD8^{+} T cells in regulating energy dissipation in lean WAT, mediated by IFNγ and the significant modulation of the abundance of resident innate immune cells and of the catecholaminergic activity within the scWAT. We also demonstrate that similar mechanisms operate in the liver of *Rag1*$^{-/-}$ mice to confer protection from lipid storage and development of steatosis in states of wasting due to altered caloric intake such as starvation. These findings provide a plausible explanation for the metabolic dysfunction in patients with diseases characterized by altered CD8^{+} T cell numbers, such as chronic parasitoses, or states associated with cachexia. Overall we demonstrate the effects of CD8^{+} T cells in energy homeostasis via regulation

of lipid metabolism in the WAT and the liver. These data suggest that targeting of $CD8^+$ T cells may provide a promising therapeutic approach in humans with obesity and other diseases associated with profoundly altered energy homeostasis.

1.4. Extended Abstract

Immunometabolism is a new emerging field of investigation, studying the interactions between the immune system and the metabolic processes in health and disease. The focus of this study was to elucidate how the adaptive immune system participates in the regulation of energy homeostasis in the adipose tissue and the liver, as depicted in the metabolic changes following exposure to environmental changes driving energy utilization rather than storage, such as temperature, or reduced caloric intake. Similar mechanisms operate in diseases associated with inability to maintain energy balance and are characterized by significant body weight loss (1).

Our experiments were designed to elucidate the contribution of the cells of the adaptive immunity in the metabolic homeostasis. We first measured a range of metabolic parameters in WT and *Rag1*$^{-/-}$ mice using the comprehensive laboratory animal monitoring system (CLAMS) and we found that *Rag1*$^{-/-}$ mice have increased metabolic activity and they can metabolize lipids more efficiently than carbohydrates, despite their similar motor and eating behaviors. These results were encouraging as they suggested that the above described effects of deficient adaptive immunity in the lipid metabolism in the liver might be part of more broad effects with the potential to provide new targetable mechanisms for dysregulated energy homeostasis.

As one of the major worldwide health problems of our times is obesity and its associated co-morbidities, we sought to assess if lymphocyte deficiency contributes in the regulation of energy homeostasis in the white adipose tissue (WAT) in basal states. Better understanding of the physiology of energy storage and dissipation in WAT, a lipid storage tissue and the primary source of the obesity associated co-morbidities, may provide better insights for specific and effective treatments for obesity. Although lymphocytes have been implicated in obesity, the crosstalk between T cells and adipocytes and its contribution, and potential targeting, in the regulation of energy homeostasis including lipid metabolism remain still unclear (2, 3). Recently, a distinct type of fat, with strong thermogenic capacity, named “beige adipose tissue” has been identified (4-6, 12). Beige adipocytes, located within the subcutaneous white adipose tissue (scWAT), are characterized by multilocular appearance characteristic of increased mitochondrial content and high expression of the mitochondrial uncoupling protein 1 (*Ucp1*), a primary mediator of thermogenesis expressed also in high abundance in brown fat (BAT) (7). The role of the innate immune system in the development of beige AT within the scWAT in mice has been extensively studied lately (8-10) and continuing efforts explore the possibilities it could serve as a possible significant target in the efforts for effective treatments of obesity.

Indeed, in our model, where *Rag1*$^{-/-}$ mice present an increased metabolic activity, histological analysis (H&E staining) of the scWAT, indicated significant increase in beige tissue formation in the *Rag1*$^{-/-}$, as compared to the WT, tissues. Further, immunofluorescence staining for characterization of *Ucp1* expression and profiling of the expression of the thermogenesis-related

genes *Ucp1, Cidea (cell-death-inducing DFFA-like effector α), Prdm16 (PR domain containing 16)* and *Dio2 (Deiodinase Type II)* in the *Rag1*$^{-/-}$ and WT scWAT identified differences in line with the increased beige adipogenesis in the former. Next we assessed if reconstitution of *Rag1*$^{-/-}$ mice with mixed (whole) splenocytes population, isolated from the spleen of WT mice, could alter the increased beige adipose depot of the *Rag1*$^{-/-}$ mice. Indeed, adoptive transfer of whole splenocytes reversed the phenotype of the *Rag1*$^{-/-}$ mice resulting in reduced areas with “beige” phenotype and downregulation of the expression of the thermogenesis-related genes. In order to assess the possible mechanisms employed by lymphocytes to inhibit beige formation, we assessed the activity of recently identified pathways critical for the induction of thermogenesis. An insight in the increased beige formation was provided by the specific input of the adrenergic pathways. As shown, *Rag1*$^{-/-}$ scWAT presented with increased expression of the relative adrenergic receptors (4, 5) in the scWAT and significant tyrosine hydroxylase (TH) expression, a marker of catecholaminergic neurons, as depicted by specific staining (11). In line with these findings, administration of prazosin, an alpha-adrenergic blocker, reduced the beige fat areas in the scWAT of *Rag1*$^{-/-}$ mice and significantly attenuated the expression of the thermogenesis-related genes. Notably, the adoptive transfer of whole splenocytes in the *Rag1*$^{-/-}$ mice reversed the increased adrenergic input observed in lymphocyte-deficient mice.

We next examined the response of *Rag1*$^{-/-}$ mice to a physiologic stimulus for ablation (12) or induction of *Ucp1* (7) expression, that is the temperature of the environment. To block *Ucp1* expression, WT and *Rag1*$^{-/-}$ mice acclimated at thermoneutral conditions (30^{o}C) for 20 days. As expected, thermoneutrality

attenuated the genotype-related differences in beige formation within the scWAT and the expression of *Ucp1*, while it had no effect on other thermogenesis-related genes such as *Cidea*, where *Rag1*$^{-/-}$ retained their increased expression. To stimulate *Ucp1* expression and induce beige AT formation, WT and *Rag1*$^{-/-}$ mice acclimated at 4^{o}C for two days (16). Interestingly, *Rag1*$^{-/-}$ mice were more capable in maintaining their body temperature than the WT mice, indicating that the beige adipose depot of the *Rag1*$^{-/-}$ mice retains its functionality and sensitivity to stimulatory challenges. To identify, the key cell, if any, of the adaptive immune system that can inhibit the formation of beige fat, we performed FACS analysis for CD4^{+} and CD8^{+} T cells, in the scWAT of *Rag1*$^{-/-}$ mice following reconstitution with the same number of CD4^{+} and CD8^{+} T cells. Our analysis revealed that the cell type that was significantly increased in the scWAT was the CD8^{+} T cells, revealing a preferential accumulation of this cell type in this tissue. Although it has been reported that in obesity, infiltration of CD8^{+} T cells in the scWAT may precede that of the macrophages and that adoptive transfer of CD8^{+} T cells to CD8-deficient mice aggravated the adipose tissue inflammation (2), there is no bibliography about the role of CD8^{+} T cells in the differentiation of WAT and most specifically, beige adipose tissue formation.

Therefore, we performed a series of studies to characterize the role of CD8^{+} T cells in beige formation and the specific mechanisms implicated. Adoptive transfer of CD8^{+} T cells in *Rag1*$^{-/-}$ mice significantly inhibited beige formation in the scWAT and led to a profound downregulation of thermogenesis and lipid catabolism genes in room temperature (RT) and cold exposure. Most importantly, CD8^{+} T cells replenishment could reverse the increased TH

expression in *Rag1*$^{-/-}$ mice, indicating a possible indirect mechanism that CD8^{+} T cells use to exert their negative effect in thermogenesis. Further studies on the metabolic profile of *CD8*$^{-/-}$ versus WT mice showed increased beige adipogenesis in the absence of CD8^{+} T cells, supporting the negative effect of these cells in the regulation of metabolic homeostasis.

Recent studies showed that the induction of beige formation requires two cytokines: IL-4 derived from eosinophils that via the induction of M2 macrophages impacts on the catecholamine-mediated induction of beige fat formation (8), and IL-13 or IL-5 derived from type 2 innate lymphoid cells (ILC2), facilitating the IL-4 effects on beige adipogenesis (13). Furthermore, removing either these cytokines, or the cells that produce them, or the macrophages, the target of these cytokines, blocked the induction of beige fat in the treated mice. To further understand the mechanism(s) behind the induced beige adipogenesis in *Rag1*$^{-/-}$ mice and how they align with the above reports, we assessed the contribution of innate immunity in this process. Initially we measured the abundance of eosinophils and ILC2s in WT, *Rag1*$^{-/-}$ mice and *Rag1*$^{-/-}$ mice reconstituted with CD8^{+} T cells in regular and cold temperatures. As expected, *Rag1*$^{-/-}$ mice that appear with increased beige formation have higher percentages of the above innate cell populations in the scWAT compared to WT mice, while in the presence of CD8^{+} T cells this population is significantly decreased. In line with the increased percentages of eosinophils and ILC2s, the intra-scWAT levels of IL-4, IL-5 and IL-13 secreted by them were significantly elevated in *Rag1*$^{-/-}$ mice compared to WT mice. Finally, transfer of CD8^{+} T cells to *Rag1*$^{-/-}$ mice, brought the levels of the above cytokines down to values similar to those measured in the WT mice.

These findings suggest an indirect effect of $CD8^+$ T cells in the regulation of beige adipogenesis mediated by altering innate immune cells and the corresponding cytokines profiles.

Finally, we studied whether the $CD8^+$ T cells inhibit beige fat formation in the scWAT via any secreted factor and we found that reconstitution of *Rag1*$^{-/-}$ mice with $CD8^+$ T cells that do not express INFγ, failed to block beiging formation. Additionally, characterization of the scWAT of *IFNγ*$^{-/-}$ and WT mice showed that the former presented with extended beige areas and increased percentages of eosinophils. The above indicate that a possible mechanism mediating the modulatory effects of the $CD8^+$ T cells in energy homeostasis could be IFNγ.

Next we sought to elucidate if the adaptive immune system deficiency had similar effects in lipid metabolism and storage in the liver of mice on hypocaloric diet, we know that at least in its early stages is a strong stimulus for liver lipid storage. We planned our experimental strategy with the assumption that in the absence of adaptive immune cells, as in the *Rag1*$^{-/-}$ mouse, increased energy utilization instead of lipid storage, is also occurring in the WAT similar to our findings in the liver. Very few studies have focused on the interactions of immune system with the metabolic functions that take part in hypocaloric states, with the bulk of them focused on the role of the innate immune system in starved mice (14, 15). For this purpose we leveraged again the *Rag1*$^{-/-}$ mice, that are deficient in functional T and B cells, Oil Red O (ORO) stained hepatic sections showed less lipid storage after starvation in *Rag1*$^{-/-}$ vs WT liver sections , whereas, in agreement, the FAO (fatty acid oxidation) pathway was significantly activated in the *Rag1*$^{-/-}$ mice.

To further assess the contribution of the missing lymphocytes as a whole in the increased liver lipid deposition of the *Rag1*$^{-/-}$, we next performed adoptive transfer of whole splenocytes isolated from a healthy WT mice. Transfer of splenocytes reversed the above phenotype in the *Rag1*$^{-/-}$ liver resulting in an increase in lipid deposition and attenuation of the FA oxidation, to levels similar to those encountered in the WT tissues. Next, we assessed the effect of specific T cell subtypes such as CD8^{+} T cells in this process. We found that transfer of CD8^{+} T cells in *Rag1*$^{-/-}$ mice promoted the storage of lipids in the liver, inhibited FA oxidation and blocked glucose synthesis in *Rag1*$^{-/-}$ liver, thus reversing or “normalizing” their phenotype similar to the effect of the mixed lymphocyte population initially attempted.

Collectively, our study demonstrates for the first time the role of CD8^{+} T cells in energy storage as reflected by the regulation of beige adipose tissue formation and liver steatosis. These findings carry potentially significant implications in the treatment of the exponentially rising number of patients with metabolic disorders, a remaining unmet medical need, or other chronic diseases altering the capacity for energy homeostasis.

2. Introduction

Obesity, a major epidemic with prevalence rates rising steadily among adults and children worldwide, is characterized by a state of chronic, low-grade inflammation due to profound infiltration of adipose tissue by inflammatory cells. This inflammatory state contributes to the development of systemic insulin resistance and progress to Type 2 diabetes. Additionally, obesity is associated with development of liver steatosis and thus, increased risk of

developing Non-Alcoholic-Fatty-Liver disease (NAFLD), which leads to hepatic deposition of lipids and the development of liver steatosis. The hypothesis I sought to address with my studies presented in this PhD thesis, is the immunometabolic properties of liver (A) and adipose tissue (B) as well through *in vivo* and *in vitro* studies in the regulation of immune-mediated pathogenesis.

2.1. The immune cells in adipose tissue

Although the inflammatory state of the white adipose tissue (WAT) in states of obesity is well described, the precise immune cell types involved in the activation of the inflammatory mechanisms in obesity over time remain uncertain. Several studies have provided evidence that in obese states pro-inflammatory classically activated macrophages (M1), neutrophils, $CD8^+$ T cells, $CD4^+$ Th1 cells and mast cells accumulate in white adipose tissue (WAT) and thus contribute to local and systemic inflammation (2, 17-19), while in lean states normal adipose tissue contains eosinophils, alternatively activated macrophages (AAMs), invariant killer T cells (iNKT), T regulatory cells and type 2 innate lymphoid cells (ILC2s) that can promote insulin sensitivity and metabolic homeostasis (3, 20-23) (Figure 2.1)

Macrophages

The WAT of lean mice is populated primarily by M2-polarized macrophages, expressing IL-10 and arginase that help maintain normal the function of adipose tissue, mainly through promoting tissue repair and angiogenesis. Initial studies have implicated the white adipose tissue infiltrating macrophages as well as the shift of resident macrophage polarization, as the key players in the development of insulin resistance during obesity (20). Early

on in the development of obesity, macrophages accumulate in visceral white adipose tissue (WAT) and reside there forming the adipose tissue macrophages (ATM) population, a polarized anti-inflammatory ("alternatively" activated) population, the so-called M2 macrophages. As adiposity increases and insulin resistance is established, ATMs undergo a phenotypic switch from the M2 to the proinflammatory ("classically" activated) M1 type, losing their protective capacity and contributing to the development of insulin resistance. M1-polarized macrophages are classically activated in the AT and get characterized by high secretion of pro-inflammatory markers such as TNF-α, IL-1β, IL-6 and Nos2, promoting the progress of insulin resistance and exerting a negative impact on the normal WAT function.

Mast cells

In addition to macrophages, one other cell of the innate immune system mediating the inflammatory response that takes place within adipose tissue is the mast cells. Mast cells are increased in the obese WAT as compared to the lean adipose tissue, indicative of the possibility for a role of this immunocyte in the pathogenesis of obesity. Genetic models of mice deficient in mast cells or even pharmacological stabilization of mast cells reversed the increase in inflammatory cytokines, chemokines and proteases in the WAT of obese mice. Further, these interventions attenuated the increased WAT and muscle angiogenesis both favor WAT expansion, in line with improved glucose homeostasis and increased energy expenditure (19).

Neutrophils

Neutrophil granulocytes are cells of the innate immune system that consist the largest fraction of white blood cells in mammals and are the first immune cells

to respond acutely upon initiation of inflammation. Especially, neutrophils support the recruitment of macrophages in the inflamed tissue through the production of cytokines and chemokines and secrete several proinflammatory proteases (24), one of which is the serine protease, neutrophil elastase (NE), a key effector in the inflammatory response (25). In states of exposure to High-Fat-Diet (HFD), the neutrophils in the AT is significantly increased leading to further release of NE that mediates development of insulin resistance, while ablation of NE in obese mice protects mice from AT inflammation associated with reduced infiltration of neutrophils and macrophages in the AT with a corresponding increase in AT insulin sensitivity (17).

Eosinophils

Eosinophils are white blood cells primarily involved in processes associated with allergic responses (26), certain microbial infections (27) and parasitoses, particularly with intestinal helminths (28). It has recently been reported that eosinophils are central for the regulation of metabolic homeostasis through supporting of adipose AAMs (29). AAMs are induced mainly by the IL-4 cytokine, derived to a great extent by eosinophils residing in the WAT. In HFD states mice with eosinophil deficiency have impaired AAMs accumulation, while they show compromised glucose tolerance, but increased adiposity and systemic insulin resistance. Interestingly, helminth infection-induced eosinophilia resulted in improved metabolic parameters and glucose tolerance, indicative of the effects of eosinophils in obesity. However, what is the network of factors behind the maintenance of eosinophils within the adipose tissue is still unknown. Recent studies indicate that IL-5 and IL-13

cytokines secreted from innate lymphoid type 2 cells (ILC2s) (30) in adipose tissue may contribute to maintain adipose eosinophils homeostasis.

Innate lymphoid type 2 cells (ILC2s)

Innate lymphoid cells (ILCs) is a newly described group of innate effector immune cells (31), that belong to the lymphoid lineage but do not have the processes for raising antigen-specific responses due to lack of T-cell receptors (32). The physiological functions of ILCs share many similarities with various T helper (TH) subsets (33, 34), while dysregulation of the ILCs abundance is associated with allergy and autoimmune diseases (35, 36). However, as emerging evidence has shown, ILCs exert tissue-specific characteristics and in the adipose tissue for example, the main role of these cells is to regulate metabolic homeostasis (29, 35). The ILCs are divided into three groups based the transcription factors that regulate their development and differentiation and the cytokines they produce (37). In this study, we have been focusing in the innate helper 2 cells (ILC2s). ILC2s were first identified in fat associated lymphoid structures in adipose tissue (30), while subsequently other groups identified ILC2s in the gut, spleen and lung (38). Upon exposure to the epithelial cytokines IL-25 and IL-33, ILC2s expand and secrete large amounts of type 2 cytokines, particularly IL-4, IL-5, IL-13 (30, 39). Recent studies have demonstrated the major role of ILC2s in the regulation of metabolic and glucose homeostasis, apart from their known role in type 2 immune responses associated with asthma and intestinal helminth infection. In fact in a recent study (23) it was shown that increased levels of these type 2 cytokines could promote the accumulation of AAMs and eosinophils in adipose tissue. Furthermore, the increased cytokine release by ILC2s seems

to be driven by IL-33, a cytokine highly expressed in the adipose tissue (40). Interestingly, mice deficient of ILC2s present with low AT eosinophils, AAMs and type 2 cytokine levels and with insulin resistance upon infection with an intestinal parasite (23).

$CD4^+$ T cells

The $CD4^+$ T cells group includes several distinct cell populations, including Th1 and Th17 cells, source of proinflammatory cytokines, and Th2 cells and Tregs, which produce anti-inflammatory cytokines. The role of $CD4^+$ T cells in obesity was addressed by studies involving adoptive transfer of T cells into mice deficient in recombination-activating genes (Rag), which as a result lack functional T and B lymphocytes. Especially, $CD4^+$ T cells transferred in a diet-induced obese (DIO) model dampened weight gain, while increased VAT mass and circulating levels of pro-inflammatory cytokines such as TNF-α and IL-6 (18). Winer et al. also proposed that it is the imbalance between the T cell subtypes that promotes adipogenesis. More specifically they showed that in obese mice the VAT resident $CD4^+$ Th1 cells are overwhelmingly increased compared to the Th2 and Treg cells

and promote the recruitment of pro-inflammatory M1 macrophages in the VAT, via induction of the release of IFN-γ, IL-1, IL-6 and TNF-α. Therefore, it is the restoration of the Th1/Treg cells balance that reverses insulin resistance in a HFD model, predominantly through Th2 cells and the production of the anti-inflammatory cytokines IL-4 and IL-13.

T regulatory cells (Tregs)

T regulatory cells are $CD4^+$ T lymphocytes characterized by high expression of the transcription factor forkhead/winged-helix transcription factor (Foxp3),

mediating the maintenance of self-tolerance and the suppression of autoreactive T cells in immunopathogenic states such as autoimmunity, allergy, inflammation, infection and tumorigenesis (41, 42). T regulatory cells are widely expressed in both lymphoid and non-lymphoid tissues, and they normally consist only 5-20% of the total $CD4^+$ T cells. However, in the visceral adipose tissue (VAT) T regulatory cells constitute half of the $CD4^+$ T cell population, suggestive of their possibly significant role in this tissue (3). Furthermore, in insulin-resistant models of obesity, Treg cells were found to be dramatically reduced specifically in the VAT, in further support of their important role in the inflammatory phenotype of the obese adipose tissue. The main mechanism of the protective action of Tregs is via controling the expansion of other T cell subtypes, and the regulation of innate immune cells, such as macrophages. The interaction of Tregs with the macrophages is facilitated as Tregs reside in the crown-like structures within the adipose tissue. Indeed, it has been shown that it is the increased influx of classically activated macrophages (M1), as well as the increased local and systemic concentrations of pro-inflammatory cytokines such as TNF-α, IFN-γ and IL- 6 that interfere with the expansion or survival of Tregs in the AT during obesity. In contrast, induction of Tregs in the adipose tissue of obese mice improved insulin sensitivity. Another study has shown that the critical molecule controlling Tregs accumulation, phenotype and function in AT is the proliferator-activated receptor gamma (PPARγ), as PPARγ expression by VAT Tregs was required for the restoration of insulin sensitivity in obese mice.

$CD8^+$ T cells

The VAT of obese mice contains high numbers of resident $CD8^+$ T cells in contrast to the low abundance of the $CD4^+$ T and Treg cells (2). Interestingly, the increased levels of $CD8^+$ T cells detected in the obese VAT was a tissue specific characteristic and not part of systemic increase in $CD8^+$ T cells, indicating the specificity of the proliferation of $CD8^+$ T cells in the AT as part of the pathogenesis of obesity. Furthermore, in the obese, as compared to the lean, VAT the $CD8^+$ T cells are activated, as the frequency of the $CD44^+CD62L^-$ effector memory cells was significantly higher as opposed to the decrease in naïve $CD44^-CD62L^+CD8^+$ T cells. In contrast to earlier studies claiming that the first cells to accumulate in obese VAT are macrophages, a more recent study has showed that the infiltration by $CD8^+$ T cells precedes the accumulation of macrophages. *In vivo*, loss and gain-of-function experiments have shown that the $CD8^+$ T cells are essential not only for the initiation, but also the maintenance of the inflammatory response. Especially, CD8 deficient mice (*$CD8^{-/-}$*) did not have any significant change in the numbers of M1/M2 macrophages neither in the levels of pro-inflammatory cytokines IL-6 and TNF-α following diet-induced obesity (DIO). However, adoptive transfer of splenic $CD8^+$ T cells in CD8 knockout mice increased the infiltration by the M1-proinflammatory macrophages, the formation of crown-like structures and the expression of IL-6 and TNF-α, aggravating adipose inflammation (2) suggesting that the $CD8^+$ T cells are important for the initiation of the inflammatory cascade. Moreover, depletion of $CD8^+$ T cells via a neutralizing antibody after establishment of obesity, confirmed the importance of $CD8^+$ T cells for the maintenance of the inflammatory response

in adipose tissues with on-going inflammation. In particular, specific anti-CD8 antibody treatment lowered the IL-6 and TNF-α levels and the M1 macrophage infiltration in the VAT of obese mice, resulting in ameliorated insulin resistance and glucose intolerance. An interesting point in Nishimura's study is that the interaction between $CD8^+$ T cells and adipocytes was sufficient to activate an inflammatory response that drove induction of the macrophage's differentiation, activation and migration to the AT. All the above provided strong evidence for a major role of the $CD8^+$ T cells in the regulation of systemic metabolism.

iNKT

Innate natural killer T cells (iNKT) consist a unique T cell population, a subpopulation of $CD4^+$ T cells, which is highly conserved and expresses invariant T cell receptors (TCRs). iNKT cells are activated when TCRs recognize glycolipid ligands such as alpha-galactosylceramide (aGC) presented by the major histocompatibility complex-like molecule CD1d (43, 44). Upon their activation, iNKT cells produce Th1 and Th2 cell cytokines (45). The immunoregulatory properties of iNKT cells underlie their use in the treatment of immune-mediated diseases such as Type 1 diabetes, multiple sclerosis and rheumatoid arthritis (RA) (46-48). Under physiological conditions, the adipose tissue is highly enriched in iNKT cells, in contrast to their low abundance in the obese fat (49). It has recently described that the adipose tissue–iNKT cells represent a unique subset with distinct Th2 cell characteristics that promotes the secretion of anti-inflammatory cytokines such as IL-10. As such this iNKT subpopulation exerts protective effects against the development of obesity-induced insulin resistance (22).

Additionally, an indirect way that iNKT cells use to eliminate AT inflammation is through phenotypic switch of tissue macrophages towards the anti-inflammatory M2 type, mediated by the increased IL-10 levels. Animal studies using altered iNKT cell numbers showed that mice lacking iNKT cells showed increased weight gain and rapid development of insulin resistance following HFD (50). Along these lines, adoptive transfer or *in vivo* activation of iNKT cells via their lipid ligand decreased body weight and systemic triaglyceride levels and improved the insulin sensitivity of mice on DIO (22). Therefore, iNKT cells are believed to confer protection against the development of dysmetabolic disease and the associated inflammation following exposure to HFD.

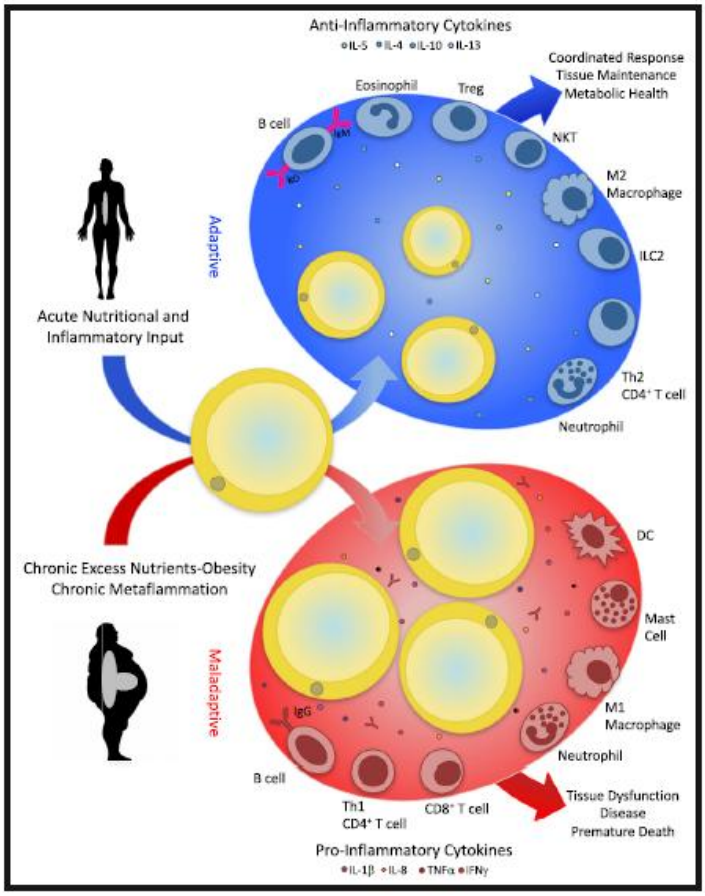

Figure 2.1. The immune cell types involved in the physiology and pathogenesis of tissue homeostasis in white adipose tissue.

In obese states, immune cells that are recruited and contribute to adipose tissue inflammation are: Monocytes, that transmigrate into the adipose tissues differentiate to proinflammatory M1-like macrophages secreting proinflammatory cytokines, $CD4^+$ T_H1, $CD8^+$ effector T cells, which secrete proinflammatory cytokines, mast cells and B cell numbers, that activate T cells, which enhance M1-like macrophage polarization. On the other, in lean states, adipose tissue is enriched in T_H2 cells, T_{reg} cells, eosinophils, ILC2s and M2-like macrophages. T_{reg} cells secrete IL-10 and also stimulate IL-10 secretion from M2-like macrophages, while eosinophils and ILC2s secrete IL-4, IL-5 and IL-13 and thus contributing to the anti-inflammatory, insulin-sensitive phenotype. (Adapted from Gokhan Hotamisligil, Immunity Review, 2017).

2.2. Physiologic functions of adipose tissue (AT)

The main function of adipose tissue (AT) under normal conditions is to store lipids, and regulate triaglycerides (Trg) and fatty acid (FA) circulating levels and to secrete adipocyte-specific derived proteins such as adipokines (Figure 2.2). The main processes to achieve the above are: (a) De novo lipogenesis (DNL), (b) Lipid storage, (c) Fatty acid Oxidation (FAO) and (d) Lipolysis.

(a) De novo lipogenesis (DNL) refers to the synthesis of fatty acid (FA) from non-lipid substrates. This is achieved by convertion of the excess carbohydrates to lipids for storage. The two central enzymes that regulate DNL are the acetyl-CoA carboxylase (ACC) and the fatty acid synthase (FAS), by using acetyl-CoA and malonyl-CoA derived from glucose or other carbon precursors to generate FAs. The expression of these lipogenic genes (FAS and ACC) is regulated by two master transcription factors: the sterol response element binding protein 1c (SREBP1c) and the carbohydrate response element binding protein (ChREBP).

(b) Another main function of adipose tissue is the ***storage of fats*** in the form of triaglycerides. The central enzyme that regulates the terminal step in triaglyceride synthesis is DGAT (diacylglycerol acyltransferase), which catalyzes the formation of triglycerides from diacylglycerol and acyl-CoA.

(c) ***Fatty acid oxidation*** *(FAO)* takes place in the AT in response to high energy demands, as the oxidation of fats yields more energy (in ATP molecules) than the carbohydrates oxidation. The process of mitochondrial FAO is termed beta-oxidation and includes four reactions. The first oxidation step involves a family of FAD-dependent Acyl-CoA dehydrogenases (Aco), while the next three steps involve a hydration, an oxidation and finally a hydrolytic reaction, all catalyzed by a multifunctional enzyme called mitochondrial trifunctional protein (MTP). MTP is composed of eight protein subunits, four alpha-subunits encoded by the Hadhα (Hydroxyacyl-CoA dehydrogenase) gene and four beta-subunits encoded by the Hadhb genes.

(d) The rate limiting step that takes place in AT is ***lipolysis***. Lipolysis is the hydrolysis of stored triaglycerides (Trg) by several distinct lipases, to diacylglycerols (DAG), monoacylglycerols and, finally, to fatty acids and glycerol. Hormone-sensitive lipase (Lipe) is a multifunctional enzyme that possesses triaglyceride (TAG), diacylglyceride (DAG), cholesterol ester and retinyl ester hydrolase activities. However, it is more specific for the initial step of lipolysis for diacylglyceride (DAG) hydrolysis. Another important enzyme responsible for the final step of lipolysis is the monoglyceride lipase (MG), which hydrolyzes monoglycerides into glycerol and fatty acids.

In addition to the enzymes above described involved in the fatty acid metabolism pathways in AT, there are several transcription factors such as peroxisome proliferator-activated receptor gamma coactivator-1a (Pgc-1α) and PPARs, important for the functions of adipocytes. Especially, Pgc-1α is a co-activator that interacts with a broad range of transcription factors involved in the control of AT metabolic homeostasis. Elevated levels of Pgc-1α are found in tissues rich in mitochondria and thus with active oxidative metabolism. PPARs Similarly the PPARs (PPAR-α, PPAR-δ, and PPAR-γ) are nuclear receptors, that are subject to transcriptional co-activation by Pgc-1α. According to several studies, increased levels of PPAR-γ are linked to adipogenesis, whereas increased levels of PPAR-α and PPAR-δ induce FA oxidation.

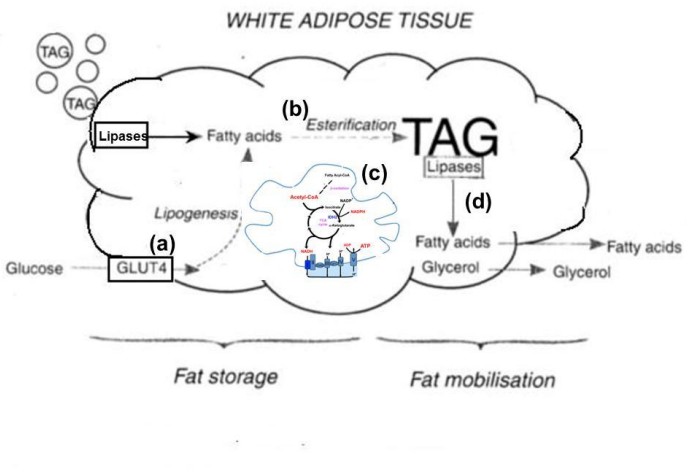

Figure 2.2. Fatty acid metabolism in the white adipose tissue (WAT):

(A) **De novo Lipogenesis**: Glucose comes into the cell through Glut4 receptors. Glucose converted into acetyl-CoA and then into FFAs

(B) **Esterification/Fat storage**: the process of assembling FAs into TAGs.

(C) **Beta-oxidation** of FAs.

(D) **Lipolysis**: lipases break down triaglycerides (TAG) to fatty acids (FAs) and glycerol.

(Adapted from Metabolic Regulation: A Human Perspective, 3rd Edition; Keith N. Frayn, February 2010, Wiley-Blackwell and modified).

2.3. Fat depots

2.3.1. White adipose tissue (ScWAT & EpiWAT)

In addition to the above described functions, AT is a highly dynamic endocrine organ actively participating in the progress of many diseases including inflammatory and infectious diseases, cancer and other states with altered energy metabolism (51). Adipose tissue depots are divided into two types: white adipose tissue (WAT) that stores energy in the form of triaglycerides, and brown adipose tissue (BAT) that dissipates energy as heat to maintain body temperature. The AT depots have specific characteristics that underlie their relative contribution to maintenance of energy balance (52).

In particular, WAT is situated under the epidermis (subcutaneous-scWAT) or inside the abdomen (visceral-VAT) surrarounding vital organs (perigonadal, mesenteric, omental and perirenal fat) (Figure 2.3A). Subcutaneous and visceral fat depots have distinct characteristics (Figure 2.3A), which support their different involvement in metabolic functions. The anatomical location of the two depots dictates their discrete roles. Thus, scWAT serves as an insulating layer located beneath the skin, to directly experience changes in environmental temperature. VAT located deeper in the abdominal cavity is subject to experience less fluctuations in external temperature. Histologically, VAT has a uniform appearance and consists primarily from single, large fat droplets and a few mitochondria, whereas the scWAT is heterogeneous and contains mature unilocular adipocytes intercalated with small multilocular

adipocytes. Increased subcutaneous (sc) fat deposition seems to have a metabolically protective role, and thus it is called the “good fat”, while increased visceral fat deposition has been linked with metabolic syndrome and is called as the “bad fat”. The main reason for the benign nature of the scWAT compared to the VAT is its increased rate of adipose turnover and the formation of new adipocytes.

Recently a new adipocyte population residing in the scWAT has been identified, the so-called brown in white (brite) or beige cells, that shares many characteristics with the brown adipocytes. Spiegelman’s group successfully cloned pre-adipocyte cell lines from the SVF of WAT and identified two types of pre-adipocytes, white and beige (4). Both types were capable to differentiate into adipocytes under standard adipogenic conditions, though, only beige cells induced a thermogenic gene program, that promotes the expression of a set of brown-fat specific genes such as *Ucp1, Cidea* and *Pgc-1 α,* when treated with beta-adrenergic agonists or upon exposure to cold (Figure 2.3A). Beige cells have different origin from that of the brown adipocytes, although it was originally falsely presumed that most beige cells arise from trans-differentiation of pre-existing, mature adipocytes (53). Wang et al using a fate-mapping technique to track white adipocytes showed that most, if not all beige cells, arise from a precursor population rather than from the pre-existing white adipocytes (54). Recent experiments have shown that beige adipocytes do not express the myogenic marker (Myf), nor the brown adipocyte specific markers but instead they possess a distinct gene signature (Figure 2.3A). This unique cell population (beige cells) is most prominent in the scWAT and thus scWAT is best positioned to acquire thermogenic

behavior characteristics, than the visceral depots that are more susceptible to development of inflammatory phenotype and the associated adverse metabolic profile. In basal states beige cells are limited in numbers and resemble white adipocytes, as per their low expression in brown adipocyte associated markers such as *Ucp1, Cidea* and *Cox7A1* (4). However, upon stimulation beige cells obtain a more brown-like phenotype as they possess comparable thermogenic potential (7). Therefore, beige cells have the unique capability to switch between an energy storage and energy dissipitation phenotype.

An interesting recent finding that reveals the significance of studying beige metabolism is that the brown fat visualized in adult humans' shares more molecular characteristics with beige fat than classical brown adipocytes. So beige adipocytes are found in the adult human and possibly they have a physiological role, as opposed to BAT, although still to be described.

2.3.2. Brown adipose tissue (BAT)

Brown adipose tissue (BAT) is mainly located subcutaneously in the intrascapular region and contains multilocular small lipid droplets and a high density of mitochondria. The origin of BAT cells is from mesodermal lineage ($Myf5^{+}$) (55) (Figure 2.3B). The main role of BAT is to regulate energy homeostasis through the production of heat (thermogenesis) in response to cold, or other stimuli engaging the peripheral nervous system, through mitochondrial uncoupling. The brown-specific mitochondrial uncoupling protein 1 (UCP1) is the essential protein responsible for the non-shivering thermogenesis, constitutively on-going in the BAT. Ucp1 is located in the inner mitochondrial membrane, which allows protons in the intermembrane space to

re-enter the mitochondrial matrix without generating ATP and thereby resulting in the production of heat (thermogenesis). Ucp1 is activated by long chain fatty acids that are produced within BAT by lipolysis upon adrenergic stimulation of BAT (56). Additionally, Ucp1 is induced by several transcription factors including the co-activator Pgc-1alpha (57). BAT also has a high rate of fatty acid, triaglycerides and glucose uptake as well as beta oxidation in line with its important role in the control of energy homeostasis. The abundance as well as the functionality of this thermogenic tissue is diminished in obese people, suggesting an inverse relationship between adiposity and BAT activity. Along these lines, stimulation of BAT can increase the basal metabolic rate and impact long-term energy balance. Additionally, mice genetically engineered to have less BAT gained more weight than control mice (58).

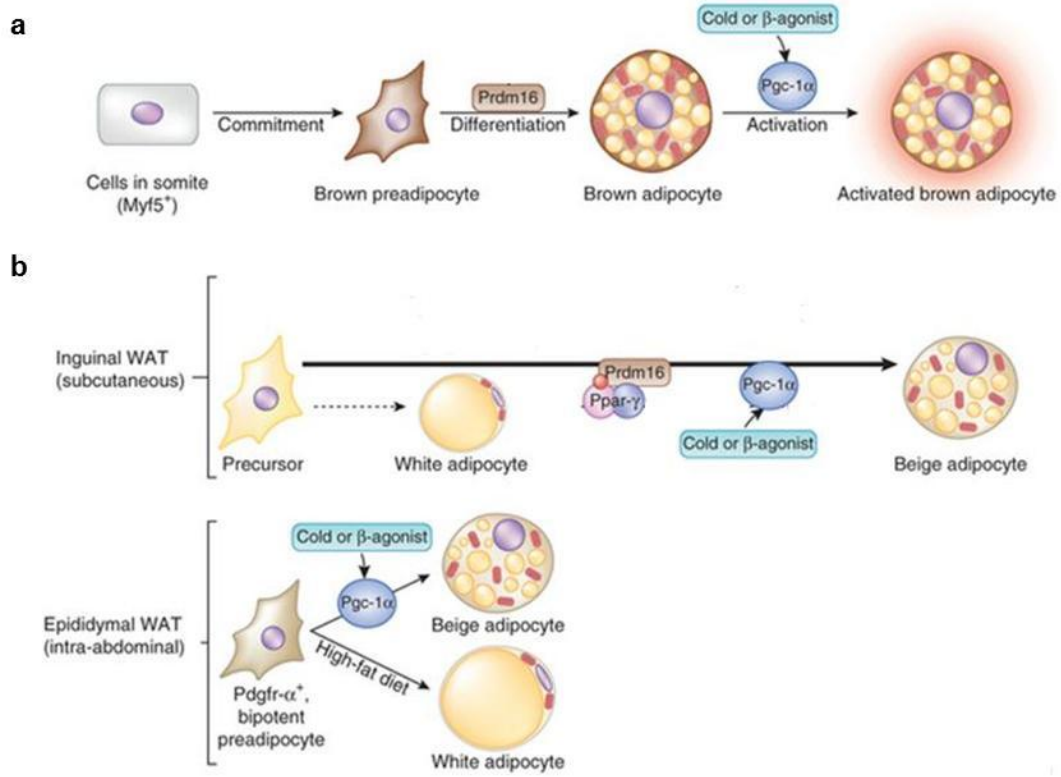

Figure 2.3. **Beige and brown adipocyte development**.

(A)In scWAT, white adipocytes derive from different progenitors from beige adipocytes. β-adrenergic stimulation or cold exposure triggers predominantly *de novo* differentiation of precursor cells (large arrow) to beige adipocytes. In eWAT, caloric excess causes bipotent progenitors to differentiate into white adipocytes, whereas β-adrenergic activators or cold exposure stimulate beige adipocyte development. (B) Brown adipocytes are derived from a *Myf5*+ progenitor population. Prdm16 drives a brown fat cell fate. Thermogenesis in brown adipocytes is activated by beta-agonists or cold exposure through beta-adrenoreceptors that activates Pgc-1a expression inducing Ucp1 expression. (Adapted from Matthew Harms & Patrick Seale Nat. Med. 2013).

2.4. Factors promoting beige adipogenesis

The known pathways to increase BAT activity are mainly associated to the rich network of sympathetic innervation and high vascularization observed in this tissue. Sympathetic stimulation leads to release of norepinephrine (NE) at the nerve endings, which binds the beta-adrenergic receptors (β-Adrs) on the brown fat cells leading to increased cAMP levels. In turn, cAMP activates protein kinase A (PKA) which mediates lipolysis, resulting to increased cytosolic FFA levels used as substrates for mitochondrial energy dissipation ultimately resulting in increased heat production (56). Therefore, known beige activators are cold exposure and beta-3 adrenergic receptor agonist treatment through activation of the SNS (Figure 2.4). Apart from known beige activators, the hormone irisin, Fgf21, natriuretic peptides, Bmp7 and meteorin are newly identified beige regulators (Figure 2.4). Contrary to BAT activators which result in a healthy phenotype, thermoneutral housing conditions (around 30^{o}C) ablate *Ucp1* expression driving an obese phenotype.

Fgf21

Fibroblast growth factor (Fgf21) is a secreted factor that acts as a hormone to regulates important metabolic processes in several tissues such as liver, epididymal WAT (eWAT) and pancreas. Initially, Fgf21 was found to regulate glucose uptake and to inhibit lipolysis in adipocytes. More recent studies identified the significant role of Fgf21 as a brown fat adipokine mediating adaptation to chronic cold exposure including induction of beige formation. Fgf21 acts in an auto-/paracrine manner to increase *Ucp1* and other thermogenic genes expression in both brown and white adipose tissue, mainly through induction of the protein levels of Pgc1alpha (Figure 2.4). Animal studies revealed the significance of Fgf21 in metabolic homeostasis, as mice deficient in Fgf21 showed impaired ability to adapt to prolonged cold exposure with diminished beige formation in the scWAT, while overexpression of Fgf21 resulted in weight loss in obese mice through increase in energy expenditure.

Irisin

Irisin is a myokine released by muscle into the circulation under exercise, following proteolytic cleavage from its cellular form, fibronectin-type III domain-containing 5 (Fndc5). Fndc5 expression was induced by the elevated Pgc-1alpha in muscle in response to exercise. Irisin induces the expression of Ucp1 and results in the corresponding scWAT browning (Figure 2.4). Thus, the beneficial effects of irisin in systemic energy expenditure include improvement in obesity-mediated insulin resistance and glucose homeostasis (59).

Bone morphogenetic protein 7 (Bmp7)

BMPs are members of the transforming growth factor-β (TGF-β) superfamily known to control multiple key pathways of embryonic development and differentiation. Different members of BMPs appear to have opposing roles in adipogenesis. BMP-7 is a potent inducer of brown preadipocyte's differentiation, and activates brown fat specific genes such as *Ucp1*, *Prdm16* (PR-domain containing 16), *Pgc-1alpha* and *PPARgamma* (Figure 2.4). Additionally, Bmp7 mediates commitment mesenchymal progenitor cells to the brown adipocyte lineage. Studies on overexpression of BMP-7 demonstrated its ability to induce the differentiation of brown adipocyte *in vitro* and *in vivo*, while deletion of Bmp7 in mice showed marked insufficiency in brown fat formation and almost complete loss of *Ucp1* expression (11, 60).

Natriuretic peptides

Natriuretic peptides are hormones identified initially as released by heart in response to cardiac stress. Atrial natriuretic peptide (ANP) and B-type natriuretic peptide (BNP) have been linked with the induction of brown and beige adipocytes through p38 MAPK activation (61). In a more recent study, mice found to have increased levels of natriuretic peptide receptors as well as beta-3-adrenergic recetpors in the scWAT following Roux-en-Y gastric bypass (RYGB), and increased expression of beige fat markers (62) (Figure 2.4).

Meteorin

Meteorin-like (Metrnl) is a Pgc-1a-4 regulated hormone induced in muscle after exercise and in adipose tissue (AT) upon cold exposure. It mainly acts through activation and recruitment of immune cells with thermogenic effects in the AT, rather than through direct effects on adipocytes. In particular,

meteorin recruits eosinophils into the AT, where they secrete IL-4 and IL-13, cytokines shown to promote the activation of the AAMs that in turn result in increased expression of thermogenesis-related genes. Interestingly, induction of Metrnl levels in mice resulted an improvement in glucose and overall metabolic homeostasis, in line with increased beige fat thermogenesis, while blockade of Metrnl significantly attenuated the chronic cold exposure-induced AAMs activation and the associated activation of thermogenic genes (10).

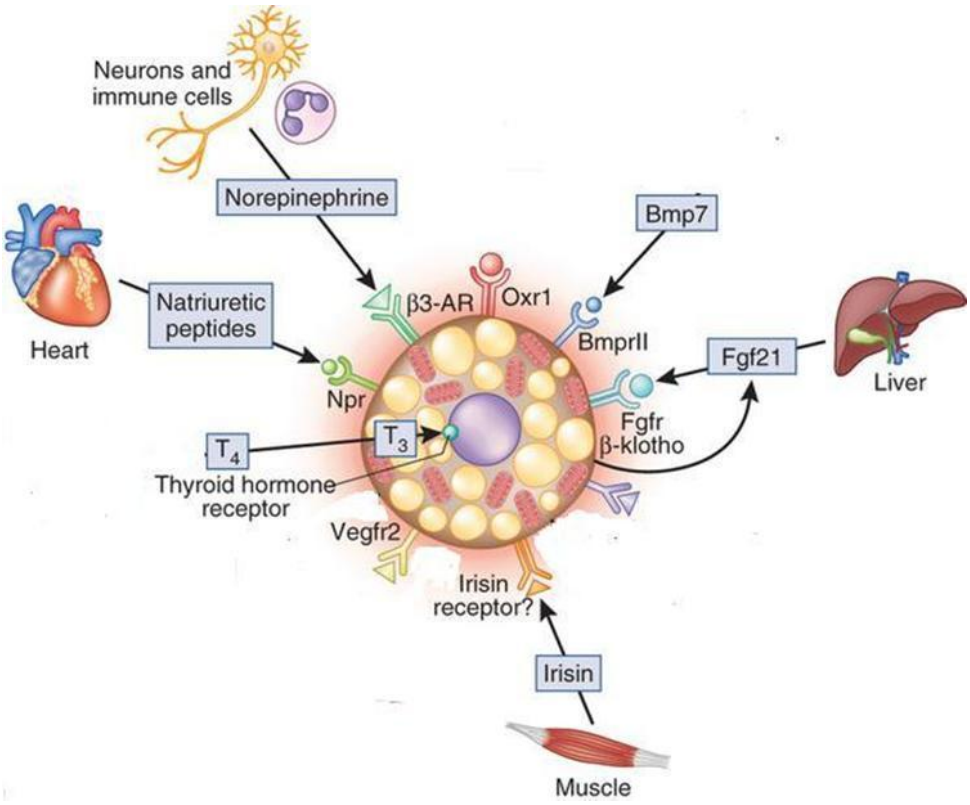

Figure 2.4. Factors promoting beige adipogenesis. (A) Norepinephrine secreted by neurons and alternatively activated macrophages (AAMs), (B) natriuretic peptides secreted by cardiac tissue, (C) fgf21 secreted by liver , (D) irisin secreted by muscle (E) and Bmp7 promotes brown fat development.

(Adapted from Matthew Harms & Patrick Seale Nat. Med. 2013)

2.5. Effect of various temperatures in beige adipogenesis

Cold exposure and beta-adrenergic activation

In mammals, maintaining body temperature in a cold environment achieved by both shivering and non-shivering thermogenesis. Non-shivering thermogenesis is mainly mediated by BAT, in which energy is dissipated in the form of heat through the action of Ucp1 in mitochondria (63). When non-shivering thermogenesis is not sufficient to cover the demands for heat, shivering thermogenesis via increase in muscle activity is also contributing.

The classic (indirect) mechanism mediated by cold to induce thermogenesis is through activation of the sympathetic nervous system (SNS) and the associated beta-adrenergic signaling (Figure 2.5). Cold is sensed by the sensory nerves in the skin, and then processing in the hypothalamus leads to activation of the SNS and finally release of norepinephrine (NE) in the brown and subcutaneous AT. Binding of NE to G protein-coupled beta-adrenergic receptors (GPCRs) on adipocytes activates the cAMP/protein kinase A (PKA)/ cAMP response-elementing binding protein pathway critical in controling the thermogenic pathway. At the same time, increased blood flow via vasodilation, and increased vascularization,is induced. However, the use of beta-adrenergic agonists to enhance energy production has many limitations due to the broad expression of beta-adrenergic receptors (beta-Adrs) in many vital organs has many limitations. Additionally, it has been recently reported that blockade of beta-adrenergic receptors did block the increased thermogenesis in response to cold, indicating that regulation of thermogenesis implicates additional mechanisms independent of the sympathetic activation. An example for the latter is a recent report showed that that cold may directly

activate thermogenesis in a cell-autonomous manner. Thus, *in vitro* studies indicated that lower temperatures could directly activate a thermogenic program in white and beige adipocytes, but failed to activate thermogenesis in brown adipocytes. This pathway was independent of the cAMP-induced beta-adrenergic activation.

Thermoneutrality

An important factor in the study of metabolism is the control of temperature. For all mammals there is a range of ambient temperatures within which the general metabolism of the organism, in the absence of any physical activity, generates sufficient heat as a byproduct of the continually ongoing metabolism so that its predetermined body temperature can be maintained. This temperature range is known as the thermoneutral zone, and at this temperature the organism demonstrates its basal metabolic rate. On mild cold exposure an animal will initially attempt to defend its body temperature and the animal will increase its endogenous heat production. This increase will occur initially through shivering thermogenesis. As emerging evidence demonstrates the “normal” animal house conditions (18-22^{o}C) impose a chronic thermal stress to mice as the environment temperature where thermal stress is eliminated was found to be around 30^{o}C for mice. In this temperature, Ucp1 is ablated resulting in accumulation of fat even with normal diets, due to impaired induction of thermogenesis (Figure 1.5). This experimental manipulation enables characterization of the role of Ucp1 and genotype-specific metabolic studies. Based on the above colony maintenance and experimentation at the commonly used housing temperature of ~22^{o}C may result in biased interpretations in metabolic studies. Combination with

studies with animals kept at thermoneutrality conditions is likely to increase the possibility of identifying genes important for metabolic functions.

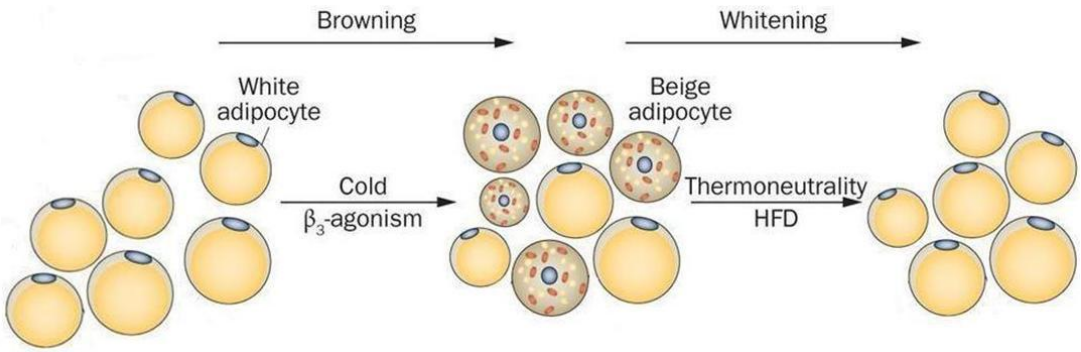

Figure 2.5. Browning and Whitening of WAT depots.

Specific WAT depots can either develop high numbers of beige adipocytes (browning) or increase lipid storage in cells that morphologically resemble classic white adipocytes (whitening), depending on environmental challenges. Browning of WAT requires cold temperatures or treatment with a beta-3 adrenergic receptor agonist, while whitening of WAT promoted by exposure to a High-Fat-Diet (HFD) or in the absence of heat stress (thermoneutrality) that reduces the rate of thermogenesis and leads to excessive lipid deposition. (Adapted from Alexander Bartelt & Joerg Heeren Nature Reviews Endocrinology 2014).

2.6. Beige adipose tissue and innate immune cells

Recent studies in the browning, i.e. beige adipocytes development, in the scWAT showed the significance of immune cells such as eosinophils, type 2 cytokines, macrophages and other myeloid cells. Thus, in response to cold, eosinophils secrete IL-4 that induces the expression of tyrosine hydroxylase (TH), the rate limiting enzyme in the synthesis of catecholamines, in alternatively activated macrophages (AAMs) (Figure 2.6). At the same time AAMs secrete type 2 cytokines; IL-4 and IL-13 promoting an anti-inflammatory profile and together with catecholamines induce the expression of

thermogenesis- and lipolysis- mediating genes in BAT and in WAT respectively. The significance of AAMs and eosinophils-derived IL-4 in the WAT browning was supported by animal studies where lack of AAMs impaired the metabolic adaptation to cold, while IL-4 administration increased thermogenic genes expression, fatty acid mobilization and energy expenditure (8). Furthermore, administration of IL-4 in pre-established models such as in thermoneutrality-driven obesity, increased the beige fat mass and the thermogenic capacity highlighting the significance of this cytokine in controling obesity (9). Additionally, genetic disruption of IL4/IL-13 signaling or TH expression prevented the cold-induced WAT beiging. To conclude, in contrast to the neuronal circuit that it is known to regulate BAT thermogenesis (64), the development and functionality of beige adipose tissue is also controlled by a parallel circuit, driven by hematopoietic cells, in particular eosinophils, type 2 cytokines and alternatively activated macrophages.

More recently, it has been reported that innate lymphoid cells type 2 (ILC2s) lay a significant role in the regulation of beige fat formation within the WAT. Initially, ILC2s have been identified in epididymal WAT of mice, where they support eosinophils and AAMs to promote glucose homeostasis. Since the ILC2-derived cytokines IL-5 and IL-13 are essential for initiating type 2 immune responses in WAT, ILC2s rightly linked with the development of beige fat in the scWAT. In line, ILC2s activation results in the proliferation of bi-potential adipocyte precursors (APs) and in their subsequent commitment to the beige fat lineage. The exact physiological signals that prime ILC2s to activate this pathway remain unknown. However, fate mapping studies showing that beige cells derive from a distinct progenitor cell population, the

Myf5- PDGFRα+ precursor cells, was important in elucidating the mechanisms driving these functions of ILC2s. IL-33 is a classic stimulus used for the activation of ILC2s and its administration led in accumulation and activation of ILC2s in the scWAT and the corresponding increase in IL-5 and IL-13 secretion (Figure 2.6). Then, IL-13 together with the eosinophils-derived IL-4 induce IL-4Rα signaling, thus promoting the expansion of PDGFRα+ adipocyte precursor cells and their commitment to the beige adipocyte lineage. Interestingly, during the development of scWAT, eosinophil-derived IL-4 seems is critical role in the expansion of PDGFRα+ adipocyte precursors to beige adipocytes.

Lastly, the role of ILC2s for adipose tissue homeostasis was revealed through gain and loss of function studies, where ILC2- and eosinophil-derived type 2 cytokines induced signaling via the IL-4α in PDGFRα+ APs promoting beige fat formation, while loss of type 2 cytokine signaling decreased the proliferation rate and number of PDGFRα APs in the scWAT.

To conclude, the mechanism by which beige fat development in scWAT is mediated by type 2 immunity is through control of the expansion and commitment of APs to the beige fat lineage and activation of mechanisms for differentiation of beige adipocytes precursors to beige adipocytes via myeloid-derived catecholamines.

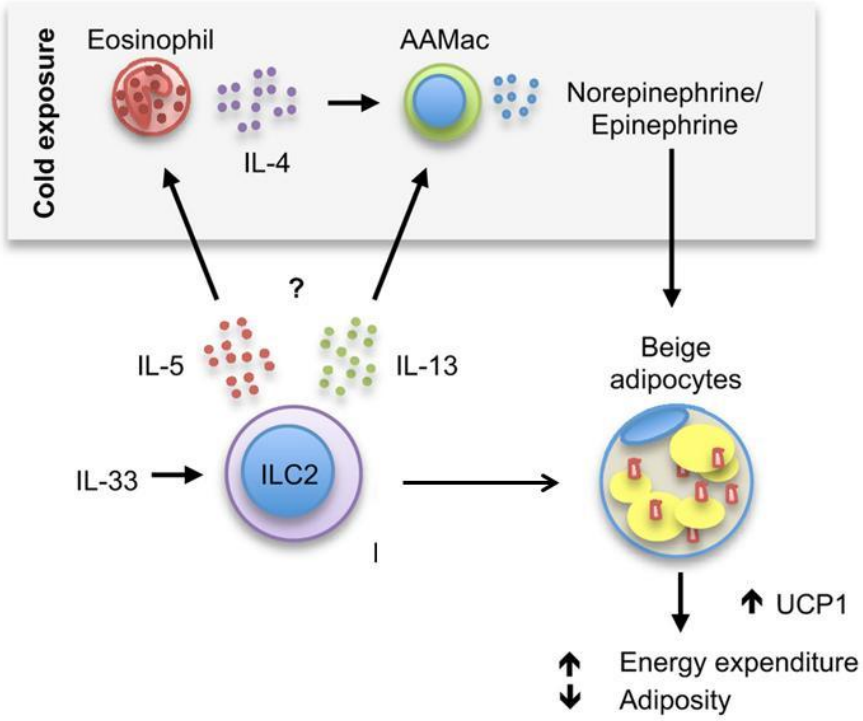

Figure 2.6. Thermogenic responses in cold exposure

The release of epithelial cell-derived cytokine IL-33 results in the activation of ILC2s, which then secrete IL-5 and IL-13 to initiate type 2 immune responses and promote recruitment of eosinophils and alternatively activated macrophages (AAMac). Cold exposure activates eosinophils to secrete IL-4 and therefore activate the secretion of norepinephrine from AAMs that induce beige adipogenesis characterized by increased Ucp1 levels.

(Adapted from Farber et al., Nature, 2015 and modified).

2.7. Liver and energy homeostasis

A very first question addressed in this PhD thesis was to elucidate common mechanisms for the maintenance of energy homeostasis between the adipose tissue and the liver, focused on those employed by the adaptive immune system. For this reason we focused in the regulation of lipid metabolism in the liver under basal conditions and upon nutrient deprivation that induces

lipolysis and the development of liver steatosis, as a first resort in the storage of energy for the anticipated upcoming demands. The metabolic process in the liver during starvation follows several steps: increased muscle proteolysis that supplies amino acids for glyconeogenesis, and increased lipolysis in the adipose tissue that supplies FFAs for glyconeogenesis, oxidation and ketogenesis, while at the same time glycogen stores are depleted. In short-term starvation, mobilization of FFAs exceeds the demand for FA oxidation, and thus surplus of FFAs are re-esterified to triaglycerides (TG), increasing the lipid deposition in the liver (Figure 2.7). A few recent studies have linked the immune system with the metabolic functions operating in the liver in starvation (14, 15). Here we provide preliminary results from our studies with mice exposed to experimental nutrient deprivation, from on-going studies in our laboratory.

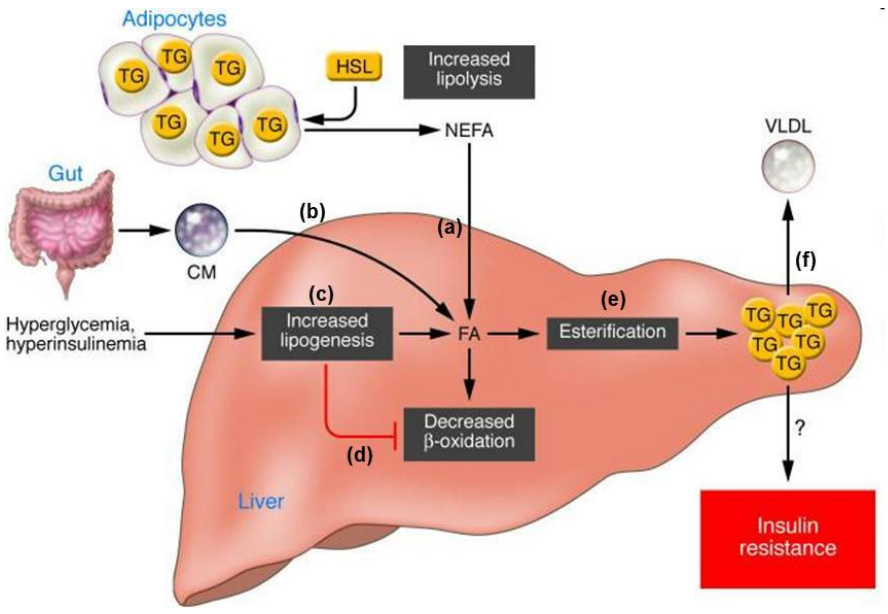

Figure 2.7. Non-Alcoholic Fatty Liver Disease (NAFLD) is an accumulation of TGs in the liver.

Molecular events resulting in intrahepatic lipid accumulation may arise from:

(A)increased uptake of FFAs from peripheral fat stored in AT. (B)Fatty acids are also taken up by the liver through the uptake of intestinally derived chylomicron (CM). (C)In addition, the combination of elevated plasma glucose (hyperglycemia) and insulin concentrations (hyperinsulinemia) promotes de novo fatty acid synthesis (lipogenesis) and (D) impairs β-oxidation, thereby contributing to the development of hepatic steatosis. (E)After the esterification step (conversion of FAs into TGs) TG can then be stored as lipid droplets within hepatocytes or secreted into the blood as VLDL. (F)Export of triaglycerides assemble Very low density lipoproteins (VLDL) (Adapted from J Clin Invest. 2008 March 3; 118(3): 829–838 and modified).

3. Results

3.1. Adipose tissue and its immunometabolic properties

The subject of this study was to evaluate the contribution of the cells of the adaptive immunity in energy homeostasis and primarily the liver and the adipose tissue within the scWAT in mice. The model we have chosen for these experiments is the *Rag1*$^{-/-}$ mouse that lack a functional adaptive immune system, as it is deficient in functional T and B cells. In order to assess the metabolic effects of the lack of adaptive immune system, we first measured a range of metabolic parameters using a comprehensive laboratory animal monitoring system (CLAMS), in WT and *Rag1*$^{-/-}$ mice over a 48-hour period. By assessment of metabolic rate, food intake, moving activity and respiratory exchange ratio (RER) (ratio of CO_2 to O_2) we showed that *Rag1*$^{-/-}$ mice have increased metabolic activity (Figure 3.1A) and that metabolize lipids more efficient than carbohydrates, despite their similar eating (Figure 3.1B) and motor behaviors (Figure 3.1C). The decreased respiratory

exchange ratio (RER) in *Rag1*$^{-/-}$ mice demonstrates the importance of lipids as their primary fuel source (Figure 3.1D). A thorough analysis of the main metabolic organs that could be involved in the development of this metabolic phenotype such as liver and adipose tissue identified the most striking differences in the latter.

3.1.1. ScWAT, EpiWAT and BAT characteristics in WT and Rag1-/- mice

Initially, inguinal (subcutaneous-Sc) and epididymal white adipose tissue (eWAT) and interscapular brown adipose tissue (BAT) from age- and weight-matched wild-type (WT) and *Rag1*$^{-/-}$ mice fed a normal diet (ND) were collected, weighed and tissue taken for further molecular and histological analysis. Interestingly, although the fat pad weight of eWAT and BAT were not significantly different between the different genotypes (Figure 3.2 A&D), the fat pad weight of scWAT of *Rag1*$^{-/-}$ was substantially reduced versus that of the WT mice (Figure 3.1G). Furthermore, histological analysis (H&E staining) of all adipose depots showed significantly reduced cell size in the scWAT of the *Rag1*$^{-/-}$ vs WT mice (Figure 3.1E), while no significant differences were detected in the eWAT or BAT adipocytes between the two genotypes (Figure 3.2 B&E). Next we assessed metabolic pathways operating in the physiologically functioning adipose depots. We found that in the eWAT (Figure 3.2C), expression of the genes related to the fatty acid (FA) oxidation pathway (*Pgc1a, Hadha, PPARα*) was significantly increased in the *Rag1*$^{-/-}$ tissues, while the expression of genes related to the FA synthesis (*Fasn*, *Acc1*), lipogenesis (*Srebp1c*) and lipolysis (*Lipe, MgII*) pathways was much lower in

the *Rag1*$^{-/-}$ tissues, indicative of increased lipid utilization in the absence of lymphocytes. In the BAT (Figure 3.2F), the expression of *Ucp1*, the key enzyme for thermogenesis, showed no significant differences between the two genotypes. Lastly, the expression of thermogenesis- (*Ucp1, Cidea, Prdm16, Fgf21*), FA oxidation- (*Hadha*) and lipolysis- (*Lipe)* related genes was significantly increased in the *Rag1*$^{-/-}$ vs the WT scWAT (Figure 3.1F). The latter was in line with the increased abundance of beige adipose tissue (AT) and the associated induced lipid oxidation in the *Rag1*$^{-/-}$ scWAT. All the above point to the scWAT as the adipose depot that is significantly altered in the mice with lymphocyte deficiency, we decided to pursue with further characterization.

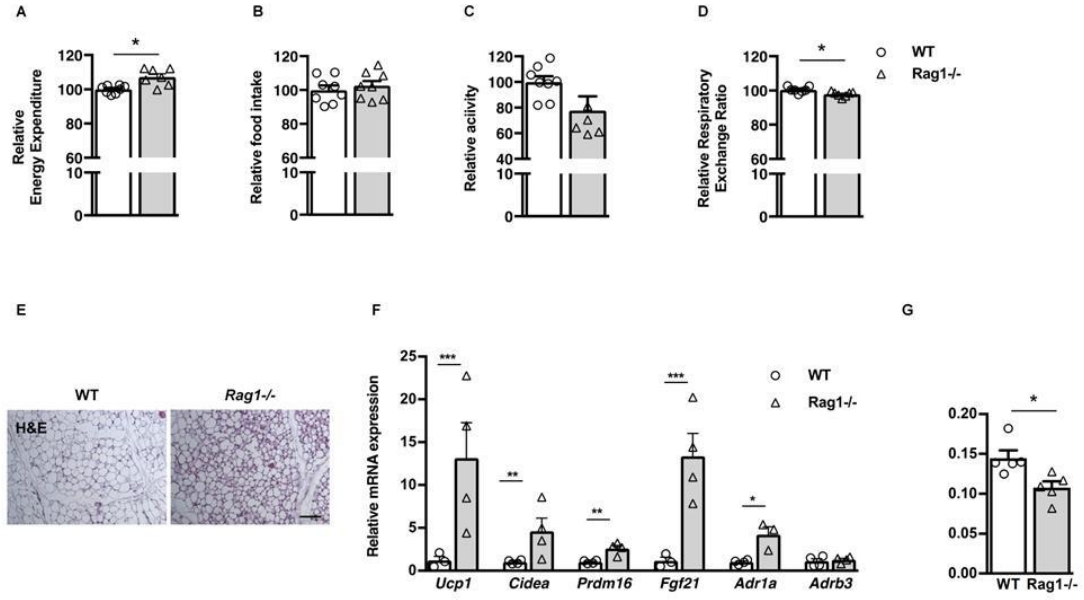

Figure 3.1. Beige tissue formation in the scWAT is increased in lymphocyte-deficient mice.

(**A-D**) Assessment of metabolic behavior using indirect calorimetry, including energy expenditure adjusted to body weight (**A**), food intake (**B**), total activity (**C**) and respiratory exchange ratio (RER) (**D**). n = 7 per group. (**E**) Representative images of hematoxylin and eosin (H&E) of the scWAT depot of age and weight-matched *Rag1*$^{-/-}$ and WT mice. Scale bar:

100µm. (**F**) Gene expression analysis of thermogenic and adrenergic receptors. Data are mean expression normalized to actin ± SEM. (**G**) Absolute weight of scWAT in age and weight-matched WT and *Rag1*$^{-/-}$ mice. The data shown are derived from one representative out of three independent experiments Data shown are derived from one representative out of two independent experiments. Data are presented as mean ± S.E.M. n≥4 per group (**E-G**). **p* < 0.05, ***p* < 0.01, ****p* < 0.001, Student's t-test.

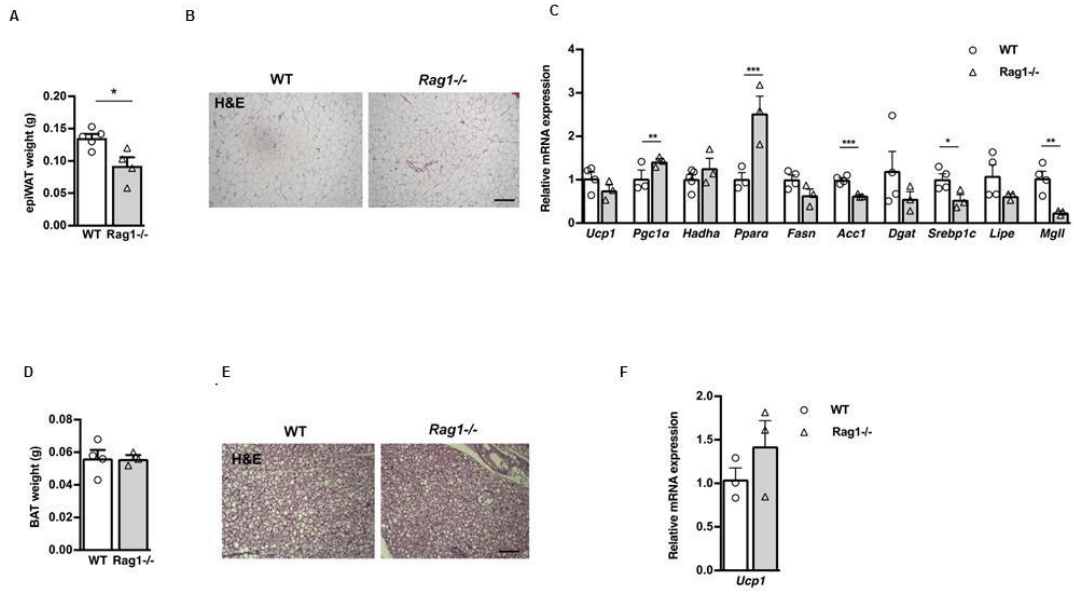

Figure 3.2. Characteristization of epididymal (epi) and subcutaneous (sc) white adipose tissue (WAT) and brown adipose tissue (BAT).

(**A**) Characterization of the absolute epiWAT weight of age and weight-matched WT and *Rag1*$^{-/-}$ mice. n=5 (**B**) Representative images of H&E staining. Scale bar: 100µm. (**C**) Gene expression analysis of *Ucp1* and lipid metabolism related genes in the above groups. Data are presented as mean expression normalized to actin ± S.E.M. n = 4 per group. Student's t-test. (**D**) Characterization of the BAT weight in age and weight-mathced WT and *Rag1*$^{-/-}$ mice. n=5 (**E**) Representative images of H&E staining in the above groups. Scale bar:100 µm. (**F**) Gene expression analysis for *Ucp1* in the above groups. n = 4 per group. Data are mean expression normalized to actin ± S.E.M. Data shown was derived from one out of two

independent experiments. P values, *p < 0.05, **p < 0.01, ***p < 0.001, 2-way Anova with Bonferroni's post test.

3.1.2. The role of splenocytes in beige adipogenesis and the implicated mechanisms

Our initial goal was to assess if reconstitution of *Rag1*$^{-/-}$ mice with whole splenocytes, a cell mixture rich in T and B cells, isolated from the spleen of WT mice, could alter the increased beige AT formation of the *Rag1*$^{-/-}$ mice. For that purpose, 5x10^{6} splenocytes were retro-orbitally injected in *Rag1*$^{-/-}$ mice once per week for a total period of two weeks. Indeed, adoptive transfer of whole splenocytes reversed the phenotype of the *Rag1*$^{-/-}$ mice as shown by the fewer areas with "beige" phenotype within the scWAT. This was confirmed by histological analysis (H&E staining) of the scWAT of WT, *Rag1*$^{-/-}$ and *Rag1*$^{-/-}$ reconstituted with splenocytes (Figure 3.3A), measurement of the relative adipocyte cell size (Figure 3.3C) and immunofluorescence staining with the key enzyme for thermogenesis, Ucp1 (Figure 3.3 A&B). Additionally, the increased expression of thermogenesis- (*Dio2, Prdm16, Cidea*) and FA oxidation- (*Hadha*) related genes in *Rag1*$^{-/-}$ mice (Figure 3.3D) was completely reversed to the WT levels after reconstitution with splenocytes. In order to assess the possible mechanisms employed by lymphocytes to inhibit beige formation, we assessed the activity of recently identified pathways critical for the induction of thermogenesis and the associated beiging of the WAT. An insight on the increased beige formation was provided by the specific input of the adrenergic pathways. According to previous studies, thermogenesis in the adipose tissue is under adrenergic control and is mediated mainly by beta-adrenergic receptors (3, 4) in the scWAT. Staining for tyrosine hydroxylase

(TH) expression provides the evidence for catecholaminergic neuronal activity (11).

As we hypothesized, *Rag1*$^{-/-}$ mice exhibited increased expression of adrenergic receptors in the scWAT (Figure 3.3D) and significantly increased TH staining as compared to the WT mice (Figure 3.3A). To determine the role of adrenergic innervation in the induction of the thermogenic program in scWAT in this model we tested whether the adoptive transfer of whole splenocytes could also affect the increased adrenergic input observed in these, lymphocyte-deficient, mice. Notably, *Rag1*$^{-/-}$ mice reconstituted with splenocytes had lower expression of adrenergic receptors and TH staining compared to the *Rag1*$^{-/-}$ mice (Figure 3.3 A&D). Additionally, administration of prazosin, an alpha-adrenergic blocker, via the drinking water for 5 days in WT and *Rag1*$^{-/-}$ mice, blocked the beige formation in the scWAT of *Rag1*$^{-/-}$ mice as shown by H&E staining (Figure 3.4A) and attenuated the expression of the thermogenesis-related (*Ucp1, Prdm16*) genes (Figure 3.4B). These findings highlight the important role of lymphocytes in the regulation of the adrenergic system-induced beige thermogenesis.

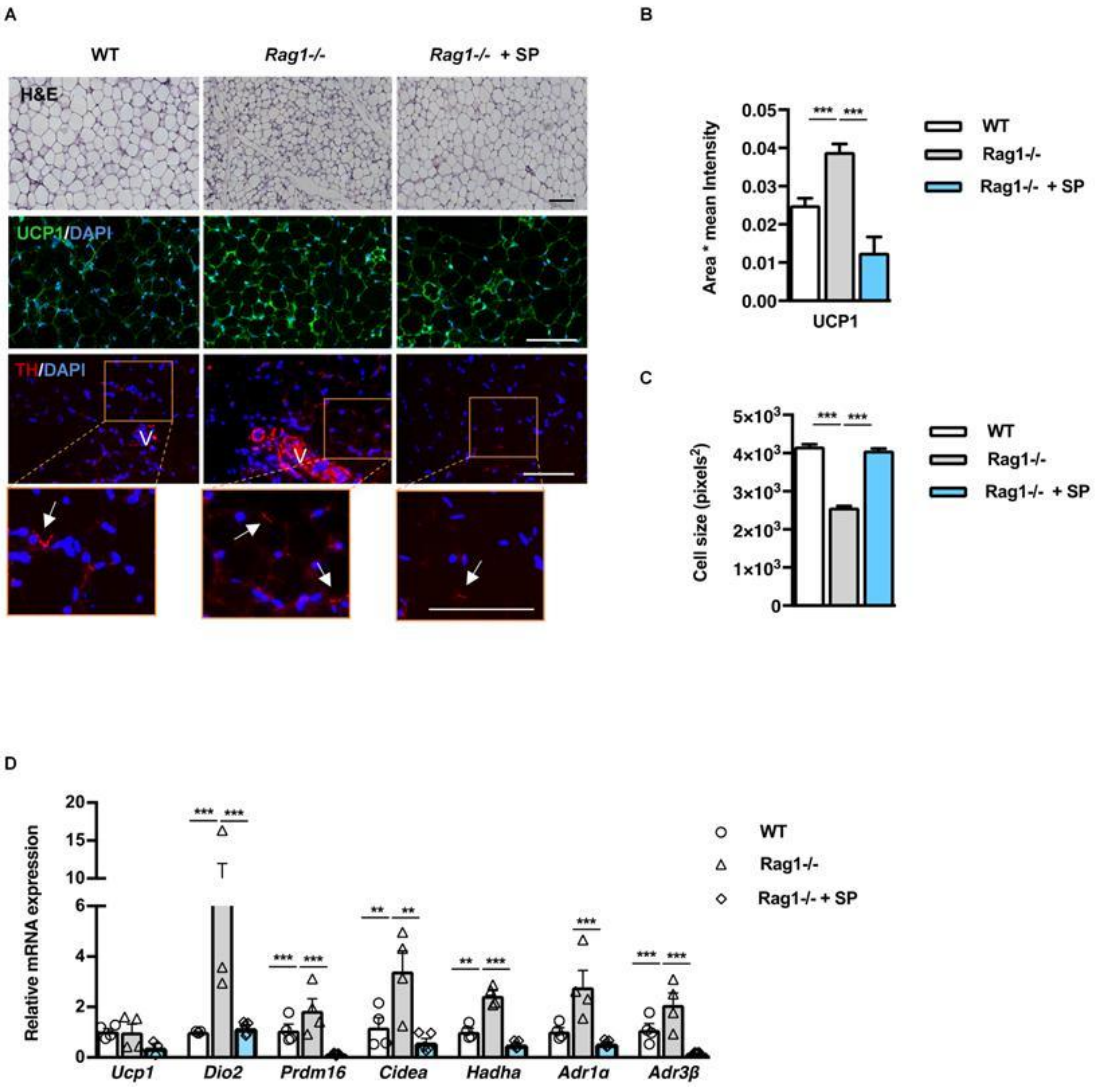

Figure 3.3. Adoptive transfer of whole splenocytes in *Rag1*$^{-/-}$ mice reverses the increased scWAT "beigeing".

(**A**)Representative images of H&E and immunofluorescence (IF) staining for UCP1 or TH from WT, *Rag1*$^{-/-}$ or *Rag1*$^{-/-}$ reconstituted with 5x10^{6} splenocytes, once/week for 2 weeks. Scale bar: 100µm. (**B**) The relative UCP1 mean area and intensity in the above groups. Values are means ± SD intensity of 15 patches for every image. n = 3 per group. (**C**) Relative scWAT adipocyte cell size of WT mice or *Rag1*$^{-/-}$ treated with either PBS or adoptively transferred with splenocytes (5x10^{6}), once/week for 2 weeks. n = 4 per group and (**D**) relative expression of beige, oxidation and adrenergic receptors genes. Data are mean expression normalized to actin ± S.E.M. n = 5 per group. Data shown above are representative from one of two

separate experiments. Data are presented as mean ± S.E.M. $^{**}p < 0.01$, $^{***}p < 0.001$. 1-way Anova with Bonferroni's post test.

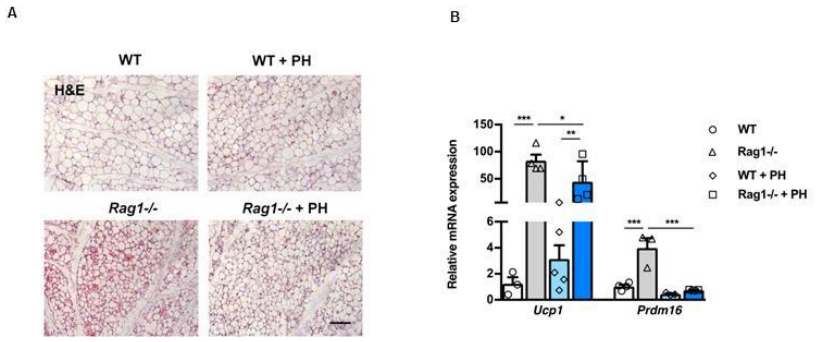

Figure 3.4. Antagonism of alpha-adrenergic signalling blocks the increased brownization of scWAT in *Rag1*$^{-/-}$ mice

(**A**) Representative images of H&E staining in the scWAT of WT, *Rag1*$^{-/-}$ and WT and *Rag1*$^{-/-}$ mice administered PH (8mg/kg) pre-diluted in PBS, via the drinking water. Control groups have received PBS containing drinking water for 5 days. Scale bar: 100μm. (**B**) Gene expression analysis of thermogenic markers in the above groups. Data shown are derived from one experiment. Data are presented as mean expression normalized to actin ± S.E.M. n = 4 per group. $^{*}p < 0.05$, $^{**}p < 0.01$, $^{***}p < 0.001$, 2-way Anova with Bonferroni's post test.

3.1.3. Thermal stress and beige adipogenesis

We next examined the response of *Rag1*$^{-/-}$ mice to physiologic stimuli that alter thermogenesis and the development of beige adipose tissue, such as exposure to thermoneutral conditions (30^{o}C) that ablates *Ucp1* expression (63, 65). For this purpose WT and *Rag1*$^{-/-}$ mice were acclimated at thermoneutral conditions (30^{o}C) for 20 days. As expected, thermoneutrality attenuated the genotype-related differences in beige formation within the scWAT, as shown by H&E staining, and the expression of *Ucp1* (Figure 3.5 A&B), while it had no effect on other thermogenesis-related genes such as *Cidea*, where *Rag1*$^{-/-}$ retained their increased expression (Figure 3.5A).

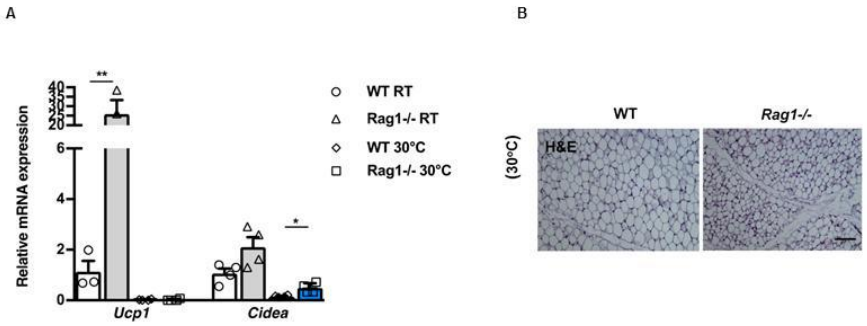

Figure 3.5. Effect of thermoneutrality, simulated by housing at 30°C for 20 days, in scWAT beiging.

(**A**) Representative images of H&E staining in the above groups. Scale bar: 100μm. (**B)** Gene expression analysis of *Ucp1* and *Cidea* in WT and *Rag1*$^{-/-}$ mice to assess the effect of thermoneutrality, simulated by housing at 30°C for 20 days. Data are mean expression normalized to actin ± S.E.M. Data shown are derived from one representative experiment. Data are presented as mean ± S.E.M. n≥4 per group. **p* < 0.05, ***p* < 0.01, Student's t-test.

3.1.4. The role of CD8+ T cells in beige adipogenesis

Next, we sought to identify the specific lymphocyte population(s) within the T and B cell deficiencies in the *Rag1*$^{-/-}$ mice that are most likely to mediate the mechanisms underlying their induced beige adipogenesis. Previous studies have described the contribution of the resident and/or infiltrated lymphocyte populations, including $CD4^+$ and $CD8^+$ T cells, to WAT biology (1, 17). In particular, the $CD8^+$ T cells have been directly associated with impaired lipid metabolism, as suggested by their striking effects in promoting high fat diet-induced liver steatosis (66). It has also been shown that $CD8^+$ T cells preceded the accumulation of macrophages in the scWAT in obese states and adoptive transfer of $CD8^+$ T cells to CD8-deficient mice aggravated adipose inflammation (1). Despite this information linking $CD8^+$ T cells to metabolic responses, the specific role of $CD8^+$ T cells in the maintenance of energy

homeostasis via regulation of beige fat formation has not been studied. We therefore sought to assess the impact of reconstitution of *Rag1*$^{-/-}$ mice with CD8^{+} T cells on the "beigeing" of the scWAT, when mice were housed in RT (22◦C). For this purpose, 5x10^{6} CD8^{+} T cells isolated from WT mouse splenocytes were transferred in the *Rag1*$^{-/-}$ mice by retro-orbital injection. The CD8^{+} T cell transfer resulted in reduced adipocyte size and smaller beige areas, as depicted by H&E staining (Figure 3.6A). Additionally, in the presence of CD8^{+} T cells the relative expression of thermogenesis- (*Ucp1, Cidea, Fgf21*) and fatty oxidation- (*Hadha, Lipe*) implicated genes (Figure 3.6B) was altered to levels similar to those found in the WT scWAT. Similarly, the expression of UCP1, the main protein indicating beige adipogenesis, was dramatically reduced in the *Rag1*$^{-/-}$ scWAT of mice reconstituted with CD8^{+} T cells as compared to the control *Rag1*$^{-/-}$ scWAT (Figure 3.6C). As well shown, a main mechanism that supports the dissipation of energy in adipose tissue depots, including the induction of beige adipogenesis, is the tissue-specific activation of the adrenergic system. In line with this, the catecholaminergic activity of Rag1$^{-/-}$ mice was significantly reduced upon reconstitution with CD8^{+} T cells. Specifically, the expression of both α1 and β3 adrenergic receptors was decreased in the presence of CD8^{+} T cells (Figure 3.6B). This data indicates that the negative effects of CD8^{+} T cells in the formation of beige fat implicate changes in local catecholaminergic activity that seem to be early in the cascade of events driving beige fat formation. To confirm that this effect is specifically mediated by the scWAT CD8^{+} T cells, we performed FACS analysis to check on the fate of the transferred cells. As shown (Figure 3.6D), FACS analysis of the scWAT stromal vascular fraction (SVF), a rich

source for T cells, followed by comparison of tissues from WT, *Rag1*$^{-/-}$ and *Rag1*$^{-/-}$ reconstituted with CD8^{+} T cells, confirmed successful homing of reconstituting cells to physiologically relevant amounts.

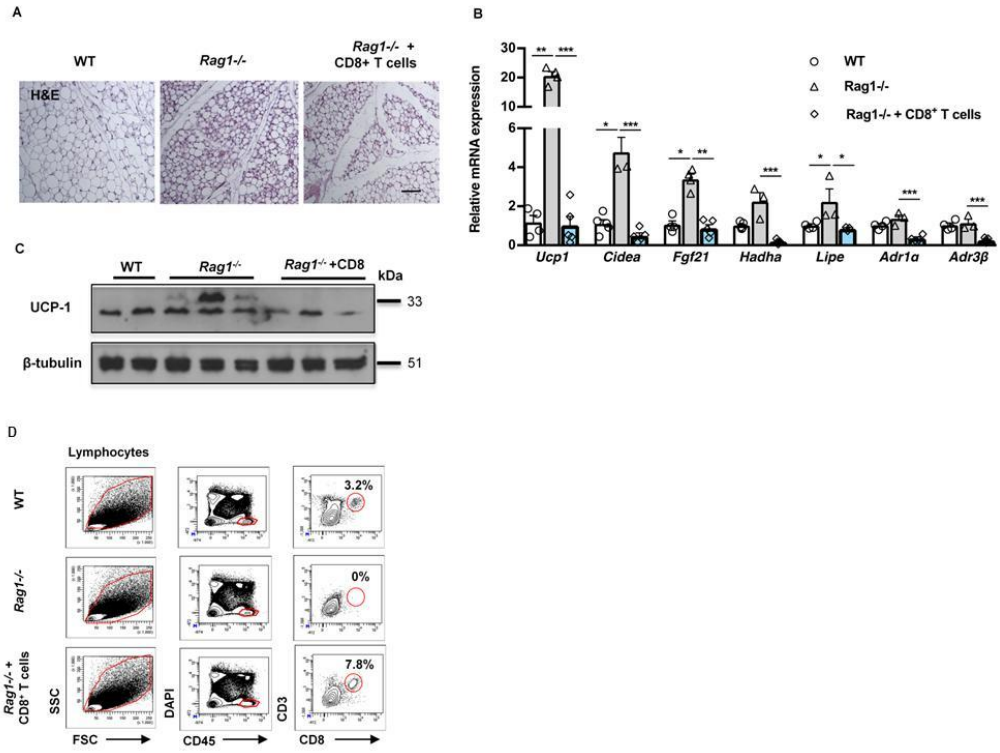

Figure 3.6. Adoptive transfer of CD8^{+} T cells in *Rag1*$^{-/-}$ mice reverses increased scWAT "beigeing" in *Rag1*$^{-/-}$ mice

Data shown in all panels are from the scWAT of WT, *Rag1*$^{-/-}$ or *Rag1*$^{-/-}$ reconstituted with 5x10^{6} CD8^{+} T cells, once/week for 2 weeks (**A**) Representative H&E staining. Scale bar: 100μm. n=3 per group. (**B**) Expression of thermogenic, lipid metabolism and adrenergic receptors genes. Data are mean expression normalized to actin ± S.E.M. n ≥ 5. Data shown are derived from one representative out of three independent experiments. *p < 0.05, **p < 0.01, ***p < 0.001, Student's t-test. (**C**) Protein expression of UCP1 and β-tubulin. (**D**)Representative gating strategy to identify mouse CD8^{+} T cells in WT and *Rag1*$^{-/-}$ mice treated either with PBS or adoptively transferred with CD8^{+} T cells (5x10^{6}), once/week for 2 weeks. Percentages of CD3ε^{+} CD8^{+} cells gated on Viable CD45^{+} DAPI^{-} cells with a low side

scatter profile are depicted. Data shown are representative of two independent experiments. Flow cytometry was performed after pooling n = 5 mice per group.

3.1.5. Interplay between cells of the innate immune system and CD8+ T cells

As has been demonstrated in a number of studies, both the relative abundance and the polarization of macrophages are important determinants for the development of insulin resistance and the associated inflammatory features of obesity. The majority of adipose tissue macrophages in baseline conditions bear characteristics of 'alternatively activated M2-like cells', while as obesity develops, they switch polarization state and 'M1-like' proinflammatory macrophages become the predominant population (19). We detected no major differences in either the percentages or absolute numbers of $CD11b^+$ $F4/80^+$ cells expressed per gram of tissue of the scWAT between WT and *Rag1*$^{-/-}$ mice, with or without reconstitution with $CD8^+$ T cells (Figure 3.7 A&B). Further, we found no evidence for altered macrophage polarization in the reconstituted experimental groups, based on assessment of M1 and M2 markers (Data not shown). These data suggest that phenotype switch or increased polarization of the scWAT macrophages is unlikely the underlying cause of the effects of lymphocyte deficiency/reconstitution on beige adipogenesis.

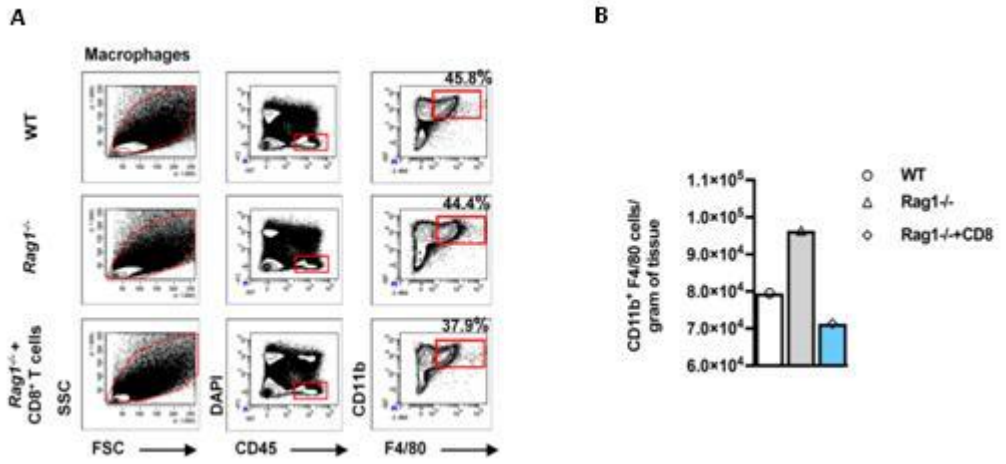

Figure 3.7. Macrophage numbers didn't significantly alter among WT, *Rag1*$^{-/-}$ and *Rag1*$^{-/-}$ reconstituted with CD8^{+} T cells (**A**) Gating strategy to identify murine CD11b^{+}F480^{+} macrophages in WT mice or *Rag1*$^{-/-}$ mice treated with PBS or adoptively transferred with CD8^{+} T cells (5x10^{6}), once/week for 2 weeks. Percentages of CD11b^{+}F480^{+} cells gated on Viable CD45^{+} DAPI^{-} cells with a low side scatter profile are depicted. Data shown are one experiment. Flow cytometry was performed after pooling n=5 mice per group. (**B**) The absolute number of resident macrophages per gram of tissue in the above treatments. Data shown are one experiment. Flow cytometry was performed after pooling n = 5 mice per group.

Recently, the critical, pivotal role of cells of the innate immune system, such as eosinophils and their secreted type 2 cytokines, in the regulation of fat beige adipogenesis has been described (7, 13). Particularly, the eosinophil derived IL-4 was shown to drive the alternative activation of M2 macrophages, which has as a consequence the induction of catecholamines that directly induce beige fat adipogenesis. The same investigators have further expanded their findings lately; by showing that type 2 innate lymphoid cells (ILC2s) drive the IL4 effects on beige adipogenesis by targeting the PDGFRa+ adipocyte precursors (13). As IL-4 has been shown to inhibit the CD8^{+} T cell activation

(67), our current findings not only complement these data but also provide additional mechanisms adding in our current understanding on the development of beige adipose tissue.

To further elucidate the contribution of these mechanism(s) in the increased beige adipogenesis in the *Rag1*$^{-/-}$ mice, we first assessed the abundance of total ILCs in the scWAT. Specifically, ILCs, for FACS sorting analysis, were defined as CD45^{+}, lineage negative (CD3^{-} CD4^{-} CD8^{-} CD19^{-} B220^{-} CD11b^{-} CD11c^{-} FceRI^{-} Gr-1^{-}Terr119^{-}), CD90.2^{+} Sca-1^{+} cells. We found that the percentage of CD90^{+}Sca-1^{+} cells gated in CD45^{+} cells in *Rag1*$^{-/-}$ scWAT was significantly higher (1.244% ± 0.117%) from that it has been described the WT scWAT (0.491% ± 0.061%) (Figure 3.8 A&B). Accordingly, the absolute number of ILCs (CD90.2^{+}Sca-1^{+}) per gram of tissue in the *Rag1*$^{-/-}$ scWAT was also significantly increased compared to WT mice (Figure 3.8C). Interestingly, reconstitution with CD8^{+} T cells brought the levels of ILC2s close to those identified in the WT scWAT and reduced the abundance of beige adipose tissue in the *Rag1*$^{-/-}$ mice. (Figure 3.8C). A similar pattern was obtained for eosinophils, defined as CD45^{+}CD11b^{+}SiglecF^{+} cells. Specifically, the percentage of eosinophils gated in CD45^{+} cells (Figure 3.8 D&E) was higher in *Rag1*$^{-/-}$ scWAT (WT: 9.667% ± 0.953%; *Rag1*$^{-/-}$: 13.900% ± 0.521%), although the absolute numbers of eosinophils did not reach significant difference between the two genotypes (Figure 3.8F). Furthermore, measurement of the intra-scWAT levels of cytokines secreted by ILC2s showed that the levels of IL-4, IL-5 and IL-13 were increased in the *Rag1*$^{-/-}$ mice versus the WT scWAT, while CD8^{+} T cell reconstitution led to profound reduction in the levels of the above cytokines (Figure 3.8G). These results

demonstrate that the interactions between innate immune cells and CD8^{+} T cells maintain the in balance beige adipogenesis and the associated energy dissipation.

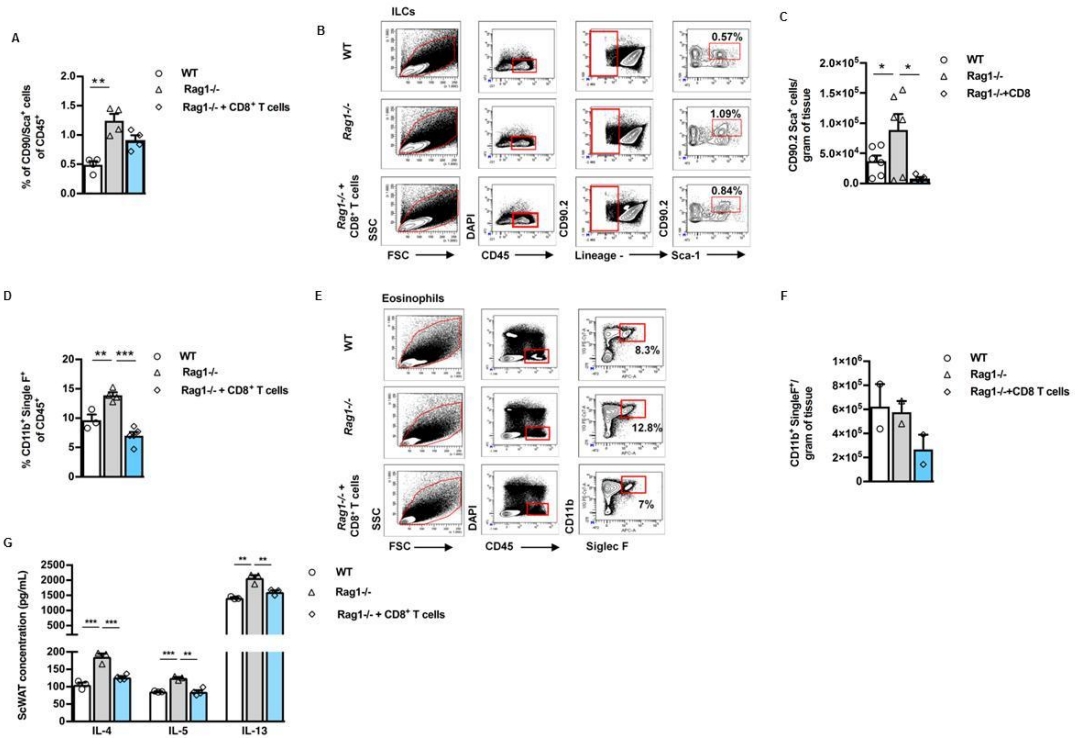

Figure 3.8. Adoptive transfer of CD8^{+} T cells in *Rag1*$^{-/-}$ mice alters the intra-scWAT number of innate cells.

(A) ILCs (CD90.2^{+} Sca-1^{+} Lin^{-}) % gated on CD45^{+} cells. n ≥ 4 per group. (B) Representative gating strategy for the identification of ILCs (CD90.2^{+} Sca-1^{+} Lin^{-}). CD90.2^{+} Sca-1^{+} Lin^{-} % gated on the viable CD45^{+}DAPI^{-} cells are depicted. Data shown are representative of two independent experiments. Flow cytometry was performed after pooling n ≥ 5 mice per group. (C) The absolute numbers of total lineage (Lin)-negative CD90.2^{+} Sca-1^{+} ILCs per gram of tissue in the scWAT of WT, *Rag1*$^{-/-}$ and *Rag1*$^{-/-}$ mice reconstituted with CD8^{+}T cells. n=5 mice per group. Data shown are representative of two independent experiments and were analyzed by Student's t-test. Values are means ± S.E.M. *p < 0.05. (D) Eosinophils (CD11b^{+} Siglec F^{+}) % gated on the viable CD45^{+}DAPI^{-} cells. n ≥ 4 per group. (E) Representative gating strategy for identification of eosinophils (CD11b^{+} Siglec F^{+}). CD11b^{+}Siglec F^{+} cells % gated

on the viable $CD45^+DAPI^-$ cells are depicted. Data shown are representative of two independent experiments. Flow cytometry was performed after pooling n ≥ 5 mice per group. (F)The absolute number of $CD11b^+$ Siglec F^+ gated on the viable $CD45^+DAPI^-$ cells per gram of tissue in the scWAT of WT, *Rag1*$^{-/-}$ and *Rag1*$^{-/-}$ mice reconstituted with $CD8^+$ T cells. n = 5 per group. Data shown are derived from one experiment. Flow cytometry was performed after pooling n ≥ 5 mice per group. (G) Intra scWAT levels of IL-4, IL-5 and IL-13. n ≥ 4 per group. Data are presented as mean ± S.E.M. **p* < 0.05, ***p* < 0.01, ****p* < 0.001, 1-way Anova with Bonferroni's post test.

3.1.6. Cold stress and beige adipogenesis

Next, we assessed if the already increased beige adipose depot of the *Rag1*$^{-/-}$ mice in baseline conditions, interferes with their capability to respond to stimuli that drive beigeing in the scWAT, such as exposure to cold. For this reason, WT and *Rag1*$^{-/-}$ mice were acclimated at 18^{o}C for two days before getting exposed to 4^{o}C for another two days (12). Interestingly, measurement of core body temperature at regular intervals throughout the two days period they were exposed to cold, showed that *Rag1*$^{-/-}$ mice were more capable than WT mice in maintaining their body temperature (Figure 3.9A), indicative of the inherent capacity of the *Rag1*$^{-/-}$ mice to expand their beige adipose compartment well above that of the WT mice.

As we have described above, $CD8^+$ T cells deficiency was proven by our experiments to play a major role in the regulation of energy by the scWAT. We assessed their role in the increased thermogenesis of the *Rag1*$^{-/-}$ mice upon exposure to cold by adoptive transfer of $5x10^6$ $CD8^+$ T cells, isolated from the spleen of WT mice. Transfer once per week for a total period of two weeks

significantly inhibited beige formation in the scWAT of *Rag1*$^{-/-}$ mice exposed to cold (4^{o}C), as shown by H&E staining (Figure 3.9B). Evaluation of the relative expression of thermogenesis- (*Ucp1, Cidea, Dio2*) and lipid catabolism- (*Hadha, Lipe*) genes following exposure to cold, showed that reconstitution with CD8^{+} T cells could reverse the increased beige induction of *Rag1*$^{-/-}$ mice to the WT levels (Figure 3.9C). However, the differences in the expression of other scWAT genes between WT and *Rag1*$^{-/-}$ mice were not as prominent as those detected in RT conditions (Figure 3.9C). Most importantly, the expression of UCP1 protein (Figure 3.9 B&D) remained significantly higher in the *Rag1*$^{-/-}$ scWAT, highlighting the contribution of the lymphocyte deficiency to beige adipogenesis even in states associated with excess beige fat development. To further elucidate the possible mechanisms utilized by the CD8^{+} T cells in the above, we first studied the activation of the adrenergic pathway as catecholamines hold a central position in the cold-induced thermogenesis process (65). As shown, Tyrosine Hydroxylase (TH), the rate limiting step in the biosynthesis of norepinephrine (68, 69) and a reliable marker for catecholaminergic neurons (11), was higher in the *Rag1*$^{-/-}$ scWAT upon exposure to cold (Figure 3.9B). Further, correction of the CD8^{+} T cells deficiency, decreased the expression of *Adr1α* and *Adr3β* (Figure 3.9C), followed by a profound decrease of tyrosine hydroxylase (TH) and Ucp1 protein expression (Figure 3.9B) in the scWAT of *Rag1*$^{-/-}$ mice exposed to cold. These findings indicate a possible, indirect, mechanism employed by CD8^{+} T cells for the blockade of thermogenesis. All the above taken together indicate that CD8^{+} T cells have a negative impact on the induction of thermogenesis in the scWAT.

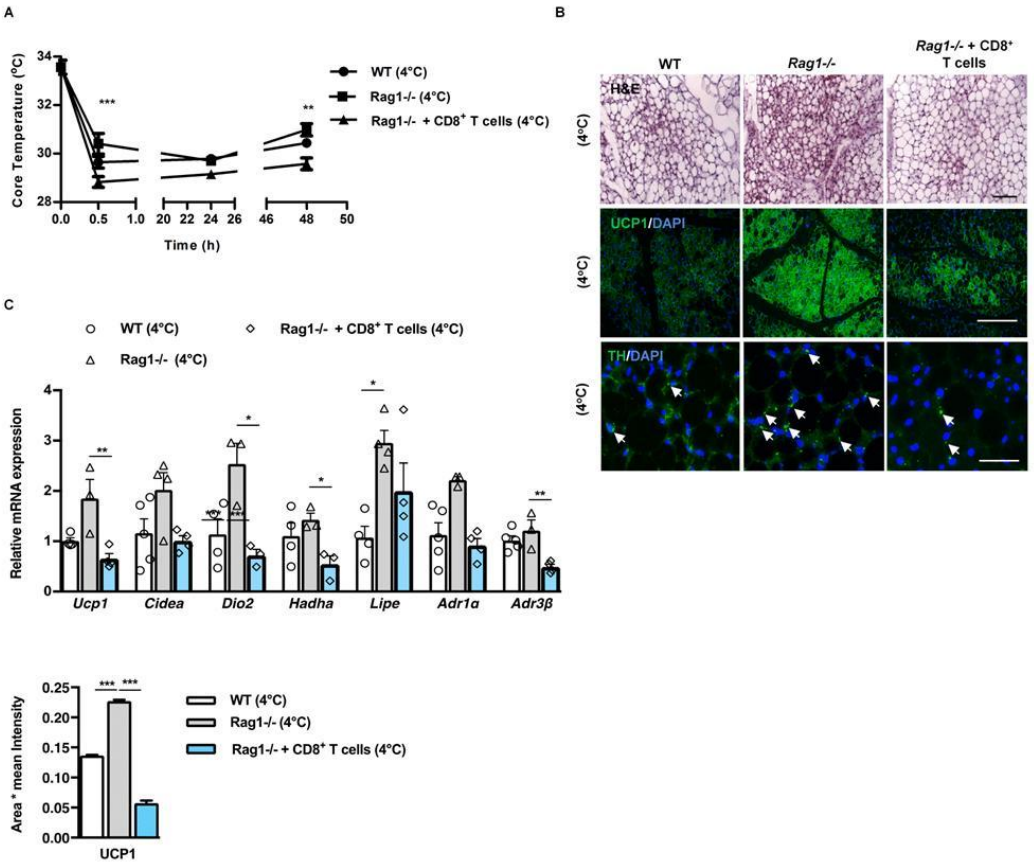

Figure 3.9. Adoptive transfer of CD8^{+} T cells inhibits increased scWAT beigeing in *Rag1*$^{-/-}$ mice exposed to cold environment.

Data shown in all panels are from the scWAT of WT, *Rag1*$^{-/-}$ or *Rag1*$^{-/-}$ reconstituted with 5x10^{6} CD8^{+} T cells, once/week for 2 weeks (A) Core temperature measurements. n ≥ 4 per group. (B) Representative images of H&E and IF staining of UCP1 and TH. Scale bar: 100μm. n ≥ 3 per group. (C) Relative expression of thermogenic, lipid metabolism and adrenergic receptors genes in the scWAT of age-matched mice, housed at 4^{o}C for 2 days at the end of the second week. Data are mean expression normalized to actin ± SEM. n ≥ 5 per group. Data shown are derived from one representative out of two independent experiments. (D) Quantitation of mean intensity of UCP1 protein expression following cold exposure in the scWAT of WT, *Rag1*$^{-/-}$ and *Rag1*$^{-/-}$ mice reconstituted with CD8^{+} T cells (5x10^{6}), once/week for 2 weeks. n = 3 per group. Data are means ± SD intensity of 15 patches for every image. ***p < 0.001. Data shown are derived from one out of two separate experiments.

Next, we assessed the effect of cold exposure in the abundance of eosinophils and ILCs residing in the scWAT. Consistent with the above results, reconstitution of *Rag1*$^{-/-}$ mice with CD8^{+} T cells led to significant reduction in the percentage of both eosinophils, out of CD45^{+} cells, (11.150% ± 0.902%) and of ILCs (1.265% ± 0.065%), gated on CD45^{+} cells, compared to those of the non-treated *Rag1*$^{-/-}$ mice (eosinophils: 17.150% ± 2.293%; ILCs:1.759% ± 0.189%) (Figure 3.10 A-D). No significant differences were identified in the absolute numbers of these cells (data not shown). As expected, the eosinophils and ILCs were significantly higher in the cold-exposed *Rag1*$^{-/-}$ as compared to WT mice (eosinophils: 6.800% ± 2.491%; ILCs: 0.943% ± 0.044%) (Figure 2.10 A-D), indicating a role for these cells in the cold-induced beigeing of *Rag1*$^{-/-}$ mice. The absolute numbers of eosinophils (WT: 34.082.84; *Rag1*$^{-/-}$: 35.087.72) and ILCs (WT: 3.393.272.00; *Rag1*$^{-/-}$: 3.810.893.00) per gram of tissue were relatively higher in *Rag1*$^{-/-}$ mice compared to WT mice.

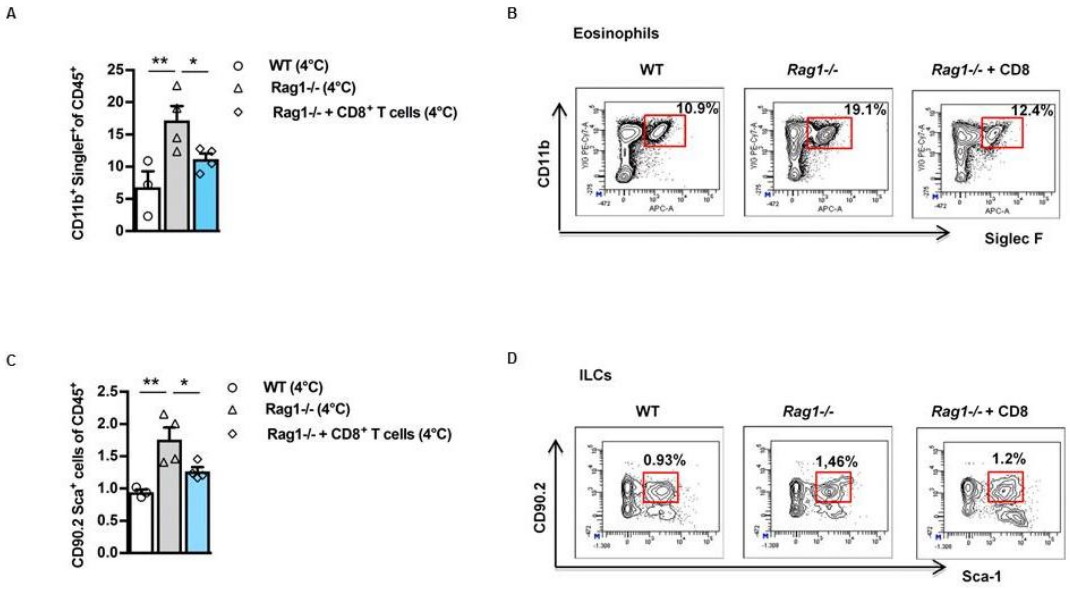

Figure 3.10: Adoptive transfer of $CD8^+$ T cells in *Rag1*$^{-/-}$ mice exposed to cold environment alters the intra-scWAT number of innate cells.

(A) Representative percentages of eosinophils ($CD11b^+$ Siglec F^+), placed at 4^oC for 2 days. Data shown are representative of two independent experiments. Flow cytometry was performed after pooling n ≥ 4 mice per group. (B) Results are expressed as percentages of $CD11b^+$Siglec F^+ eosinophils, gated on the viable $CD45^+DAPI^-$ cells. n ≥ 4 per group. (C) Representative percentages of ILCs positive for $CD90.2^+$ $Sca\text{-}1^+$ Lin^-, in WT mice or *Rag1*$^{-/-}$ treated either with PBS or adoptively transferred with $CD8^+$ T cells ($5x10^6$), once/week for 2 weeks, and placed at 4^oC for 2 days, are depicted on the flow cytometry plots. Data shown are representative of two independent experiments. Flow cytometry was performed after pooling n ≥ 4 mice per group. (D) Results are expressed as percentages of $CD90.2^+$ $Sca\text{-}1^+$ Lin^- gated on the viable $CD45^+DAPI^-$ cells. n ≥ 4 per group. Data are presented as mean ± S.E.M. **p* < 0.05, ***p* < 0.01, ****p* < 0.001, 1-way Anova with Bonferroni's post test.

3.1.7. CD8+ T cells, the main lymphocytes regulating beige adipogenesis

To strengthen our hypothesis that the absence of $CD8^+$ T cells in *Rag1*$^{-/-}$ mice accounted for the increased beigeing in their scWAT, we compared the phenotype of the scWAT between $CD8^+$ T cell-deficient (*CD8*$^{-/-}$) and WT mice. Initially, we performed indirect calorimetry in age and weight-matched *CD8*$^{-/-}$ and WT mice, using CLAMS and we found increased expenditure of energy in the former (Figure 3.11A). This could be explained by the increase in total activity of the *CD8*$^{-/-}$ mice (Figure 3.11B), while their food consumption was similar to that of the WT mice (Figure 3.11C). Additionally, RER was found to be lower in the *CD8*$^{-/-}$ mice suggesting that in the absence of $CD8^+$ T cells mice shift to preferential utilisation of fatty acids, rather than carbohydrates, as their energy resource (Figure 3.11D). In line with the above described

metabolic profile, we found that *CD8*$^{-/-}$ mice exhibited significant expansion of the beige fat areas within the scWAT, higher percentage of eosinophils content (Figure 3.11G) and increased expression of beige-driving genes such as *Ucp1*, *Cidea* and *Dio2* (Figure 3.11 E&F), when compared to the WT mice. Further, exposure to cold environment led in the anticipated activation of beige adipogenesis (Figure 3.11 H&I) and the associated increase in eosinophils in scWAT (Figure 3.11J). The absolute number of eosinophils per gram of tissue was 1.285.714 in the *CD8*$^{-/-}$ mice, versus 842.105 in the WT mice in accordance with all the above. Finally, to further confirm the contribution of $CD8^+$ T cells in beige adipogenesis we conducted complementary studies in age and weight-matched WT mice, treated either with anti-CD8 Ab or control IgG. Interestingly, in the treated WT mice, that the $CD8^+$ T cells were depleted, the expression of beige adipogenesis-driving genes, such as *Ucp1*, *Cidea* and *Dio2,* was significantly increased (Figure 3.12A). These findings provide the evidence on the impact of $CD8^+$ T cell depletion in the development of beige fat within the scWAT, a critical process in the dissipation of energy by the WAT (Figure 3.12A).

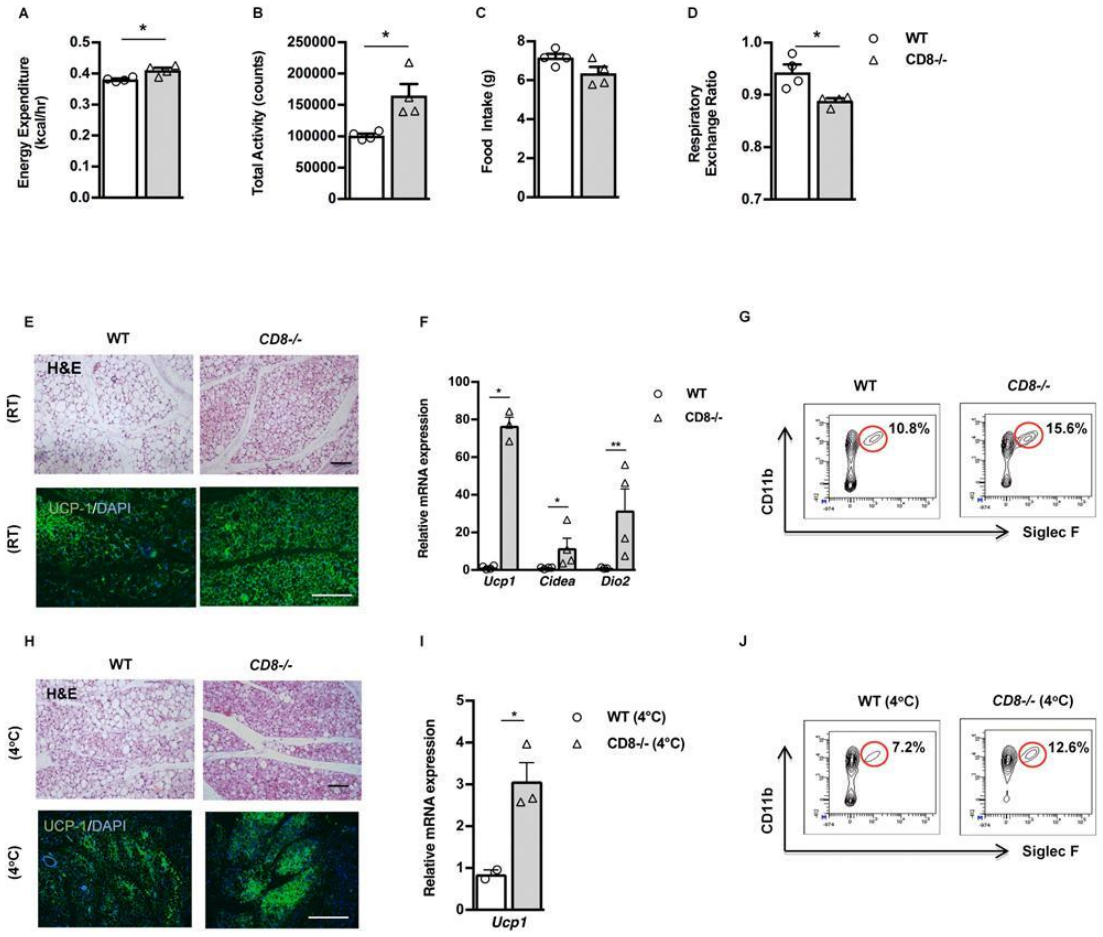

Figure 3.11. *CD8*$^{-/-}$ mice display increased beigeing of scWAT and thermogenic capacity.

(A-D) Assessment of metabolic behavior using indirect calorimetry, including energy expenditure adjusted to body weight (A), total activity (B), food intake (C) and respiratory exchange ratio (RER) (D). n = 4 per group. Data shown are derived from one experiment (E) Representative images of H&E staining in scWAT of WT and *CD8*$^{-/-}$ mice. Scale bar: 100µm. n=3 per group. (F) Relative expression of beige genes such as *Ucp1, Cidea and Dio2* in scWAT of *CD8*$^{-/-}$ versus WT mice. Data are mean expression normalized to actin ± S.E.M. n ≥ 4 per group. Data shown are derived from one representative out of two independent experiments (G) Single cell suspensions prepared from scWAT, harvested from either WT or *CD8*$^{-/-}$, mice, were gated on the viable CD45^{+}DAPI^{-} cells and then depicted as percentages of Siglec F^{+} and CD11b^{+} cells to identify eosinophils. Flow cytometry was performed after pooling n ≥ 5 mice per group. (H) Representative image from H&E staining of scWAT from

WT and *CD8*$^{-/-}$ mice exposed to cold. Scale bar: 100μm. n=3 per group. (I) Relative expression of *Ucp1* gene in scWAT from *CD8*$^{-/-}$ mice and WT mice. Data are mean expression normalized to actin ± S.E.M. n ≥ 4 per group. Data are presented as mean ± S.E.M. *p < 0.05, Student's t-test. Data shown are derived from one experiment. (J) Single cell suspensions from scWAT of WT and *CD8*$^{-/-}$ mice subjected to exposure at 4°C for 2 days, were gated on the viable CD45^{+}DAPI^{-} cells and then analyzed for Siglec F and CD11b expression to measure eosinophils. Flow cytometry was performed after pooling n ≥ 5 mice per group.

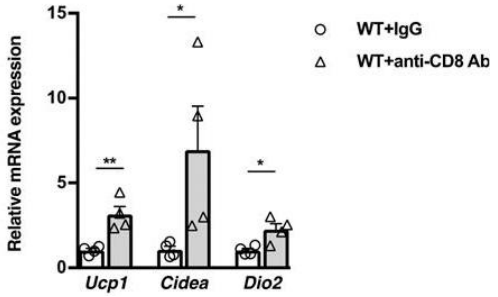

Figure 3.12. Impact of CD8^{+} T cell depletion in the development of beige adipogenesis

(A) Relative expression of beige genes (*Ucp1, Cidea, Dio2*) of age and weight-matched WT either received anti-CD8 antibody or IgG. n=4. Data are mean expression normalized to actin ± S.E.M. *p < 0.05, **p < 0.01. t-test.

3.1.8. IFNγ negatively regulates beige adipogenesis

To further elucidate the specific factor(s) underlying the effects of CD8^{+} T cells in beige adipogenesis, we next measured the scWAT content in IFNγ, a cytokine secreted in large amounts by activated CD8^{+} T cells. Further, IFNγ has been implicated in the regulation of the function of resident innate immune cells within the scWAT, including ILC2s (66). Interestingly, more recently found that adipose ILC1 IFN-γ contributes to M1 macrophage polarization and thus promote obesity associated insulin resistance (67). To

confirm the role of CD8-derived IFNγ in this process, we reconstituted *Rag1*$^{-/-}$ mice with CD8^{+} T cells isolated from the spleen of healthy WT or *IFNγ* –deficient (*Ifnγ*$^{-/-}$) mice and compared the result in beige adipogenesis within the scWAT. In contrast to the reduction in UCP1 expression in the scWAT following reconstitution with WT CD8^{+} T cells, reconstitution with *IFNγ*–deficient CD8^{+} T cells had no effect on the UCP1 expression in the scWAT (Figure 3.13 A&B). Additionally, reconstitution of *Rag1*$^{-/-}$ mice with CD8^{+} T cells derived from *Ifnγ*$^{-/-}$ mice resulted in a small increase of ILCs in the scWAT of *Rag1*$^{-/-}$ mice, in contrast to the decrease following reconstitution with WT CD8^{+} T cells (Figure 3.13C).

Next, we sought to understand the importance of IFNγ itself in beige adipogenesis, by comparing beiging of the scWAT in *Ifnγ*$^{-/-}$ and WT mice. In accordance with our previous findings, IFNγ deficiency was associated with significant expansion of the beige areas in the scWAT, as depicted by H&E staining and a profound reduction in the adipocyte cell size (Figure 3.14A). Importantly, the *Ifnγ*$^{-/-}$ scWAT displayed increased numbers of eosinophils (Figure 3.14B) and of ILCs (Figure 3.14C), as compared to the WT scWAT. These results are consistent with the mechanisms employed by CD8^{+} T cells to inhibit beige formation. Furthermore, a significant increase was noted in the absolute numbers of eosinophils (WT: 810.000; *Ifnγ*$^{-/-}$: 1.100.000) and of ILCs per gram of tissue in *Ifnγ*$^{-/-}$ compared to WT scWAT (Figure 3.14D).

Collectively, our results demonstrate that the inhibitory effects of CD8^{+} T cells on the formation of beige fat are exerted at several levels, including regulation of the catecholaminergic input to the scWAT and compromised abundance of cells of innate immunity (eosinophils, ILCs). The latter accounts for the

decreased levels of cytokines secreted by the resident immune cells, such as IL-4, IL-5 and IL-13 (Figure 3.15), shown to promote “beigeing” of scWAT as discussed above.

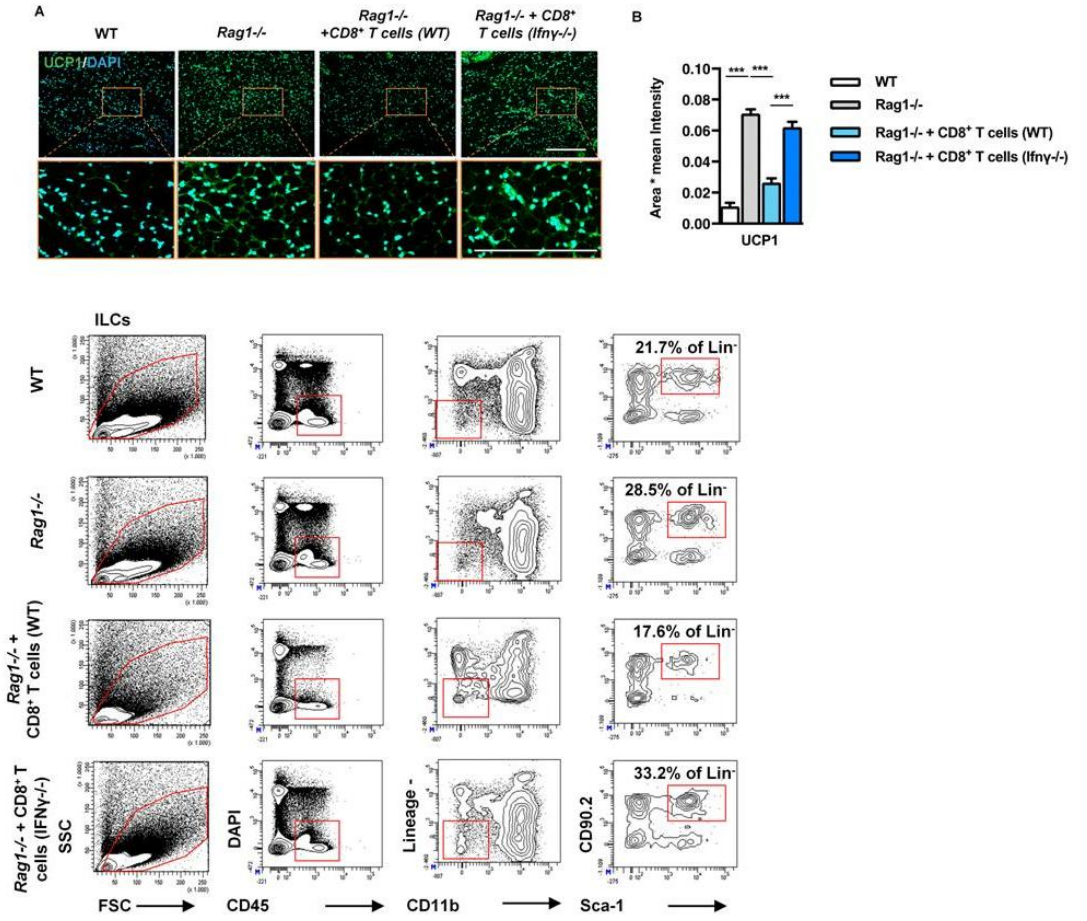

Figure 3.13. IFNγ deficiency is associated with increase in total ILCs in the scWAT.

(A)Representative images of UCP1 IF staining in the scWAT of WT or *Rag1*$^{-/-}$ mice treated either with PBS or adoptively transferred with 5x10^{6}, WT-derived or *Ifnγ*$^{-/-}$-derived CD8^{+} T cells, once/week for 2 weeks. Scale bar: 100μm. (B) The relative UCP1 mean intensity in the above groups. Data were analysed by Two-Way ANOVA. Values are means ± SD intensity of 15 patches for every image. n = 3 per group. ***p < 0.001. (C) Gating strategy for the identification of lineage (Lin)-negative CD90.2^{+} Sca-1^{+} ILCs of WT or *Ifnγ*$^{-/-}$ scWAT, pre-gated on live CD45^{+} DAPI^{-} cells. Percentage of cells stained positive for CD90.2^{+} Sca-1^{+} is depicted on the flow cytometry plots. Data shown are from one single experiment. Flow cytometry was performed after pooling n ≥ 4 mice per group.

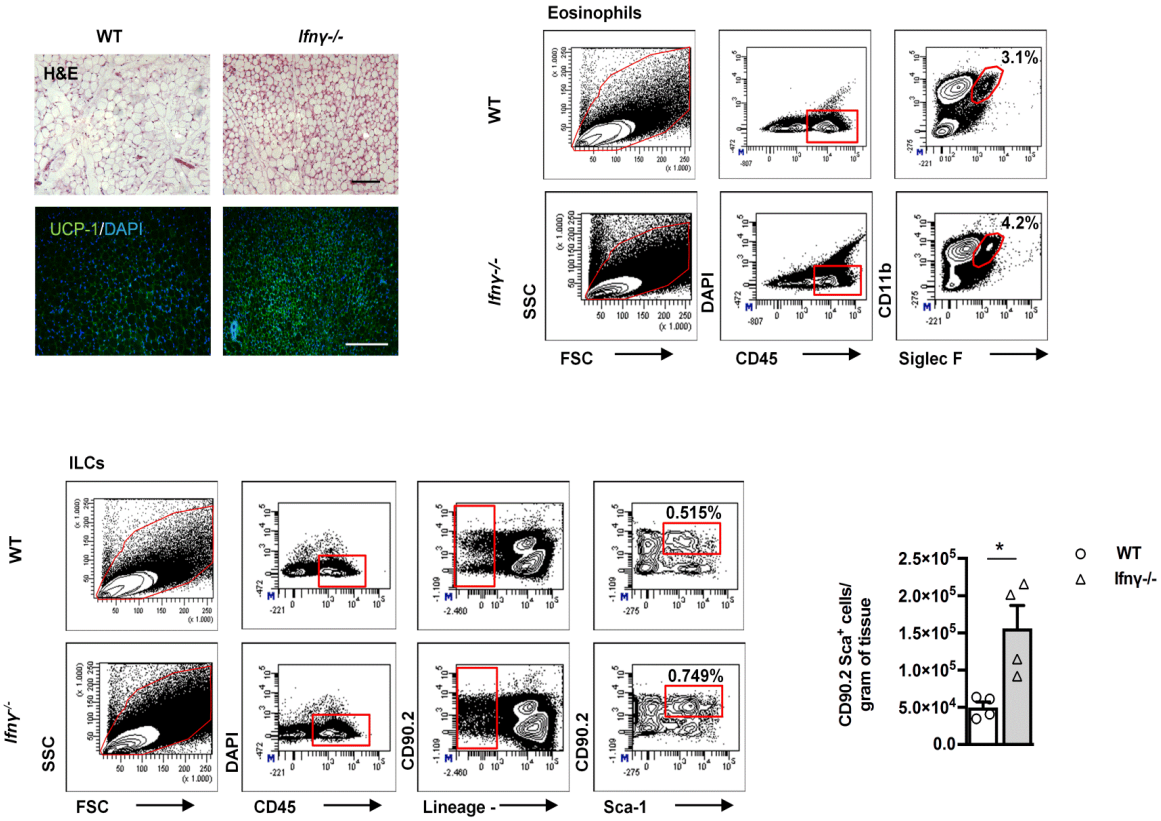

Figure 3.14. Increased "beigeing" and eosinophils in the scWAT of *Ifnγ*$^{-/-}$ mice.

(A) Representative images of H&E and UCP1 IF staining of scWAT from WT and *Ifnγ*$^{-/-}$ mice. Scale bar: 100μm. n=3 per group. Data shown are derived from one experiment. (B) Gating strategy for the identification of eosinophils gated on viable CD45^{+} DAPI^{-} cells and further identified into CD11b^{+} Siglec F^{+} cells. Data shown are depicted as percentages. Flow cytometry was performed after pooling n ≥ 4 mice per group. (C) Gating strategy for the identification of total ILCs in WT mice or *Rag1*$^{-/-}$ treated with either PBS or adoptively transferred with 5x10^{6} either WT CD8^{+} T cells or CD8^{+} T cells derived from *Ifnγ*$^{-/-}$ mice, once/week for 2 weeks. Percentages of cells positive for CD90.2^{+} Sca-1^{+} Lin^{-} gated on the viable CD45^{+}DAPI^{-} cells are depicted on the flow cytometry plots. Flow cytometry was performed after pooling n ≥ 4 mice per group. (D) Absolute numbers of total ILCs (CD90.2^{+}

Sca-1^{+} Lin^{-}) per gram of tissue in scWAT of WT and *Ifnγ*$^{-/-}$ mice. n=5 per group. Data are presented as mean ± S.E.M. **p* < 0.05, Student's t-test.

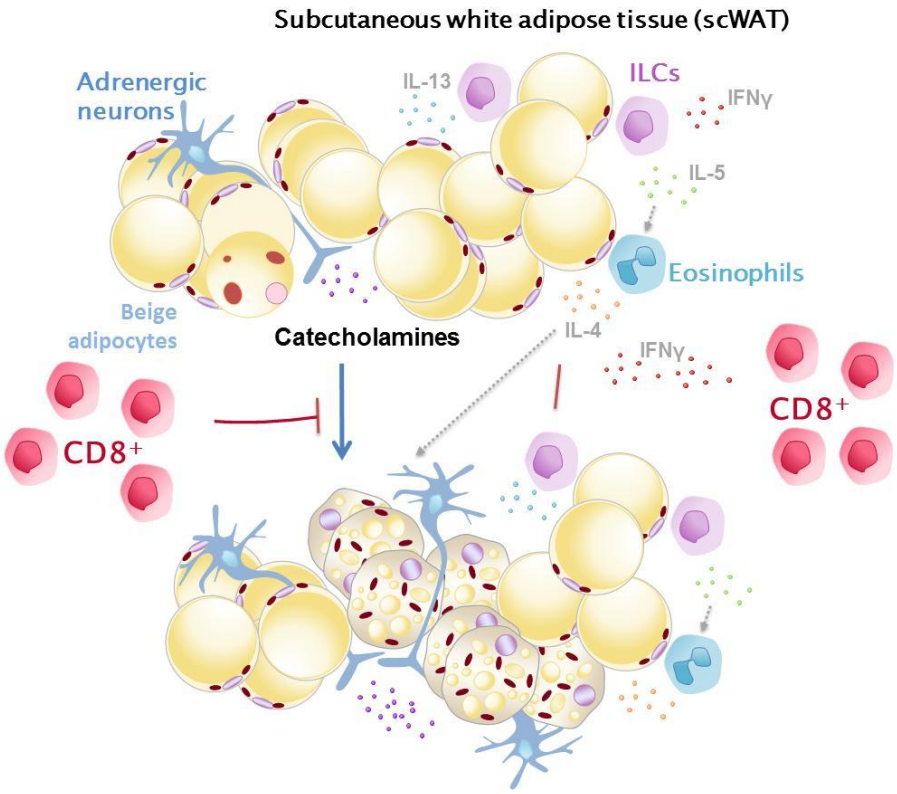

Figure 3.15. Schematic representation of the effects of the CD8^{+} T cells in the beigeing of the scWAT.

CD8^{+} T cells inhibit beige adipose tissue development in the scWAT by modulating the catecholaminergic input to scWAT and reducing the abundance of implicated innate immune cells and the associated cytokines such as IL4, IL5 and IL13 shown to induce beige fat formation (25). scWAT CD8^{+} T cells derived IFNγ is a major mediator of these effects of the CD8^{+} T cells.

3.2. Liver and its immunometabolic properties

Based on the findings described above about the significant impact of lymphocyte deficiency on lipid oxidation resulting in increased scWAT beiging, we next sought to understand if similar effects were also exerted on the lipid oxidation taking place on the liver. First, we characterized the expression (Figure 3.16) of critical genes for fatty acid (FA) oxidation- and carbohydrate metabolism in age- and weight-matched WT and *Rag1*$^{-/-}$ mice. Our findings revealed increased expression of genes involved in FA oxidation (*Cpt1c, Aco, Hadha*) and glucose metabolism (*Pepck, G6Pase, HK*) in *Rag1*$^{-/-}$ vs the WT liver tissues extracted from mice housed under baseline conditions. These findings clearly demonstrate that *Rag1*$^{-/-}$ mice utilize FA and glucose more efficiently than WT mice for energy production (Figure 3.16). This data are in line with the effect of lymphocyte deficiency in energy utilization in the WAT indicating common mechanisms driving the increase in metabolic activity in the primary organs involved in lipid metabolism. The metabolic effects of lymphocyte deficiency on liver were rescued by reconstitution of *Rag1*$^{-/-}$ mice with CD8^{+} T cells isolated from the spleen of WT mice (Figure 3.16), as described for the scWAT above.

To better understand the physiological relevance of this effect we used an experimental manipulation that unmasks the capability of this system to operate in extreme conditions such as hypocaloric diet-induced liver steatosis. For this purpose we subjected age- and weight- matched WT and *Rag1*$^{-/-}$ mice to starvation, a model resembling the wasting of human patients associated with a number of severe diseases. Oil-Red-O (ORO)-staining of hepatic tissue sections from WT and *Rag1*$^{-/-}$ mice that had undergone

starvation for 24hrs, revealed significantly lower lipid accumulation (i.e. fewer red droplets as shown in Figure 3.17A&B) in the *Rag1*$^{-/-}$ livers. In contrast profound steatosis detected in the livers of the starved WT mice, confirming the success of the model to increase lipid storage in this tissue. Gene expression analysis confirmed the increased activation of genes involved in lipid oxidation (*Pgc-1α, Aco, Cpt1α)* and glucose metabolism (*Pepck, G6Pase, HK*) in the *Rag1*$^{-/-}$ as compared to the WT tissues (Figure 3.17C & D). To further assess the contribution of the missing lymphocytes in the decreased hepatic lipid storage of the *Rag1*$^{-/-}$, we next performed adoptive transfer of whole splenocytes isolated from healthy WT mice as described on the WAT studies above. Again, transfer of splenocytes reversed the liver phenotype of *Rag1*$^{-/-}$ mice, as shown by the increase in lipid storage and attenuation of FA oxidation to levels similar to those found in the WT tissues (Figure 3.17A-C). However, the presence of splenocytes had no effect at glucose metabolism of these mice (Figure 3.17D). To confirm that lack of the same T cell subpopulation, i.e. the CD8^{+} T cells, is the key driver of the increased lipid oxidation as demonstrated for the scWAT above, adoptive transfer of CD8^{+} T cells was done in the *Rag1*$^{-/-}$ mice. Indeed, CD8^{+} T cells accelerated the lipid storage in the liver of the reconstituted *Rag1*$^{-/-}$ mice resulting in the development of hepatic steatosis. Downregulation of hepatic *Hadha*, *Pepck and G6Pase* gene expression in *Rag1*$^{-/-}$ mice following starvation for 24hours (Figure 3.18) complemented the phenotypic data.

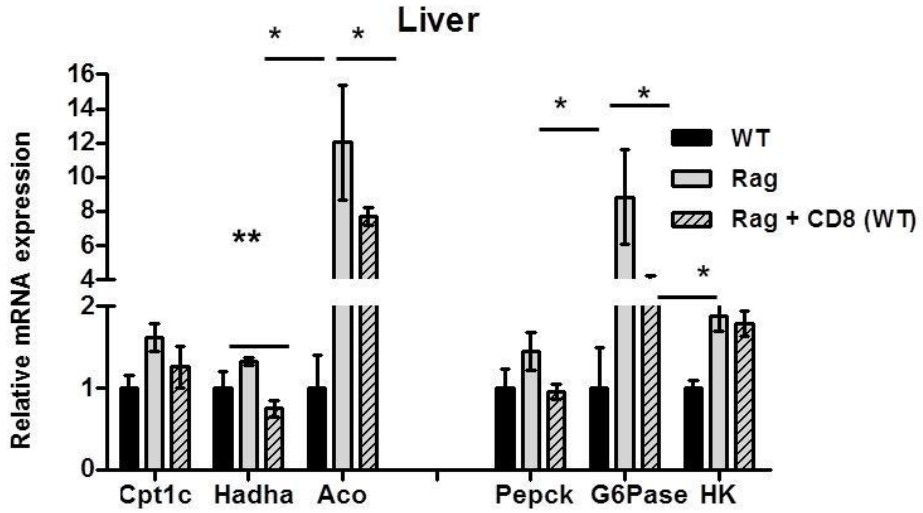

Figure 3.16. Characteristization of hepatic tissues in WT, *Rag1*$^{-/-}$ and *Rag1*$^{-/-}$ reconstituted with CD8^{+} T cells.

(**A**)Relative expression of genes implicated in the FA oxidation pathway (*Hadha*, Aco, *Cpt1c*) and carbohydrate metabolism (*Pepck, G6Pase,HK).* Data are mean expression normalized to actin ± S.E.M. n ≥ 4. Data shown are derived from one representative out of two independent experiments. *p < 0.05, **p < 0.01, Student's t-test.

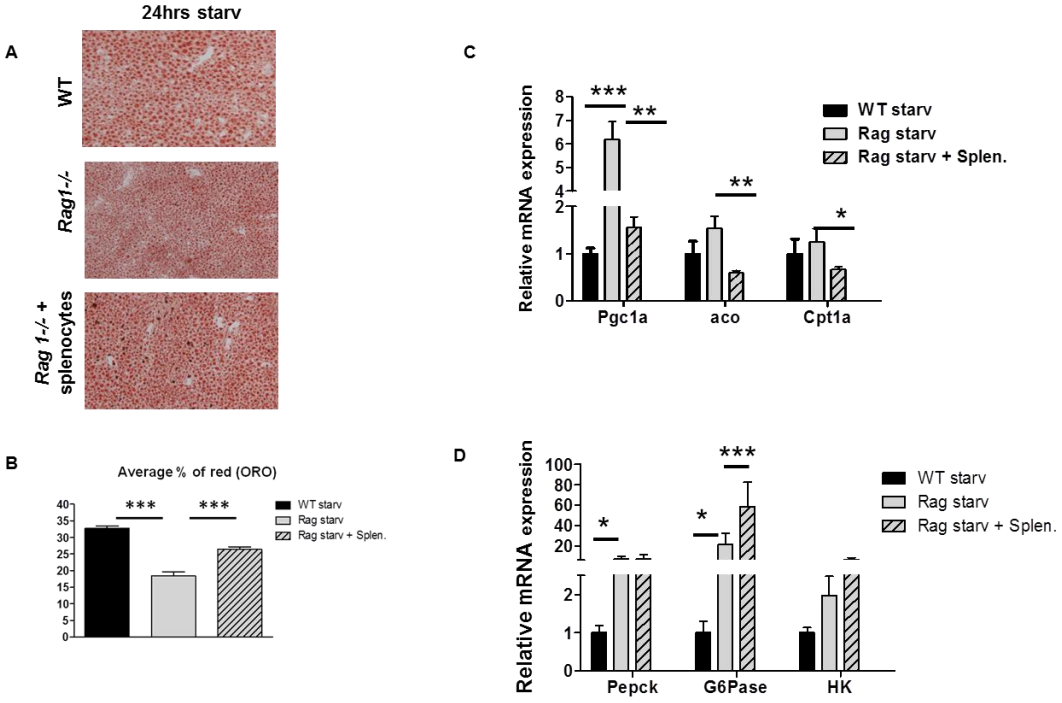

Figure 3.17. Characteristization of liver in WT, *Rag1*$^{-/-}$ and *Rag1*$^{-/-}$ reconstituted with splenocyte cells under 24hrs starvation.

Representative Oil Red O (ORO) staining (A) of liver samples in above groups and .average % measurement of red (B).Relative expression of genes implicated in the FA oxidation pathway (*Pgc1α*, Aco, *Cpt1c*) (C) and carbohydrate metabolism (*Pepck, G6Pase, HK*). (D) Data are mean expression normalized to actin ± S.E.M. n ≥ 5. Data shown are derived from one representative out of two independent experiments. **p* < 0.05, ***p* < 0.01, ****p* < 0.001, Student's t-test.

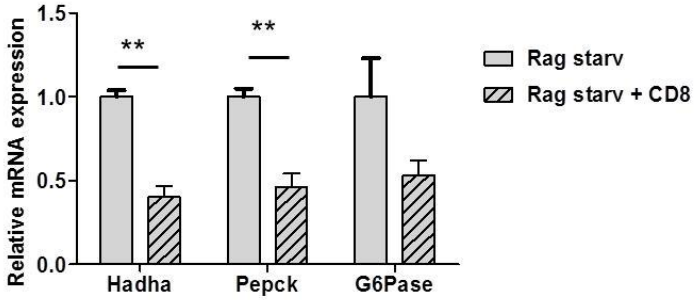

Figure 3.18. Characteristization of liver in *Rag1*$^{-/-}$ vs *Rag1*$^{-/-}$ reconstituted with CD8^{+} T cells under 24hrs starvation.

Relative mRNA expression of *Hadha* gene implicated in the FA oxidation pathway and genes (*Pepck, G6Pase*) of glucose metabolism. Data are mean expression normalized to actin ± S.E.M. n ≥ 4. Data shown are derived from one representative experiment. ***p* < 0.01, Student's t-test.

4. Discussion

In this thesis, we sought to understand the contribution of the adaptive immune system in the regulation of energy homeostasis in the adipose tissue (AT) and the liver. In particular, we leveraged the capabilities of transgenic

mouse models, like the *Rag1*$^{-/-}$ mice, to unmask the significance of T cells in response to metabolic adaptations to environmental stressors, such as temperature, or nutrient availability, such as fasting.

The interplay between the AT and the liver is necessary for the maintenance of the energy homeostasis (68). Our studies described here, clearly demonstrate that the most striking effects of the adaptive immune system in lipid metabolism/storage are driven by the T lymphocytes and are very critical for the processes operating in the AT. It has been previously shown that in obesity the recruitment of CD8^{+} T cells in the AT precedes the extensively studied accumulation of macrophages (2) thought for a long time as the primary event driving the increased secretion of TNF-a, IL-2, IFNγ and chemokines such as RANTES (20). In support of these findings, *CD8*$^{-/-}$ mice are protected from M1 macrophage infiltration and subsequent AT dysfunction found in obesity. Despite the number of studies showing the cascade of events as it concerns leukocyte recruitment in the AT in obesity, the explicit role of the various T cells subtypes in the control of energy homeostasis has not been elucidated. We demonstrate that it is the CD8^{+} T cell deficiency that plays the most critical role in the induction of beige adipogenesis in the scWAT of *Rag1*$^{-/-}$ mice and we characterized the mechanisms involved. Thus, we used several complementary approaches such as CD8^{+} T cell reconstitution in Rag1-deficient, as well as *CD8*$^{+-/-}$ and *Ifnγ*$^{-/-}$ mice. As shown several mechanisms involved in the immune plasticity and homeostatic functions of WAT are cooperating to mediate the inhibitory effects of CD8^{+} T cells in the dissipation of energy by the subWAT. These mechanisms include (i) regulation of catecholaminergic signaling and (ii) induction of eosinophils

and ILCs abundance in the subWAT, and their associated stimulatory effect on beige adipogenesis, in a manner dependent on IFNγ (Figure 3.15). Thus, $CD8^+$ T cells orchestrate several pathways involved in the immune plasticity and homeostatic functions of WAT (Figure 3.6-13).

In reference to the catecholaminergic activity, an insight on the increased formation of beige adipose tissue in the *Rag1*$^{-/-}$ mice based on previous reports on thermogenesis and on the development of beige adipose tissue was given by experimental manipulation of the adrenergic system. As known, the central nervous system senses exposure to cold and elicits a sympathetic outflow to the adipose depots to induce thermogenesis and maintain core body temperature. Norepinephrine (NE), secreted by sympathetic neurons, binds to beta-adrenergic receptors on adipose depots and triggers a signaling cascade to activate thermogenesis and lipolysis. FFAs released by lipolysis are oxidized by mitochondria and bind to UCP1 to activate its function and thus induce beiging. In our study we confirmed activation of this pathway in response to relevant experimental manipulation and in particular its operation at a more activated state in the *Rag1*$^{-/-}$ versus the WT scWAT. Thus, we identified that in the absence of lymphocytes the expression of AdR(s) and TH, the rate-limiting enzyme for the synthesis of catecholamines, are increased in the scWAT. Additionally, there is a drastic reduction of beiging upon treatment with the α-blocker prazosin hydrochloride, indicating the critical contribution of the increased catecholaminergic input in the beige adipogenesis in *Rag1*$^{-/-}$ mice. Although several effects of α-adrenergic activation on lymphocytes have been reported (69), the potential effects of lymphopenia or lymphocytosis on catecholamine production and actions

remain unknown(70). Notably, the *Rag1*$^{-/-}$ mice retain their ability to activate their catecholaminergic system despite the identified constitutive activation in the AT, as demonstrated by sensitivity to temperature changes, including acclimatization or cold exposure. In further support of the retained plasticity of their catecholaminergic system, upon reconstitution of the missing CD8^{+} T cells, *Rag1*$^{-/-}$ mice showed reversal of their increased catecholaminergic activity to level similar to that of the WT mice.

It is well demonstrated that innate cells are major players in the regulation of the adipose tissue responses to various physiological challenges, including shifting to increase in beige adipogenesis of the scWAT. The interaction between adipocytes and cells of type 2 immunity has been the focus of a number of recent studies. In particular, it has been shown that beige fat development is mediated by ILC2s, eosinophils, and the secretion of type 2 immunity cytokines, that all together act to drive the differentiation of precursor cells to the smaller, multilocular beige adipocytes in specific WAT depots (13, 71). In line, mice lacking eosinophils exhibit weight gain, insulin resistance and increased accumulation of M1 proinflammatory macrophages in the AT, while mice overexpressing eosinophils demonstrate decreased adiposity and improved insulin sensitivity when fed a HFD. Further, mice lacking ILC2s had significantly reduced eosinophils and AAMs in the visceral white adipose depot (VAT), which is correlated with a healthier metabolic phenotype. Consistent with these studies, our findings in the *Rag1*$^{-/-}$ mice showed increased ILCs in the scWAT that could be dramatically decreased, to levels resembling those in the WT tissue, upon reconstitution with CD8^{+} T cells. Furthermore, *Rag1*$^{-/-}$ mice displayed also increased IL-4 levels in the

scWAT, in addition to the ILCs-secreted cytokines. Importantly, the macrophage content of the scWAT of *Rag1*$^{-/-}$ mice did not differ from that of the WT tissue, as we initially hypothesized based on their deficiency in cells of the adaptive immunity. Furthermore, we found no difference in the expression of anti-inflammatory macrophages (M2)-specific markers between the two genotypes, suggesting that the enhanced catecholaminergic signaling and beige adipogenesis in *Rag1*$^{-/-}$ mice it is not due to alterations in macrophage numbers or their polarization. These data taken together indicate a CD8^{+} T cell deficiency–mediated mechanism for beige adipogenesis independent of alteration in M2 macrophage numbers in further confirmation of the multifaceted regulation of this process (72). Interestingly, adoptive transfer of CD8^{+} T cells in *Rag1*$^{-/-}$ mice could reverse the abundance of both the eosinophils and the ILCs and the increased abundance of beige adipocytes. In line with the pronounced beige phenotype of the scWAT *Rag1*$^{-/-}$ mice we demonstrate increased expression of key genes involved in lipid oxidation, an effect directly linked to the CD8^{+} T cells as indicated by the down regulation following reconstitution with CD8^{+} T cells.

The dramatic effect of the replenishment of the missing CD8^{+} T cells in the scWAT phenotype, led us to the hypothesis that CD8^{+} T cells is the critical cell population involved in this process and the potential contribution of other T cells population might be secondary. To further support our hypothesis for the contribution of CD8^{+} T cells in beige adipogenesis we studied the metabolic phenotype of *CD8*$^{-/-}$ mice that confirmed our hypothesis (Figure 2.14). Further, our preliminary evidence from parallel studies in *CD4*$^{-/-}$ mice suggested that CD4^{+} T cells may also modulate beige adipogenesis, although

in a less consistent and robust manner. Of course, the $CD4^+$ T cell pool is more diverse and more amenable to regulation by the specific experimental conditions applied. To conclusively elucidate the exact position of this T cell subpopulation in the steps involved in the development of beige fat, a whole new study will be required in the future. Moreover, although this study has focused on the $CD8^+$ T cell–mediated regulation of beiging in the scWAT, the main fat depot with beiging capability, it is also conceivable that $CD8^+$ T cells act also on other fat depots, such as epiWAT and BAT. Preliminary studies in our model confirmed the negative effect of $CD8^+$ T cells in lipid utilization in eWAT and BAT, although to a much lesser extent than in the scWAT that has the inherent capacity to expand significantly its beige depot (Data not shown).

Next, we sought to elucidate the mechanisms mediating the effects of $CD8^+$ T cells in beige adipogenesis, starting with molecules secreted by the $CD8^+$ T cells. A main molecule secreted in high amounts by the activated $CD8^+$ T cells as well shown in a number of studies, is IFNγ. Some early studies reported increased INFγ activity in WAT in mice and humans, and higher amounts secreted from the T cells of patients with type 2 diabetes (73-76). Another study has shown that IFNγ (77) could inhibit glucose and lipid metabolism in primary human adipocytes *in vitro*. Interestingly, obese *Ifnγ*$^{-/-}$ mice show improved insulin sensitivity and decreased adipocyte size, suggesting beneficial effects of IFN-γ deficiency in energy utilization (78). We found that *Ifnγ*$^{-/-}$ mice have significant induction of beige fat development and increased number of ILCs and eosinophils in the scWAT (Figure 3.14), all in line with activation of the mechanisms mediating utilization of energy in the WAT depot. Reconstitution of the *Rag1*$^{-/-}$ mice with $CD8^+$ T cells from *Ifnγ*$^{-/-}$ mice,

did not affect the beige fat abundance in the scWAT, in contrast to the inhibitory (ablating) effect from the transfer of WT $CD8^+$ T cells. These findings taken together provide additional support to our hypothesis on the role of the $CD8^+$ T cells in beige adipogenesis and indicate IFN-γ as a main part of the mediating mechanism. The counterargument on the latter would be that $CD8^+$ T cells are not the only source of IFN-γ, as NK cells and ILC1 have been also shown as IFN-γ sources in the adipose tissue(79). In an interesting study of Timothy et al. identified a new subset of ILC cells, the ILC1 cells, that selectively accumulate in the AT following diet induced obesity (HFD-induced obesity) and secrete IFNγ (67). These cells were shown to accumulate preferentially in the scWAT and to secrete higher amounts of IFNγ during HFD as compared to other known IFNγ producing lymphocytes such as the $CD8^+$ T cells. The understanding of the specifics of energy homeostasis is an emerging field of investigation and new knowledge is constantly provided by the vast majority of ongoing studies worldwide.

The inhibitory effects of IFN-γ on beige adipogenesis may be both direct as shown by the studies with the *Ifnγ*$^{-/-}$ or indirect via the dose- and context-dependent effects on other regulators of beige adipogenesis. Notably, TH overexpression has been shown to decrease the production of IFN-γ (69), while challenge of PBMCs with IFN-γ resulted in decreased TH expression and of the associated catecholamine production (69, 80). All the above and our findings indicate the operation of multiple interacting networks among $CD8^+$ T cells, innate immune cells, IFN-γ, and other secreted factors driving beige adipocyte development.

Emerging evidence demonstrates the significance of the interactions between immune cells and metabolic networks in the pathogenesis of severe diseases such as insulin resistance, autoimmune diseases or cancer. Lately, a number of anti-inflammatory, biological treatments such as anti-TNFa and anti-IL-1 (Anakinra)(81), anti-IL-1beta (gevokizumab, canakinumab, LY2189102) have been suggested as of potential benefit for the treatment of insulin resistance and dysregulated glucose metabolism (82). However, anti-TNFa (CDP571, Ro 45-2081,etanercept) failed to improve insulin sensitivity in obese patients, although it successfully reduced blood glucose levels (83). Furthermore, anti-inflammatory agents such as salicylates (84, 85) and thiazolidinediones (86) have been used to control insulin resistance and reduce blood glucose levels of diabetic patients with variable efficacy (87). Our findings raise the possibility for the potential benefits of targeted therapeutic interventions to leverage the effect of the $CD8^+$ T cells on the blockade of energy dissipation (6) that might provide one of the arms for combination therapies.

The liver is a main site for essential metabolic functions, such as proteolysis, lipolysis, glyconeogenesis, fatty acid oxidation, ketogenesis and amino acid processing, all tightly controlled by insulin and other metabolic hormones. Thus, altered metabolic states, such as hypercaloric diet as well as prolonged fasting, promote lipid storage insulin resistance, and metabolic dysregulation. Compared to the wealth of information on the role of immune cells in the metabolic processes taking place in the adipose tissue depots, the relevant knowledge on the operating mechanisms in the liver is limited. In support of our findings on the effects of $CD8^+$ T cells on energy homeostasis, strategies targeting the inhibitory effect of $CD8^+$ T cells on the liver have been proposed

for the treatment of severe steatohepatitis and the associated hepatic carcinogenesis (88). Here we show that the absence of functional adaptive immune system, such as the *Rag1*$^{-/-}$ mice, is protective from the starvation-induced development of hepatic steatosis (NAFLD), via further activation of lipid oxidation (Figure 3.16). We showed that transfer of whole splenocytes isolated from healthy WT mice could inhibit the increased lipid oxidation in the liver of the *Rag1*$^{-/-}$ mice, to levels similar to those found in the WT tissues, confirming the importance of T cells in this process (Figure 3.17 A-D). Interestingly, in agreement with the recently described role of CD8^{+} T cells in liver damage and development of steatohepatitis (88), we showed that adoptive transfer of CD8^{+} T cells in *Rag1*$^{-/-}$ mice led to development of hepatic steatosis following 24hrs starvation and attenuated FA oxidation and glucose metabolism similar to the effects of fasting in WT mice (Figure 3.18). Studies focused at the cellular and molecular level are needed to elucidate the specific factors operating in the mechanisms driving the effects of CD8^{+} T cells on liver metabolism.

In summary, our results provide evidence for the critical involvement of lymphocytes in hepatic lipid metabolism during severely compromised calorie intake, as has been described for high fat diet previously (18, 88). These findings raise the possibility of immunotherapy as a putative therapeutic strategy against severe liver steatosis, a common side effect of various therapeutic interventions and of disease-induced pathological processes such as in a number of chronic infections. Given the differences between the human and rodent metabolic responses to severe stressors and therapeutic

agents such as the biologics, these studies should ideally focus on analyses of human samples from relevant clinical studies.

5. Material and Methods

5.1. In vivo experimental design

Age-matched (8-12 weeks) male mice of *Rag1*$^{-/-}$, *CD8*$^{-/-}$ and *IFNγ*$^{-/-}$ genotype on C57BL/6 background, were purchased from Jackson Laboratories and maintained in a pathogen-free, temperature controlled, 12hr light and dark cycle environment in accredited animal facilities at the Biomedical Research Foundation of the Academy of Athens. Wild type (WT) mice on C57BL/6J background were kindly provided by the animal facilities at the BRFAA and age and weight-matched (22-25 gr) with the above genotypes. Animals were given free access to food and water. All mice used for experimentation are provided by the colonies maintained in our facility for several generations, in order to normalize facility-dependent changes in metabolic and other functions. Male mice 8-12 weeks of age were used at the start of each experiment. Mice were allocated randomly in experimental groups for each genotype. Mice were fasted for 4hours and then anesthesized with inhaled isoflurane (Abbott) and sacrificed by cervical dislocation. The liver and fat pads were removed from the mouse and weighed. Once the organ was weighed left fat pads of the mice were kept for RNA extraction while the right fat pads were fixed in 4% PFA overnight (O/N) or 10% formalin solution (Sigma) and embedded in paraffin for sectioning.

5.2. Serum Sample Collection

Blood was collected from each mouse after overnight (O/N) fasting via retro-orbital bleeding using a heparinized micro-hematocrit capillary tube (Fisherbrand). Blood samples were centrifuged at 7.000rpm for 7min in order to separate the serum from the red blood cells (RBCs). Serum was then placed in -80^{o}C until further analysis.

5.3. Cold exposure experiments

Eight-week-old male mice WT and *Rag1*$^{-/-}$ were housed individually in plastic cages to avoid thermogenesis and divided into two groups that were counterbalanced by body mass. For the cold exposure studies, control groups were acclimated at room temperature (24^{o}C), whereas cold exposure groups were adapted for two days at 18^{o}C and next kept at 4^{o}C for another two days. Adaptation period is important to avoid high death rate. Body temperature was measured at room temperature (24^{o}C), at 18^{o}C and every 30 minutes for the first 4 hours at 4^{o}C. Core temperature were measured using a YSI TELE-Thermometer recorder (Simpson electric Co).

5.4. Thermoneutrality experiment

Eight-week-old WT and *Rag1*$^{-/-}$ mice on C57BL/6 mice were singly caged and housed at 28-30^{o}C, with a 12-hour light-dark cycle and free access to a standard chow diet for 20 days. Mice were housed in controlled temperature room in animal facilities at the Biomedical Research Foundation of the Academy of Athens (BRFAA).

5.5. Cell transfer experiments

Splenocytes from 8-12 week old C57BL/6 mice on regular diet were isolated and homogenized between two glass slides**.** Single cell suspensions were prepared by passing cell suspension through a 40µm nylon cell strainer (BD Falcon) and washed with RPMI 1640 medium containing 10% fetal bovine serum (FBS) and 1% penicillin/streptomycin (400xg for 7min). In order to remove red blood cells, splenocytes were resuspended in a Red Blood Cell Lysis Buffer (Sigma) (1ml for each spleen) 1 minute at room temperature (RT) and washed with 15 ml of RPMI full medium at 300xg for 10minutes. Then, cells were resuspended in 900µl Macs Buffer (PBS supplemented with 0,5% BSA and 2mM EDTA, sterile filtered) and 100µl mouse CD8a (Ly-2) microbeads (Miltenyi Biotec, Cat#130-049-401) was added per 10^8 total cells. After 15 minutes incubation at 4^o-8^oC , cells were washed with 10ml per 10^8 cells, centrifuged at 300xg for 10 minutes and resuspended in 500µl of Macs buffer for each 10^8 cells. Then, the cell suspension was loaded on a MACS column (LS) (Miltenyi Biotec) which was placed in the magnetic field of a Macs Separator (Miltenyi Biotec). Before use, macs column (LS) was rinsed and cleaned with 3ml of Macs Buffer according to the provider. The magnetically labeled $CD8^+$ cells are retained in the column, while the unlabeled cells (cell fraction depleted of $CD8^+$ cells) run through. After, the unlabeled cells were collected and column washed 3 times with 3 ml of Macs Buffer, each time once the column reservoir is empty. Then, the column was removed from the separator and placed on a suitable collection tube. Magnetically labeled cells were collected in 5 ml Macs Buffer by firmly applying the plunger supplied with the column.

To examine the effects of T cells in beige adipogenesis, 12-week-old *Rag1*$^{-/-}$ mice fed a chow diet were used for adoptive transfer of splenocytes, cells rich in B and T cells. Additionally, *Rag1*$^{-/-}$ mice, kept either at 24^{o}C or 4^{o}C, were adoptively transferred with CD8^{+} T cells. Splenocytes were obtained from the spleen of lean C57BL/6 WT mice, dissociated into single-cell suspensions and red blood cells were removed. CD8^{+} T cells were purified from the spleen of WT C57BL/6 male mice using mouse CD8α (Ly-2) microbeads (130-049-401) according to the protocol (Miltenyi Biotec). A total of 5x10^{6} splenocytes contained 15-20% CD8^{+} T cells (around 8x10^{5}) or 5x10^{6} CD8^{+} T cells were injected retro-orbitally weekly and sacrificed after 2 weeks. Control groups have received retro-orbital injections of PBS. Purity of CD8^{+} T cells injected was measured by FACS analysis and was >85%. Homing of CD8^{+} T cells in the scWAT were confirmed by flow cytometry analysis.

To examine the effects of T cells in liver deposition, 12-week-old *Rag1*$^{-/-}$ mice fed either a regular diet or deprived of food for 24hours received 5x10^{6} splenocytes or CD8^{+} T cells retro-orbitally in 100µl PBS (once weekly) for 2 weeks. At the same period, control groups have received retro-orbital injections of PBS. Homing of CD8^{+} T cells in the scWAT was confirmed by FACS analysis.

5.6. Adrenergic blockade

Alpha-adrenergic blockade was achieved by administration of prazosine hydrochloride (Sigma), a selective α1-adrenergic antagonist, in drinking water (8mg/kg) for 5 days.

5.7. In vivo depletion of CD8+ T cells

WT mice were received 200ug of anti-CD8 antibody (BE0004-1 Bio X Cell) or normal rat IgG (Control) (Bio X Cell) by the i.p route at days 0, 2, and 6. . Mice were euthanized at day 10 for further analysis. The depletion was assessed at days 24 h after the treatment with mAbs by flow cytometric (FC) blood analysis.

5.8. Tissue Homogenization protocol for Elisa

Subcutaneous adipose tissue from mice were weighed and homogenized with 600µl cold HBSS (1X) supplemented with proteinase inhibitors (1:200) by using a tissue homogenizer. The homogenates were centrifuged at 1.800 x rpm for 15 minutes at 4^{o}C and the supernatant was stored at -80^{o}C until analyzed. IL-4, IL-5 and IL-13 protein levels were determined by using Elisa (mouse IL-4, IL-5, IL-14 Elisa Ready-SET-Go! ® - eBioscience).

5.9. Tissue preparation for flow cytometry analysis

Subcutaneous white adipose tissue (scWAT) was isolated, after careful removal of lymph nodes, and kept on ice in 3cm dishes including 1ml buffer I (PBS with 1mM $CaCl_2$ and 0,5% BSA). scWAT was finely minced and washed with buffer I at 500xg at 4^{o}C for 10 minutes to remove erythrocytes and free leukocytes. After centrifugation remove the floating tissue (upper phase) and dispersed by shaking into DMEM (high glucose) medium containing fresh collagenase (2mg/ml) and 0,5% BSA depending on tissue weight (1ml/ tissue gr) at 37^{o}C for 30-40 minutes with gentle agitation. Cell suspension was topped up to 10ml by adding DMEM medium, passed through 100µm filters to generate single-cell suspensions and centrifuged at 300Xg for 5 minutes to

separate floating adipocytes from the SVF pellet. Then, cell pellet was resuspended in Facs buffer (PBS with 0,1% BSA and 2.5mM EDTA) and stained with the indicated antibodies.

5.10. Flow cytometry analysis

ScWAT was processed and stained with fluorochrome conjugated monoclonal antibody combinations for ILC staining. Monoclonal antibodies used for flow cytometry were as follows: allophycocyanin (APC)-anti-CD45 (30-F11; Biolegend); phycoerythrin (PE)-anti-CD3 (145-2C11; Biolegend); phycoerythrin (PE)-anti-CD4 (E121.19; Biolegend); PE-anti CD8 (53-6.7; Biolegend); PE-anti CD19 (6D5; Biolegend); PE-anti-B220 (RA3-6B2; Biolegend); Fluorescein isothiocyanate (FITC)-CD11b (M1/70; Biolegend); PE-anti CD11c (N418; Biolegend); PE-anti FceRI (MAR-1; Biolegend); PE-anti Gr-1 (RB6-8C5; Biolegend); PE-anti Ter119 (Ter/119; Biolegend); Peridinin-chlorophyll proteins (PercP)-anti-CD90.2 ((53-2.1; Biolegend); Phycoerythrin/Cy7 (PE/Cy7)-anti-Sca1 (D7; Biolegend) and Alexa 488-Gata3 (16E10A23; Biolegend). Representative gating schemes for each population are shown in Figure 3D. ILCs are identified as $CD45^+$, lineage negative ($CD3^-$ $CD4^-$ $CD8^-$ $CD19^-$ $B220^-$ $CD11b^-$ $CD11c^-$ $FceRI^-$ $Gr\text{-}1^-$ $Terr119^-$) $CD90.2^+$ $Sca\text{-}1^+$ cells. Subcutaneous white adipose tissues were processed and stained with fluorochrome conjugated monoclonal antibody combinations for eosinophil staining. Eosinophils were identified as $CD45^+$, $CD11b^+$ and Siglec F^+ cells. Representative gating schemes are shown in Figure 3F. Trafficking of $CD45^+CD3^+CD8^+$ in the subcutaneous white adipose tissue was assessed using the following monoclonal antibodies: (APC)-anti-CD45 (30-F11; Biolegend); Fluorescein isothiocyanate (FITC)-anti-CD3 (145-2C11;

Biolegend) and PeCy7-anti-CD8 (53-6.7; Biolegend). Representative gating schemes are shown in Supplemental Figure 2A. Macrophage assessment of the subcutaneous adipose tissue was assessed by staining with the following fluorochrome conjugated monoclonal antibodies: allophycocyanin (APC)-anti-CD45 (30-F11; Biolegend); Fluorescein isothiocyanate (FITC)-anti $CD11b^+$ (M1/70; Biolegend); and Phycoerythrin (PE) $F480^+$ (BM8; eBioscience). Representative gating schemes are shown in Figure 3.7. Samples were analyzed on a FACSAria III (Becton Dickinson). As indicated, data were expressed as percentages of $CD45^+$ hematopoietic cells. Live lymphocytes were gated by DAPI exclusion, size, and granularity based on forward- (FS) and side-scatter (SS). Data were analyzed using BD FACSDiVa software. Appropriate isotype-matched controls for all antibodies were used to determine positive staining.

5.11. Western blot

Tissues were harvested in RIPA buffer (ThermoFisher Scientific) with 1% protease and 1% phosphatase inhibitors (ThermoFisher Scientific). 20 ng of protein was loaded into each well of a 4-12% Bis-Tris polyacrylamide gel (ThermoFischer Scientific) and transferred to nitrocellulose membrane (ThermoFischer Scientific). Protein-bound membranes were blocked for 30 minutes with 5% non-fat dry milk in 0.1% tris-buffered saline with Tween (TBST) and incubated with rabbit anti-Ucp1 antibody (ab10983, Abcam) or anti-tubulin (ab15568, Abcam) in blocking buffer overnight at 4°C. Membranes were treated with HRP-conjugated secondary antibodies diluted 1:5000 in blocking buffer for two hours and rinsed with Pierce ECL chemiluminescent solution (Thermo Fischer Scientific). Membranes were immediately read in a

Kodak Image Station 4000mm PRO and protein levels were quantified using ImageJ Software. Commercially available.

5.12. Indirect calorimetry

Metabolic measurement was performed using an Oxymax indirect calorimetry system (Columbus Instruments, Columbus, OH). In short, preweighed mice were housed individually in specifically designed Oxymax calorimeter chambers with ad libitum access to the diet and water for 72h with a 12-h light/12-h dark cycle in an ambient temperature of 22°C. Mice were singly housed for 2 days prior to transferring into the calorimeter chamber.). VO_2, VCO_2 and rates were determined under Oxymax system settings as follows: air flow, 0.6 l/min, sample flow, 0.5 l/min. The system was calibrated against a standard gas mixture to measure O_2 consumed (VO_2, ml/kg/h) and CO_2 generated (VCO_2, ml/kg/h). Metabolic rate, respiratory quotient (ratio of VCO_2/VO_2, RER), and activity (counts) were evaluated over a 48-h period. Energy expenditure was calculated as the product of the calorific value of oxygen (3.815+1.232 x respiratory quotient) and the volume of O_2 consumed. Energy expenditure (kcal/hr/kg), respiratory quotient (ratio of VCO_2/VO_2, RER), food intake (g) and activity (counts) were evaluated over a 48-h period. The results were normalized and compared to the WT group per cohort that was set as 100%.

5.13. Histological studies

H&E staining

Paraffin-embedded samples are suitable for H&E staining which can reveal the morphology and size of adipocytes or hepatocytes. In addition, H&E

staining also detects intracellular fine organelles such as mitochondria and other cell types such as inflammatory cells.

Paraphormaldehyde-fixed, paraffin-embedded tissue sections of approximately 5µm were cut in a microtome (Leica RM2265) and incubated in a tissue processor center for rapid melting at 60^{o}C for 10 minutes. Sections then were deparaffinized and rehydrated through a graded series of ethanol (VWR) 100% to water: two changes of xylol (VWR) (deparaffinization) for ten minutes each; two changes of 100% ethanol for three minutes each; 95% ethanol for two minutes; 75% ethanol for two minutes; 50% ethanol for two minutes; and rinsed in tap water. Afterwards, slides were treated with Harris Hematoxylin (VWR) for 30 seconds, washed shortly with water (three dips) until clear and then stained with eosin (VWR) for one minute, followed again by a washing step (three dips). Sections were dehydrated: 80% ethanol for 30 seconds; 90% ethanol for 30 seconds; two changes of 100% ethanol for one minute each and two changes of xylol for ten minutes each. Slides were then protected with a coverslip using a permount gel mount (DPX) (VWR). Images were taken using a Brightfield microscope (LEICA DMLS2). Adipocyte cell size was measured by automated software developed in our lab using the Matlab.

Pas staining

Periodic Acid-Schiff (PAS) Staining was applied to identify glycogen storage. The purpose of this method is to identify carbohydrate macromolecules through chemical reaction. Periodic acid oxidizes the glucose residues and creates aldehydes, which react with Schiff reagent producing purple colour.

Paraffin-embedded samples were used for Pas staining. 5μm sections were cut in a microtome and let dry overnight (O/N) before use. Slides were deparaffinized and rehydrated as described previously. Afterwards, slides were treated with 0,5% periodic acid solution (VWR), prepared fresh before use, rinsed in distilled water and incubated for 15min at room temperature (RT) with Schiff's reagent (VWR). Sections were becoming light pink color during this step. Then, slides were washed with lukewarm tap water (40^{o}C) for 5min and immediately sections turn dark pink color. Sections were dehydrated as described previously and covered using a synthetic mounting medium (DPX).

Oil Red O staining

Oil Red O staining identifies lipid droplets in bright red. Oil Red O stock solution was made by dissolving 0,5% Oil Red O (Sigma) in 99% isopropyl alcohol using the very gentle heat of a water bath (37^{o}C) and overnight (O/N) stirring at room temperature (RT). The mixture sits overnight before being filtered through a Whatman paper. Working solution of Oil Red O was freshly prepared by mixing Oil Red O stock solution into distilled water (3:2)

Fresh liver pieces for Oil Red O staining were preserved in optimal cutting temperature (O.C.T.) compound (VWR) and stored at -80^{o}C. Frozen sections (10μm) were cut in a microtome cryostat (Leica CM3050 S), dried for 30 minutes and fixed with 10% formalin for 30 minutes. The slides washed three times with PBS for 5 minutes and rinsed with 60% isopropyl alchohol to completely dry. The slides were then incubated in the Oil Red O working solution for 30 minutes followed by rinse in 60% isopropyl alcohol to remove

any remaining debris. Then, slides washed 5 times with PBS. and covered using a synthetic mounting medium (DPX).

Immunofluorescence

For immunofluorescence staining, PFA-fixed, paraffin-embedded inguinal subcutaneous adipose tissue (SAT) sections, 5µm thick, were deparaffinized and hydrated. Then the SAT sections were blocked with PBS containing 10% normal goat serum (NGS) for 1 hour and a half. The sections were rinsed 3 times for 5 min in 1XPBS and then incubated with the primary antibody, overnight at 4^{o}C. The next day, tissue slides washed three times for 5 minutes with 1XPBS and then incubated with the secondary antibody for 2 hours. Then, tissue slides washed again (3 times for 5min) and nuclei were stained using DAPI (Sigma).

For detection of tyrosine hydroxylase (TH), the rate limiting enzyme of catecholamine synthesis, a rabbit anti-TH antibody (Millipore)-AB152 were used (1:1000) as a primary antibody and a goat anti-rabbit Alexa Fluor-488-conjugated secondary antibody (Invitrogen) (1:500) was used to stain the nerve fibers. Antibodies were diluted in PBS containing 10% NGS.TH^{+} parenchymal nerve fibers (i.e fibers closely associated to adipocytes in the depots) were counted. Perivascular fibers (those in contact with arterioles and venules) were not considered in the quantitative analysis. Six randomly selected areas, representative of the depot, were studied in the inguinal subcutaneous depot of each animal using a Confocal inverted microscope {LEICA TCS SP5 (DMI6000)}. The density of TH-immunoreactive fibers was calculated as the number of fibers per 100 adipocyte

For detection of UCP-1 (uncoupling protein 1), a mitochondrial inner membrane protein specifically expressed at high levels in brown adipose tissue mitochondria, a rabbit anti-UCP-1 antibody (Abcam) were used (1:300) as a primary antibody and a goat anti-rabbit Alexa Fluor-488-conjugated secondary antibody (1:500) secondary antibody. Another washing step was followed by 4,6-diamidin-2-phenylindol (DAPI) incubation and further washing steps before the sections were mounted using vectashield mounting medium (Vector). Antigen retrieval was done before blocking by treating slides with 0,1% w/v pronase (protease from Streptomyces griseus-Sigma) solution for 10 minutes at 37^{o}C (proteolytic-induced epitope retrieval method). Antibodies were diluted in PBS containing 1% BSA (Sigma). For UCP1 quantification, patches (15 patches for every image, sized 128X128 pixels) of images were randomly selected and the mean intensity of the staining was measured. Images were obtained using a bright field LEICA DMLS2 microscope.

5.14. RNA isolation

10mg piece of tissue of interest was dissected on dry ice and homogenized in TRI reagent. In case of adipose tissue (epididymal or subcutaneous), the whole tissue was homogenized to prevent spatial differences. Samples were incubated in Tri Reagent (Sigma) for 5minutes at 4^{o}C and then chloroform (Sigma) was added to each sample. Samples were shaken vigorously for 15 seconds and left on ice for 15 minutes. The samples were then centrifuged at 13.000rpm for 20 minutes at 4^{o}C, resulting in two phases, including lower DNA/protein containing red phenol chloroform phase and colorless aqueous upper phase containing RNA. The aqueous phase was transferred to a fresh tube and mixed with 0.5ml isopropyl alcohol (FisherScientific). Samples were

stored at -80^{o}C for 30 minutes and centrifuged at 13.000xg for 30 minutes at 4^{o}C. The precipitated total RNA formed a white pellet at the bottom of the tube. The supernatant was removed and RNA pellet was washed three times with 1ml per tube of 70% ethanol in diethylpyrocarbonate (DEPC) water. The sample was vortexed and spun at 8.000rpm for 10 minutes at 4^{o}C. RNA was air-dried briefly without complete drying in order to preserve solubility. The pellet was dissolved in DEPC H_20. To minimize secondary structure formation, heat denature all RNA samples at 65^{o}C for 3 minutes. It was then stored at -80^{o}C until quantification. The same procedure is followed for RNA extraction from cells, adding a washing step of cells with PBS prior to scraper.

5.15. RNA quantification

To measure RNA concentration a small quantity of the RNA sample (1µl) was measured at 260nm on a Nanophotometer P330 (Implen). The concentration of RNA was determined using the Beer-Lambert law, which predicts a linear change in absorbance with concentration. An A260 reading of 1,0 is equivalent to about 40µg/ml of RNA and the OD at 260 nm is used to determine the RNA concentration. RNA has its absorption maximum at 260nm and the ratio of the absorbance at 260 and 280nm was used to assess the RNA purity. Pure RNA has an A260/A280 range of 1,8-2,0.

5.16. RNA cleaning

For the removal of contaminated genomic DNA in RNA samples, the Ambion DNA-free Kit was used (Ambion, Cat#AM1906). Each RNA sample was treated with 1µl rDNase I and 0,1 volume of 10X Dnase I Buffer was added. Samples were incubated at 37^{o}C for 30 minutes. Following incubation, 0,1 volume of resuspended DNase inactivation reagent was added, mixed well

with samples and incubated at room temperature for 2 minutes. Samples were then centrifuged at 10.000xg for 2 minutes and the supernatant (RNA) was transferred to a fresh tube and stored at -80^{o}C until further use.

5.17. Reverse transcription (RT)-PCR

cDNA was synthesized using reverse transcriptase (RT). Reverse transcriptase is an enzyme that translates RNA to DNA. This creates one DNA (cDNA) strand complementary to the RNA strand in a DNA-RNA hybrid. Reverse transcriptase needs a primer to start the DNA synthesis. Random hexamers contain six and six nucleotides put together at random and bind at several locations in the total RNA and cDNA synthesis starts from there. RNaseout is used to avoid RNA degradation.

For cDNA synthesis, 1-2µg RNA was diluted to a final volume of 6µl and 2µl random hexamer primers (Invitrogen) (1:20) were added. Samples were denatured at 75^{o}C for 5minutes and quickly chilled on ice to avoid secondary structures. After denaturation, 4µl 5X First Strand Buffer {250mM Tris-HCl (pH 8.3 at room temperature), 375mM KCl, 15mM $MgCl_2$} (Invitrogen), 4µl dNTPs (dATP, dCTP,dGTP,dTTP) (5mM) (Invitrogen), 2µl DTT (dithiothreitiol) (0,1M) (Invitrogen), 1µl RNaseout (Recombinant ribonuclease inhibitor) (40units/ul) (Invitrogen) and 1µl M-MLV reverse transcriptase (Invitrogen) (200units) were added to each sample and incubated at 25^{o}C for 10 minutes, followed by incubation 45 minutes at 42^{o}C. Reaction was inactivated at 95^{o}C for 10 minutes. Reaction was carried out in a thermocycler (Peltier Thermal Cycler) PTC-200 (MJ Research). The generated cDNA was then used as template for quantitative real time PCR (RT-PCR) reactions.

5.18. Quantitative real time PCR (RT-PCR)

To determine the expression levels of genes of interest, quantitative real-time PCR was performed, using SYBR green-based system. cDNA was diluted 1:5 in a 20µl reaction volume; each reaction was performed in duplicate. PCR was carried out on a ABI Prism Sequence Detection System 7000 (Applied Biosystems) using the RT² SYBR® Green qPCR Master Mix (Qiagen) with the following cycle parameters 50^{o}C for 2min, 95^{o}C for 10 min, 95^{o}C for 0:15 sec, 60^{o}C for 0:1min for 40 cycles. Fold change in mRNA expression was determined using the ΔΔCT method, with all genes normalized to β-actin. Primer sequences are listed in the table1. Gene expression levels were normalised to *actin* for in vivo and to cyclophilin for in vitro experiments and calculated according to the $2^{-\Delta\Delta Ct}$ method.

5.19. Statistical Analysis

Data are presented as mean±SEM. Differences were analyzed by each appropriate test (Student's t-test for single comparisons, ANOVA for multiple, followed by post hoc Bonferroni's Multiple Comparison Test or two-way repeated measures ANOVA for body weight using Prism (GraphPad). A P value less than 0.05 was considered significant. Statistical significance is presented as *P < 0.05, **P < 0.01, ***P < 0.001.

5.20. Table1: List of primers

Gene	Forward	Reverse
Actin	5′-CCCAGGCATTGCTGACAGG- 3′	5′-TGGAAGGTGGACAGTGAGGC-3′
Pgc1α	5′-TCACCCTCTGGCCTGACAAATCTT- 3′	5′-TTTGATGGGCTACCCACAGTGTCT- 3′
Pgc1β	5'-ATTGAACAAAGCTGCTTCCGTCCG-3'	5'-GTGGCAGTGGAACATCAACAGCAT-3'
Pparα	5′-AAGAACCTGAGGAAGCCGTTCTGT- 3′	5′-GCAGCCACAAACAGGGAAATGTCA-3′
Cpt1α	5′-GTCAAGCCAGACGAAGAACA- 3′	5′-CGAGAAGACCTTGACCATAG-3′
Hadha	5′-AGCAAGTGTTCAAAGGGCTGAACG- 3′	5′-TGTGCTTTACACCGAGGTCCTCAA- 3′
Adipoq	5'-GGAGATGCAGGTCTTCTTG-3'	5'-TTCTCCAGGCTCTCCTTT-3'
Ucp1	5'-TCTTCTCAGCCGGAGTTTCAGCTT-3'	5'-ACCTTGGATCTGAAGGCGGACTTT-3'
Cidea	5'-ATCACAACTGGCCTGGTTACG-3'	5'-TACTACCCGGTGTCCATTTCT-3'
Prdm16	5'-CAGCACGGTGAAGCCATTC-3'	5'-GCGTGCATCCGCTTGTG-3'
Fndc5	5'-ATGAAGGAGATGGGGAGGAA-3'	5'-GCGGCAGAAGAGAGCTATAACA-3'
Fgf21	5'-TACACAGATGACGACCAAGA-3'	5'-GGCTTCAGACTGGTACACAT-3'
Mrc1	5'-TGATTACGAGCAGTGGAAGC-3'	5'-GTTCACCGTAAGCCCAATTT-3'
Arg1	5'-AGACCACAGTCTGGCAGTTG-3'	5'-CCACCCAAATGACACATAGG-3'
Tnfα	5'-TCTCATGCACCACCATCAAGGACT-3'	5'-ACCACTCTCCCTTTGCAGAACTCA-3'
Nos2	5'-CAGAGGACCCAGAGACAAGC-3'	5'-CCTGGCCAGATGTTCCTCTA-3'
Dio2	5'-CAGTGTGGTGCACGTCTCCAATC-3'	5'-TGAACCAAAGTTGACCACCAG-3'
Adr1a	5'-GGGTCCTTCTTCCCGAATTT-3'	5'-GCTGGAGCATGGGTATATGATAG-3'
Adr3b	5'-TGAAACAGCAGACAGGGACA-3'	5'-TCT TGACACTCCCTCAGCAC-3'
Fasn	5'-CTCCGTGGACCTTATCACTA-3'	5'-CTGGGAGAGGTTGTAGTCAG-3'
Acc1	5'-TAACAGAATCGACACTGGCTGGCT-3'	5'-ATGCTGTTCCTCAGGCTCACATCT-3'
Dgat	5'-TCATGGGTGTCTGTGGGTTA-3'	5'-CAGAGTGAAACCAGCCAACA-3'
Srepb1c	5'-TGGCTTGGTGATGCTATGTT-3'	5'-TAAGGGGTTGGGAGTAGAGG-3'
Lipe	5’-AAGGACTTGAGCAACTCAGA-3’	5’-TTGACTATGGCTGACGTGTA-3’
MgII	5’-GACGGACAGTACCTCTTTTG-3’	5’-AGAAAAGTAGGTTGGCCTCT-3’

5.21. Study Approval

All experimental procedures reported here were approved by the competent veterinary authority of the Prefectures of Athens, Greece, in accordance to the National Registration (Presidential Decree 56/2013) in harmonization to the European Directive 63/2010.

6. References

1. Petruzzelli, M., Schweiger, M., Schreiber, R., Campos-Olivas, R., Tsoli, M., Allen, J., Swarbrick, M., Rose-John, S., Rincon, M., Robertson, G., et al. A switch from white to brown fat increases energy expenditure in cancer-associated cachexia. *Cell Metab* 20:433-447.
2. Nishimura, S., Manabe, I., Nagasaki, M., Eto, K., Yamashita, H., Ohsugi, M., Otsu, M., Hara, K., Ueki, K., Sugiura, S., et al. 2009. CD8+ effector T cells contribute to macrophage recruitment and adipose tissue inflammation in obesity. *Nat Med* 15:914-920.
3. Feuerer, M., Herrero, L., Cipolletta, D., Naaz, A., Wong, J., Nayer, A., Lee, J., Goldfine, A.B., Benoist, C., Shoelson, S., et al. 2009. Lean, but not obese, fat is enriched for a unique population of regulatory T cells that affect metabolic parameters. *Nat Med* 15:930-939.
4. Wu, J., Bostrom, P., Sparks, L.M., Ye, L., Choi, J.H., Giang, A.H., Khandekar, M., Virtanen, K.A., Nuutila, P., Schaart, G., et al. 2012. Beige adipocytes are a distinct type of thermogenic fat cell in mouse and human. *Cell* 150:366-376.
5. Ishibashi, J., and Seale, P. 2010. Medicine. Beige can be slimming. *Science* 328:1113-1114.
6. Harms, M., and Seale, P. 2013. Brown and beige fat: development, function and therapeutic potential. *Nat Med* 19:1252-1263.
7. Shabalina, I.G., Petrovic, N., de Jong, J.M., Kalinovich, A.V., Cannon, B., and Nedergaard, J. 2013. UCP1 in brite/beige adipose tissue mitochondria is functionally thermogenic. *Cell Rep* 5:1196-1203.
8. Nguyen, K.D., Qiu, Y., Cui, X., Goh, Y.P., Mwangi, J., David, T., Mukundan, L., Brombacher, F., Locksley, R.M., and Chawla, A. 2011. Alternatively activated macrophages produce catecholamines to sustain adaptive thermogenesis. *Nature* 480:104-108.
9. Qiu, Y., Nguyen, K.D., Odegaard, J.I., Cui, X., Tian, X., Locksley, R.M., Palmiter, R.D., and Chawla, A. 2014. Eosinophils and type 2 cytokine signaling in macrophages orchestrate development of functional beige fat. *Cell* 157:1292-1308.
10. Rao, R.R., Long, J.Z., White, J.P., Svensson, K.J., Lou, J., Lokurkar, I., Jedrychowski, M.P., Ruas, J.L., Wrann, C.D., Lo, J.C., et al. 2014. Meteorin-like is a hormone that regulates immune-adipose interactions to increase beige fat thermogenesis. *Cell* 157:1279-1291.

11. Schulz, T.J., Huang, P., Huang, T.L., Xue, R., McDougall, L.E., Townsend, K.L., Cypess, A.M., Mishina, Y., Gussoni, E., and Tseng, Y.H. 2013. Brown-fat paucity due to impaired BMP signalling induces compensatory browning of white fat. *Nature* 495:379-383.
12. Cohen, P., Levy, J.D., Zhang, Y., Frontini, A., Kolodin, D.P., Svensson, K.J., Lo, J.C., Zeng, X., Ye, L., Khandekar, M.J., et al. 2014. Ablation of PRDM16 and beige adipose causes metabolic dysfunction and a subcutaneous to visceral fat switch. *Cell* 156:304-316.
13. Lee, M.W., Odegaard, J.I., Mukundan, L., Qiu, Y., Molofsky, A.B., Nussbaum, J.C., Yun, K., Locksley, R.M., and Chawla, A. 2015. Activated type 2 innate lymphoid cells regulate beige fat biogenesis. *Cell* 160:74-87.
14. Shen, J., Ren, H., Tomiyama-Miyaji, C., Watanabe, M., Kainuma, E., Inoue, M., Kuwano, Y., and Abo, T. 2009. Resistance and augmentation of innate immunity in mice exposed to starvation. *Cell Immunol* 259:66-73.
15. Martin, S.A., Douglas, A., Houlihan, D.F., and Secombes, C.J. 2010. Starvation alters the liver transcriptome of the innate immune response in Atlantic salmon (Salmo salar). *BMC Genomics* 11:418.
16. Lim, S., Honek, J., Xue, Y., Seki, T., Cao, Z., Andersson, P., Yang, X., Hosaka, K., and Cao, Y. 2012. Cold-induced activation of brown adipose tissue and adipose angiogenesis in mice. *Nat Protoc* 7:606-615.
17. Talukdar, S., Oh da, Y., Bandyopadhyay, G., Li, D., Xu, J., McNelis, J., Lu, M., Li, P., Yan, Q., Zhu, Y., et al. 2012. Neutrophils mediate insulin resistance in mice fed a high-fat diet through secreted elastase. *Nat Med* 18:1407-1412.
18. Winer, S., Chan, Y., Paltser, G., Truong, D., Tsui, H., Bahrami, J., Dorfman, R., Wang, Y., Zielenski, J., Mastronardi, F., et al. 2009. Normalization of obesity-associated insulin resistance through immunotherapy. *Nat Med* 15:921-929.
19. Liu, J., Divoux, A., Sun, J., Zhang, J., Clement, K., Glickman, J.N., Sukhova, G.K., Wolters, P.J., Du, J., Gorgun, C.Z., et al. 2009. Genetic deficiency and pharmacological stabilization of mast cells reduce diet-induced obesity and diabetes in mice. *Nat Med* 15:940-945.
20. Lumeng, C.N., Bodzin, J.L., and Saltiel, A.R. 2007. Obesity induces a phenotypic switch in adipose tissue macrophage polarization. *J Clin Invest* 117:175-184.
21. Cipolletta, D., Feuerer, M., Li, A., Kamei, N., Lee, J., Shoelson, S.E., Benoist, C., and Mathis, D. 2012. PPAR-gamma is a major driver of the accumulation and phenotype of adipose tissue Treg cells. *Nature* 486:549-553.
22. Lynch, L., Nowak, M., Varghese, B., Clark, J., Hogan, A.E., Toxavidis, V., Balk, S.P., O'Shea, D., O'Farrelly, C., and Exley, M.A. 2012 Adipose tissue invariant NKT cells protect against diet-induced obesity and metabolic disorder through regulatory cytokine production. *Immunity* 37:574-587.
23. Molofsky, A.B., Nussbaum, J.C., Liang, H.E., Van Dyken, S.J., Cheng, L.E., Mohapatra, A., Chawla, A., and Locksley, R.M. 2013. Innate

lymphoid type 2 cells sustain visceral adipose tissue eosinophils and alternatively activated macrophages. *J Exp Med* 210:535-549.
24. Mantovani, A., Cassatella, M.A., Costantini, C., and Jaillon, S. 2011 Neutrophils in the activation and regulation of innate and adaptive immunity. *Nat Rev Immunol* 11:519-531.
25. Pham, C.T. 2006. Neutrophil serine proteases: specific regulators of inflammation. *Nat Rev Immunol* 6:541-550.
26. Martin, L.B., Kita, H., Leiferman, K.M., and Gleich, G.J. 1996. Eosinophils in allergy: role in disease, degranulation, and cytokines. *Int Arch Allergy Immunol* 109:207-215.
27. Zu, L., He, J., Jiang, H., Xu, C., Pu, S., and Xu, G. 2009. Bacterial endotoxin stimulates adipose lipolysis via toll-like receptor 4 and extracellular signal-regulated kinase pathway. *J Biol Chem* 284:5915-5926.
28. Hotamisligil, G.S., and Erbay, E. 2008. Nutrient sensing and inflammation in metabolic diseases. *Nat Rev Immunol* 8:923-934.
29. Wu, D., Molofsky, A.B., Liang, H.E., Ricardo-Gonzalez, R.R., Jouihan, H.A., Bando, J.K., Chawla, A., and Locksley, R.M. 2011. Eosinophils sustain adipose alternatively activated macrophages associated with glucose homeostasis. *Science* 332:243-247.
30. Moro, K., Yamada, T., Tanabe, M., Takeuchi, T., Ikawa, T., Kawamoto, H., Furusawa, J., Ohtani, M., Fujii, H., and Koyasu, S. 2010 Innate production of T(H)2 cytokines by adipose tissue-associated c-Kit(+)Sca-1(+) lymphoid cells. *Nature* 463:540-544.
31. Spits, H., and Di Santo, J.P. The expanding family of innate lymphoid cells: regulators and effectors of immunity and tissue remodeling. *Nat Immunol* 12:21-27.
32. Walker, J.A., Barlow, J.L., and McKenzie, A.N. 2013. Innate lymphoid cells--how did we miss them? *Nat Rev Immunol* 13:75-87.
33. Veldhoen, M., and Withers, D.R. 2010. Immunology. Innate lymphoid cell relations. *Science* 330:594-595.
34. Spits, H., and Cupedo, T. 2012. Innate lymphoid cells: emerging insights in development, lineage relationships, and function. *Annu Rev Immunol* 30:647-675.
35. Liang, H.E., Reinhardt, R.L., Bando, J.K., Sullivan, B.M., Ho, I.C., and Locksley, R.M. 2011. Divergent expression patterns of IL-4 and IL-13 define unique functions in allergic immunity. *Nat Immunol* 13:58-66.
36. Chang, Y.J., Kim, H.Y., Albacker, L.A., Baumgarth, N., McKenzie, A.N., Smith, D.E., Dekruyff, R.H., and Umetsu, D.T. 2011. Innate lymphoid cells mediate influenza-induced airway hyper-reactivity independently of adaptive immunity. *Nat Immunol* 12:631-638.
37. Lanier, L.L. 2013. Shades of grey--the blurring view of innate and adaptive immunity. *Nat Rev Immunol* 13:73-74.
38. Spits, H., and Di Santo, J.P. 2011. The expanding family of innate lymphoid cells: regulators and effectors of immunity and tissue remodeling. *Nat Immunol* 12:21-27.
39. Hurst, S.D., Muchamuel, T., Gorman, D.M., Gilbert, J.M., Clifford, T., Kwan, S., Menon, S., Seymour, B., Jackson, C., Kung, T.T., et al. 2002. New IL-17 family members promote Th1 or Th2 responses in the

lung: in vivo function of the novel cytokine IL-25. *J Immunol* 169:443-453.
40. Miller, A.M., Asquith, D.L., Hueber, A.J., Anderson, L.A., Holmes, W.M., McKenzie, A.N., Xu, D., Sattar, N., McInnes, I.B., and Liew, F.Y. 2010 Interleukin-33 induces protective effects in adipose tissue inflammation during obesity in mice. *Circ Res* 107:650-658.
41. Zheng, Y., and Rudensky, A.Y. 2007. Foxp3 in control of the regulatory T cell lineage. *Nat Immunol* 8:457-462.
42. Sakaguchi, S., Yamaguchi, T., Nomura, T., and Ono, M. 2008. Regulatory T cells and immune tolerance. *Cell* 133:775-787.
43. Brigl, M., and Brenner, M.B. 2004. CD1: antigen presentation and T cell function. *Annu Rev Immunol* 22:817-890.
44. Matsuda, J.L., Naidenko, O.V., Gapin, L., Nakayama, T., Taniguchi, M., Wang, C.R., Koezuka, Y., and Kronenberg, M. 2000. Tracking the response of natural killer T cells to a glycolipid antigen using CD1d tetramers. *J Exp Med* 192:741-754.
45. Bendelac, A., Savage, P.B., and Teyton, L. 2007. The biology of NKT cells. *Annu Rev Immunol* 25:297-336.
46. Berzins, S.P., Smyth, M.J., and Baxter, A.G. 2011. Presumed guilty: natural killer T cell defects and human disease. *Nat Rev Immunol* 11:131-142.
47. Swann, J.B., Coquet, J.M., Smyth, M.J., and Godfrey, D.I. 2007. CD1-restricted T cells and tumor immunity. *Curr Top Microbiol Immunol* 314:293-323.
48. Wu, L., and Van Kaer, L. 2009. Natural killer T cells and autoimmune disease. *Curr Mol Med* 9:4-14.
49. Lynch, L., O'Shea, D., Winter, D.C., Geoghegan, J., Doherty, D.G., and O'Farrelly, C. 2009. Invariant NKT cells and CD1d(+) cells amass in human omentum and are depleted in patients with cancer and obesity. *Eur J Immunol* 39:1893-1901.
50. Martin-Murphy, B.V., You, Q., Wang, H., De La Houssaye, B.A., Reilly, T.P., Friedman, J.E., and Ju, C. 2014. Mice lacking natural killer T cells are more susceptible to metabolic alterations following high fat diet feeding. *PLoS One* 9:e80949.
51. Odegaard, J.I., and Chawla, A. 2013. The immune system as a sensor of the metabolic state. *Immunity* 38:644-654.
52. Tchkonia, T., Thomou, T., Zhu, Y., Karagiannides, I., Pothoulakis, C., Jensen, M.D., and Kirkland, J.L. 2013. Mechanisms and metabolic implications of regional differences among fat depots. *Cell Metab* 17:644-656.
53. Himms-Hagen, J., Melnyk, A., Zingaretti, M.C., Ceresi, E., Barbatelli, G., and Cinti, S. 2000. Multilocular fat cells in WAT of CL-316243-treated rats derive directly from white adipocytes. *Am J Physiol Cell Physiol* 279:C670-681.
54. Wang, Q.A., Tao, C., Gupta, R.K., and Scherer, P.E. 2013. Tracking adipogenesis during white adipose tissue development, expansion and regeneration. *Nat Med* 19:1338-1344.
55. Seale, P., Bjork, B., Yang, W., Kajimura, S., Chin, S., Kuang, S., Scime, A., Devarakonda, S., Conroe, H.M., Erdjument-Bromage, H., et

al. 2008. PRDM16 controls a brown fat/skeletal muscle switch. *Nature* 454:961-967.
56. Fedorenko, A., Lishko, P.V., and Kirichok, Y. 2012. Mechanism of fatty-acid-dependent UCP1 uncoupling in brown fat mitochondria. *Cell* 151:400-413.
57. Barbera, M.J., Schluter, A., Pedraza, N., Iglesias, R., Villarroya, F., and Giralt, M. 2001. Peroxisome proliferator-activated receptor alpha activates transcription of the brown fat uncoupling protein-1 gene. A link between regulation of the thermogenic and lipid oxidation pathways in the brown fat cell. *J Biol Chem* 276:1486-1493.
58. Gaudet, A.D., Fonken, L.K., Gushchina, L.V., Aubrecht, T.G., Maurya, S.K., Periasamy, M., Nelson, R.J., and Popovich, P.G. miR-155 Deletion in Female Mice Prevents Diet-Induced Obesity. *Sci Rep* 6:22862.
59. Bostrom, P., Wu, J., Jedrychowski, M.P., Korde, A., Ye, L., Lo, J.C., Rasbach, K.A., Bostrom, E.A., Choi, J.H., Long, J.Z., et al. 2012. A PGC1-alpha-dependent myokine that drives brown-fat-like development of white fat and thermogenesis. *Nature* 481:463-468.
60. Tseng, Y.H., Kokkotou, E., Schulz, T.J., Huang, T.L., Winnay, J.N., Taniguchi, C.M., Tran, T.T., Suzuki, R., Espinoza, D.O., Yamamoto, Y., et al. 2008. New role of bone morphogenetic protein 7 in brown adipogenesis and energy expenditure. *Nature* 454:1000-1004.
61. Bordicchia, M., Liu, D., Amri, E.Z., Ailhaud, G., Dessi-Fulgheri, P., Zhang, C., Takahashi, N., Sarzani, R., and Collins, S. 2012. Cardiac natriuretic peptides act via p38 MAPK to induce the brown fat thermogenic program in mouse and human adipocytes. *J Clin Invest* 122:1022-1036.
62. Neinast, M.D., Frank, A.P., Zechner, J.F., Li, Q., Vishvanath, L., Palmer, B.F., Aguirre, V., Gupta, R.K., and Clegg, D.J. 2015. Activation of natriuretic peptides and the sympathetic nervous system following Roux-en-Y gastric bypass is associated with gonadal adipose tissues browning. *Mol Metab* 4:427-436.
63. Cannon, B., and Nedergaard, J. 2011. Nonshivering thermogenesis and its adequate measurement in metabolic studies. *J Exp Biol* 214:242-253.
64. Morrison, S.F., Nakamura, K., and Madden, C.J. 2008. Central control of thermogenesis in mammals. *Exp Physiol* 93:773-797.
65. Ye, L., Wu, J., Cohen, P., Kazak, L., Khandekar, M.J., Jedrychowski, M.P., Zeng, X., Gygi, S.P., and Spiegelman, B.M. 2013. Fat cells directly sense temperature to activate thermogenesis. *Proc Natl Acad Sci U S A* 110:12480-12485.
66. Molofsky, A.B., Van Gool, F., Liang, H.E., Van Dyken, S.J., Nussbaum, J.C., Lee, J., Bluestone, J.A., and Locksley, R.M. 2015 Interleukin-33 and Interferon-gamma Counter-Regulate Group 2 Innate Lymphoid Cell Activation during Immune Perturbation. *Immunity* 43:161-174.
67. O'Sullivan, T.E., Rapp, M., Fan, X., Weizman, O.E., Bhardwaj, P., Adams, N.M., Walzer, T., Dannenberg, A.J., and Sun, J.C. Adipose-Resident Group 1 Innate Lymphoid Cells Promote Obesity-Associated Insulin Resistance. *Immunity* 45:428-441.

68. Ye, D.W., Rong, X.L., Xu, A.M., and Guo, J. Liver-adipose tissue crosstalk: A key player in the pathogenesis of glucolipid metabolic disease. *Chin J Integr Med* 23:410-414.
69. Huang, H.W., Zuo, C., Chen, X., Peng, Y.P., and Qiu, Y.H. 2016. Effect of tyrosine hydroxylase overexpression in lymphocytes on the differentiation and function of T helper cells. *Int J Mol Med* 38:635-642.
70. Wolf, Y., Boura-Halfon, S., Cortese, N., Haimon, Z., Sar Shalom, H., Kuperman, Y., Kalchenko, V., Brandis, A., David, E., Segal-Hayoun, Y., et al. Brown-adipose-tissue macrophages control tissue innervation and homeostatic energy expenditure. *Nat Immunol* 18:665-674.
71. Brestoff, J.R., Kim, B.S., Saenz, S.A., Stine, R.R., Monticelli, L.A., Sonnenberg, G.F., Thome, J.J., Farber, D.L., Lutfy, K., Seale, P., et al. 2014. Group 2 innate lymphoid cells promote beiging of white adipose tissue and limit obesity. *Nature* 519:242-246.
72. Fischer Katrin, H.H.R., Kevin Jhun 2017. Alternatively activated macrophages do not synthesize catecholamines or contribute to adipose tissue adaptive thermogenesis. *Nature Medicine* 23:623-630.
73. Duffaut, C., Zakaroff-Girard, A., Bourlier, V., Decaunes, P., Maumus, M., Chiotasso, P., Sengenes, C., Lafontan, M., Galitzky, J., and Bouloumie, A. 2009. Interplay between human adipocytes and T lymphocytes in obesity: CCL20 as an adipochemokine and T lymphocytes as lipogenic modulators. *Arterioscler Thromb Vasc Biol* 29:1608-1614.
74. Kintscher, U., Hartge, M., Hess, K., Foryst-Ludwig, A., Clemenz, M., Wabitsch, M., Fischer-Posovszky, P., Barth, T.F., Dragun, D., Skurk, T., et al. 2008. T-lymphocyte infiltration in visceral adipose tissue: a primary event in adipose tissue inflammation and the development of obesity-mediated insulin resistance. *Arterioscler Thromb Vasc Biol* 28:1304-1310.
75. O'Rourke, R.W., Metcalf, M.D., White, A.E., Madala, A., Winters, B.R., Maizlin, II, Jobe, B.A., Roberts, C.T., Jr., Slifka, M.K., and Marks, D.L. 2009. Depot-specific differences in inflammatory mediators and a role for NK cells and IFN-gamma in inflammation in human adipose tissue. *Int J Obes (Lond)* 33:978-990.
76. Rocha, V.Z., Folco, E.J., Sukhova, G., Shimizu, K., Gotsman, I., Vernon, A.H., and Libby, P. 2008. Interferon-gamma, a Th1 cytokine, regulates fat inflammation: a role for adaptive immunity in obesity. *Circ Res* 103:467-476.
77. McGillicuddy, F.C., Chiquoine, E.H., Hinkle, C.C., Kim, R.J., Shah, R., Roche, H.M., Smyth, E.M., and Reilly, M.P. 2009. Interferon gamma attenuates insulin signaling, lipid storage, and differentiation in human adipocytes via activation of the JAK/STAT pathway. *J Biol Chem* 284:31936-31944.
78. Rocha, A.M., Souza, C., Rocha, G.A., de Melo, F.F., Clementino, N.C., Marino, M.C., and Queiroz, D.M. The serum levels of the cytokines involved in the Th17 and Th1 cell commitment are increased in individuals with borderline thrombocytopenia. *J Hematol Oncol* 6:28.
79. Jiao, Y., Huntington, N.D., Belz, G.T., and Seillet, C. Type 1 Innate Lymphoid Cell Biology: Lessons Learnt from Natural Killer Cells. *Front Immunol* 7:426.

80. Cosentino, M., Zaffaroni, M., Ferrari, M., Marino, F., Bombelli, R., Rasini, E., Frigo, G., Ghezzi, A., Comi, G., and Lecchini, S. 2005. Interferon-gamma and interferon-beta affect endogenous catecholamines in human peripheral blood mononuclear cells: implications for multiple sclerosis. *J Neuroimmunol* 162:112-121.
81. Donath, M.Y., and Shoelson, S.E. Type 2 diabetes as an inflammatory disease. *Nat Rev Immunol* 11:98-107.
82. Cavelti-Weder, C., Babians-Brunner, A., Keller, C., Stahel, M.A., Kurz-Levin, M., Zayed, H., Solinger, A.M., Mandrup-Poulsen, T., Dinarello, C.A., and Donath, M.Y. Effects of gevokizumab on glycemia and inflammatory markers in type 2 diabetes. *Diabetes Care* 35:1654-1662.
83. Stanley, T.L., Zanni, M.V., Johnsen, S., Rasheed, S., Makimura, H., Lee, H., Khor, V.K., Ahima, R.S., and Grinspoon, S.K. TNF-alpha antagonism with etanercept decreases glucose and increases the proportion of high molecular weight adiponectin in obese subjects with features of the metabolic syndrome. *J Clin Endocrinol Metab* 96:E146-150.
84. Pierce, J.W., Read, M.A., Ding, H., Luscinskas, F.W., and Collins, T. 1996. Salicylates inhibit I kappa B-alpha phosphorylation, endothelial-leukocyte adhesion molecule expression, and neutrophil transmigration. *J Immunol* 156:3961-3969.
85. Yuan, M., Konstantopoulos, N., Lee, J., Hansen, L., Li, Z.W., Karin, M., and Shoelson, S.E. 2001. Reversal of obesity- and diet-induced insulin resistance with salicylates or targeted disruption of Ikkbeta. *Science* 293:1673-1677.
86. Hauner, H. 2002. The mode of action of thiazolidinediones. *Diabetes Metab Res Rev* 18 Suppl 2:S10-15.
87. Hundal, R.S., Petersen, K.F., Mayerson, A.B., Randhawa, P.S., Inzucchi, S., Shoelson, S.E., and Shulman, G.I. 2002. Mechanism by which high-dose aspirin improves glucose metabolism in type 2 diabetes. *J Clin Invest* 109:1321-1326.
88. Wolf, M.J., Adili, A., Piotrowitz, K., Abdullah, Z., Boege, Y., Stemmer, K., Ringelhan, M., Simonavicius, N., Egger, M., Wohlleber, D., et al. 2014. Metabolic Activation of Intrahepatic CD8(+) T Cells and NKT Cells Causes Nonalcoholic Steatohepatitis and Liver Cancer via Cross-Talk with Hepatocytes. *Cancer Cell* 26:549-564.

JCI insight

CD8+ T cells in beige adipogenesis and energy homeostasis

Maria Moysidou, … , Triantafyllos Chavakis, Katia P. Karalis

JCI Insight. 2018;3(5):e95456. https://doi.org/10.1172/jci.insight.95456.

Research Article Metabolism

Although accumulation of lymphocytes in the white adipose tissue (WAT) in obesity is linked to insulin resistance, it remains unclear whether lymphocytes also participate in the regulation of energy homeostasis in the WAT. Here, we demonstrate enhanced energy dissipation in Rag1$^{-/-}$ mice, increased catecholaminergic input to subcutaneous WAT, and significant beige adipogenesis. Adoptive transfer experiments demonstrated that CD8$^+$ T cell deficiency accounts for the enhanced beige adipogenesis in Rag1$^{-/-}$ mice. Consistently, we identified that CD8$^{-/-}$ mice also presented with enhanced beige adipogenesis. The inhibitory effect of CD8$^+$ T cells on beige adipogenesis was reversed by blockade of IFN-γ. All together, our findings identify an effect of CD8$^+$ T cells in regulating energy dissipation in lean WAT, mediated by IFN-γ modulation of the abundance of resident immune cells and of local catecholaminergic activity. Our results provide a plausible explanation for the clinical signs of metabolic dysfunction in diseases characterized by altered CD8$^+$ T cell abundance and suggest targeting of CD8$^+$ T cells as a promising therapeutic approach for obesity and other diseases with altered energy homeostasis.

JCI insight

RESEARCH ARTICLE

CD8+ T cells in beige adipogenesis and energy homeostasis

Maria Moysidou,[1,2] Sevasti Karaliota,[1] Elisavet Kodela,[1,2] Maria Salagianni,[1] Yassemi Koutmani,[1] Antonia Katsouda,[1] Konstantia Kodella,[1] Panagiotis Tsakanikas,[1] Styliani Ourailidou,[1] Evangelos Andreakos,[1] Nikolaos Kostomitsopoulos,[1] Dimitris Skokos,[3] Antonios Chatzigeorgiou,[4] Kyoung-Jin Chung,[4] Stefan Bornstein,[4] Mark W. Sleeman,[5] Triantafyllos Chavakis,[4] and Katia P. Karalis[1,4,6]

[1]Clinical, Experimental Surgery & Translational Research, Biomedical Research Foundation Academy of Athens, Athens, Greece. [2]University of Crete, School of Medicine, Heraklion, Crete, Greece. [3]Regeneron Pharmaceuticals Inc., Tarrytown, New York, USA. [4]Technische Universität Dresden, School of Medicine, Dresden, Germany. [5]Department of Physiology, Monash University, Clayton, Victoria, Australia. [6]Endocrine Division, Boston Children's Hospital, Boston, Massachusetts, USA.

Although accumulation of lymphocytes in the white adipose tissue (WAT) in obesity is linked to insulin resistance, it remains unclear whether lymphocytes also participate in the regulation of energy homeostasis in the WAT. Here, we demonstrate enhanced energy dissipation in Rag1$^{-/-}$ mice, increased catecholaminergic input to subcutaneous WAT, and significant beige adipogenesis. Adoptive transfer experiments demonstrated that CD8$^+$ T cell deficiency accounts for the enhanced beige adipogenesis in Rag1$^{-/-}$ mice. Consistently, we identified that CD8$^{-/-}$ mice also presented with enhanced beige adipogenesis. The inhibitory effect of CD8$^+$ T cells on beige adipogenesis was reversed by blockade of IFN-γ. All together, our findings identify an effect of CD8$^+$ T cells in regulating energy dissipation in lean WAT, mediated by IFN-γ modulation of the abundance of resident immune cells and of local catecholaminergic activity. Our results provide a plausible explanation for the clinical signs of metabolic dysfunction in diseases characterized by altered CD8$^+$ T cell abundance and suggest targeting of CD8$^+$ T cells as a promising therapeutic approach for obesity and other diseases with altered energy homeostasis.

Introduction

Obesity, a major epidemic with prevalence rates rising steadily among adults and children worldwide, is characterized by excessive accumulation of white adipose tissue (WAT). Obesity is normally associated with the development of a low-grade inflammatory response within WAT, attributed initially to the infiltration of macrophages in the adipose tissue as well as a shift in macrophage polarization (1). Additionally, further cells of innate and adaptive immunity, such as mast cells (2), eosinophils (3), neutrophils (4), type 2 innate lymphoid cells (ILC2s) (5), and CD4$^+$ (6) and CD8$^+$ T cells (7) as well as Tregs (8, 9), have been implicated as either positive or negative regulators of adipose tissue function and of insulin resistance. A major feature of the adipose tissue is its inherent capacity to act as an energy storage and/or energy dissipation site (10). This dual function has been linked to the distinct WAT and brown adipose tissue (BAT) depots respectively, and the high expression of the mitochondrial uncoupling protein 1 (Ucp1) in the latter (11, 12). A series of recent studies identified multilocular cells with energy-dispensing activity, named "beige" adipocytes (13–16), within the subcutaneous WAT (scWAT). Beige adipocytes may derive either from PDGFRα$^+$, Sca1$^+$, and CD34$^+$ precursor cells (17) or via transdifferentiation of white adipocytes (18, 19). Beige adipocytes (15, 16), similar to the brown adipocytes, express Ucp1, are expanded in response to challenges such as cold exposure, and, when activated, increase fatty acid oxidation (20). Recent findings indicate that, in adult humans, what has been thought as brown fat is more likely formed by beige, rather than brown, adipocytes (16), confirming the significance of beige adipose depot in adulthood. As shown, induction of adipose tissue thermogenesis and/or browning of white fat promote efficient whole-body energy expenditure (21). Emerging evidence suggests novel roles for innate immune cells in regulating energy dissipation via the scWAT (22–24). More importantly, increased numbers of ILC2s in the scWAT have been shown to promote beiging by stimulating the proliferation of PDGFRα$^+$ progenitors via secretion of the interleukins IL-5 and -13 (17). Eosinophils have

Authorship note: MM and SK are co–first authors.

Conflict of interest: The authors have declared that no conflict of interest exists.

Submitted: May 31, 2017
Accepted: February 1, 2018
Published: March 8, 2018

Reference information:
JCI Insight. 2018;3(5):e95456.
https://doi.org/10.1172/jci.insight.95456.

been shown to interact with M2-like macrophages in promoting beige adipogenesis as well (22, 24), while M1 macrophages inhibit scWAT beiging in obesity (25, 26). On the contrary, nothing has been reported so far about a function of lymphocytes on beige adipogenesis, which is the subject of the present work.

In this study, we demonstrate increased beige adipogenesis in the scWAT of Rag1$^{-/-}$ lymphocyte-deficient mice accompanied by increased efficiency in lipid utilization in their WAT depots. We also show that the major immune cell type driving the development of this phenotype is the CD8$^+$ T cell. We provide evidence that CD8$^+$ T cells can modify the catecholaminergic activity of WAT and affect the number of ILCs and eosinophils as well as the cytokines involved in regulating their functions. Our findings suggest that these effects of the CD8$^+$ T cells are mediated via secreted factors and, particularly, IFN-γ. Overall, our study highlights the important role of lymphocytes in the regulation of beige adipose tissue formation via direct interaction with cells of innate immunity and modulation of the catecholaminergic activity.

Results

Lymphocyte deficiency induces beige adipogenesis. Given the emerging evidence on the role of immune cells in the regulation of metabolism, we first assessed the potential effects of lymphocyte deficiency in systemic metabolic activity. To this end, we performed indirect calorimetry in age- and weight-matched Rag1$^{-/-}$ and WT male mice, using a comprehensive laboratory animal monitoring system (CLAMS). To our surprise, Rag1$^{-/-}$ mice dissipated more energy than WT mice, despite their similar eating and motor behaviors (Figure 1, A–C, and Supplemental Figure 1, A–C; supplemental material available online with this article; https://doi.org/10.1172/jci.insight.95456DS1). Additionally, the respiratory exchange ratio (RER) was found to be lower in Rag1$^{-/-}$ mice (Figure 1D and Supplemental Figure 1D), which was suggestive of an increased utilization of fatty acids as their energy substrate. In agreement, the epididymal WAT (epiWAT) was of lower weight in Rag1$^{-/-}$ mice (Supplemental Figure 1, E and F). Further, gene expression profiling revealed a significant shift in the expression of factors involved in lipid catabolism in the Rag1$^{-/-}$ epiWAT, indicating the impact of lymphocyte deficiency in the regulation of this process (Supplemental Figure 1G).

The increased energy expenditure that has been identified in the Rag1$^{-/-}$ mice raised the possibility for associated enhancement of brown and/or beige adipogenesis. Even though we found no differences between the Rag1$^{-/-}$ and WT BAT, as per weight, H&E analysis, or Ucp1 expression (Supplemental Figure 1, H–J), H&E staining of the scWAT identified substantially increased abundance of beige adipose tissue in Rag1$^{-/-}$, as compared with WT, biopsies (Figure 1E). In agreement, the expression of genes associated with beige adipogenesis, such as Ucp1, cell death–inducing DFFA-like effector a (Cidea), PR domain-containing 16 (Prdm16), and Fgf21 (Figure 1F) (13, 27), was significantly induced in the Rag1$^{-/-}$ scWAT. Finally, the weight of the Rag1$^{-/-}$ scWAT was significantly lower, in accordance with its higher content in small, energy-dissipating, rather than in large, primarily lipid-storing, adipocytes (Figure 1G). These findings suggest that lymphocyte deficiency promotes energy dissipation by inducing beige adipogenesis in the lipid-storing WAT, while it has no apparent effect on BAT, the primary thermogenic depot (12). A mechanistic insight on the increased formation of beige adipose tissue in the Rag1$^{-/-}$ mice was provided by the increased expression of the gene encoding the adrenergic receptor (AdR) 1α (AdR1α) and a similar trend for the AdRβ3 gene in the Rag1$^{-/-}$ scWAT (Figure 1F). Further, treatment of Rag1$^{-/-}$ mice with the selective α-1 AdR antagonist prazosin hydrochloride via the drinking water for 5 days led to reduced amounts of beige adipose tissue (Supplemental Figure 1K) and significant attenuation in the corresponding expression of Ucp1 and Prdm16 (Supplemental Figure 1L). Taken together, these results indicate that the increased beige adipogenesis in Rag1$^{-/-}$ mice is associated with induction of adrenergic activity, a physiologically relevant pathway, in the WAT depot (14).

To further confirm the specificity of the Rag1$^{-/-}$ scWAT phenotype, we repeated the experiment at thermoneutrality, i.e., at a housing temperature of 30°C (28). Following housing of all groups at thermoneutrality conditions for 20 days, Ucp1 expression decreased significantly in both WT and Rag1$^{-/-}$ mice (Figure 1H), as expected by the well-shown sensitivity of this factor to temperature changes (28–30). No differences in the weight of the scWAT were found between the two genotypes when housed in thermoneutrality conditions (data not shown). However, in Rag1$^{-/-}$ scWAT genes associated with beige adipogenesis, such as Cidea, were found to be at significantly higher levels as compared with the WT scWAT (Figure 1H). The latter is in line with the corresponding histological analysis that showed profound abundance of beige fat areas in the scWAT of the Rag1$^{-/-}$ mice (Figure 1I).

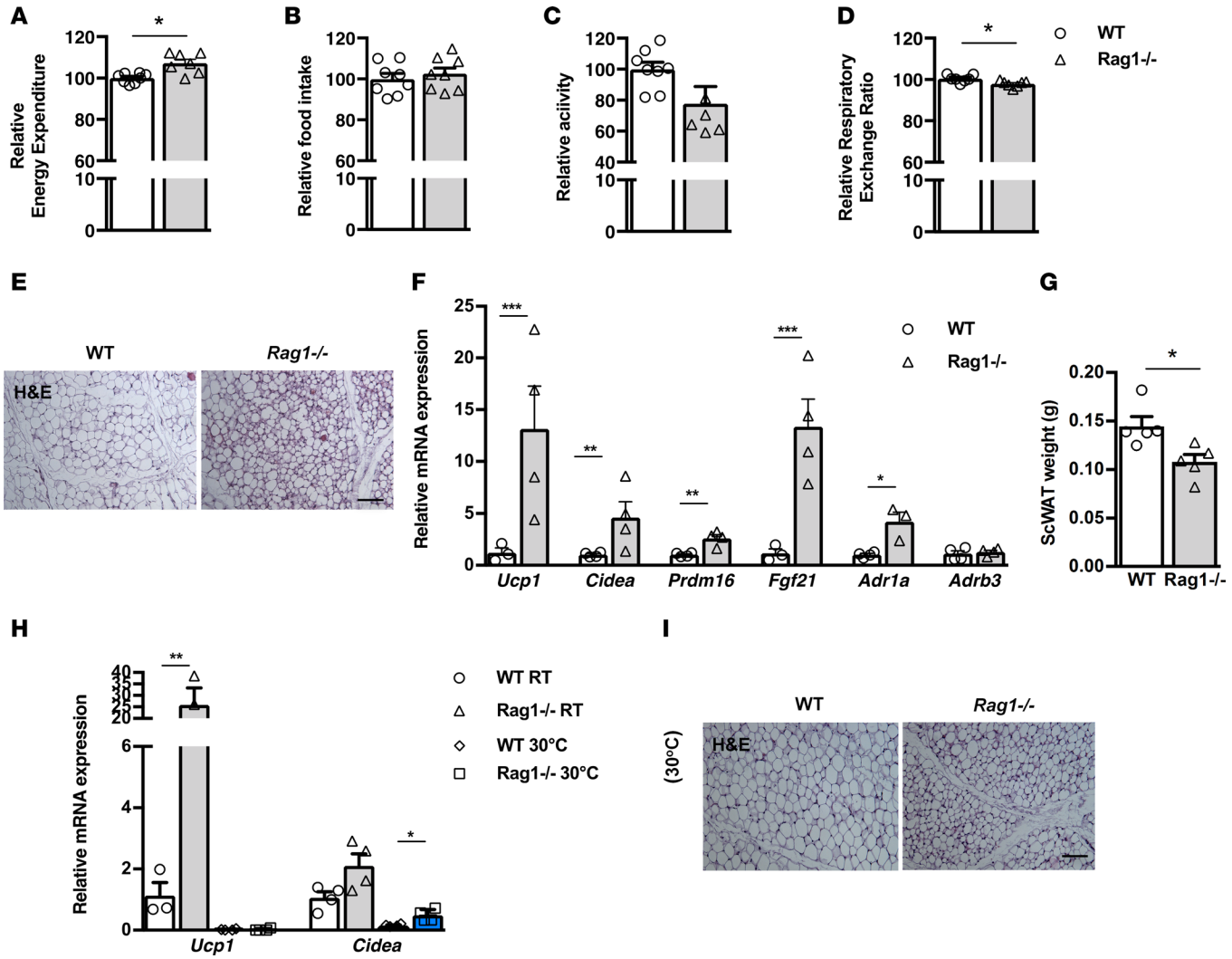

Figure 1. Beige tissue formation in the scWAT is increased in lymphocyte-deficient mice. (**A–D**) Assessment of metabolic behavior using indirect calorimetry, including energy expenditure adjusted to body weight (**A**), food intake (**B**), total activity (**C**), and respiratory exchange ratio (RER) (**D**). $n = 7$ per group. (**E**) Representative H&E-stained images of the scWAT depot of age- and weight-matched Rag1$^{-/-}$ and WT mice. Scale bar: 100 μm. (**F**) Gene expression analysis of thermogenic and adrenergic receptors. Data are shown as mean expression normalized to actin ± SEM. (**G**) Absolute weight of scWAT in age- and weight-matched WT and Rag1$^{-/-}$ mice. The data shown are derived from 1 representative of 3 independent experiments. (**H**) Gene expression analysis of Ucp1 and Cidea in WT and Rag1$^{-/-}$ mice to assess the effect of thermoneutrality, simulated by housing at 30°C for 20 days. Data are shown as mean expression normalized to actin ± SEM. (**I**) Representative H&E-stained images in the above groups. Scale bar: 100 μm. Data shown are derived from 1 representative of 2 independent experiments. Data are presented as mean ± SEM. $n \geq 4$ per group (**E–I**). *$P < 0.05$, **$P < 0.01$, ***$P < 0.001$, Student's t test.

Next, we sought to confirm that lymphocyte deficiency is indeed the primary underlying reason for the enhanced beige adipogenesis in Rag1$^{-/-}$ mice by reconstituting mice with splenocytes isolated from WT mice. This procedure reversed the phenotype of the Rag1$^{-/-}$ scWAT, as it resulted in significant elimination of the extent of the beige fat areas, resembling those found in the WT scWAT (Figure 2, A and B). Splenocyte reconstitution also led to increased adipocyte size (Figure 2C), an additional indication for the increase in energy storage, while it reduced the expression of thermogenic and lipid oxidation-related genes to levels comparable to those in the WT tissues (Figure 2D). The weight of WT scWAT was not altered, compared with the Rag1$^{-/-}$ tissue, following reconstitution with splenocytes (data not shown). Further, reconstitution of the Rag1$^{-/-}$ mice with splenocytes reduced the expression of TH, the rate-limiting step in catecholamine synthesis (Figure 2A) and of the AdR1α and AdRβ3 genes (Figure 2D). These data provide additional evidence for the link between lymphocyte deficiency and increased adrenergic activation.

CD8$^+$ T cell transfer abrogates beige adipogenesis in Rag1$^{-/-}$ mice. Next, we sought to identify the specific lymphocyte population missing in the Rag1$^{-/-}$ mice, possibly underlying the induction in their beige adi-

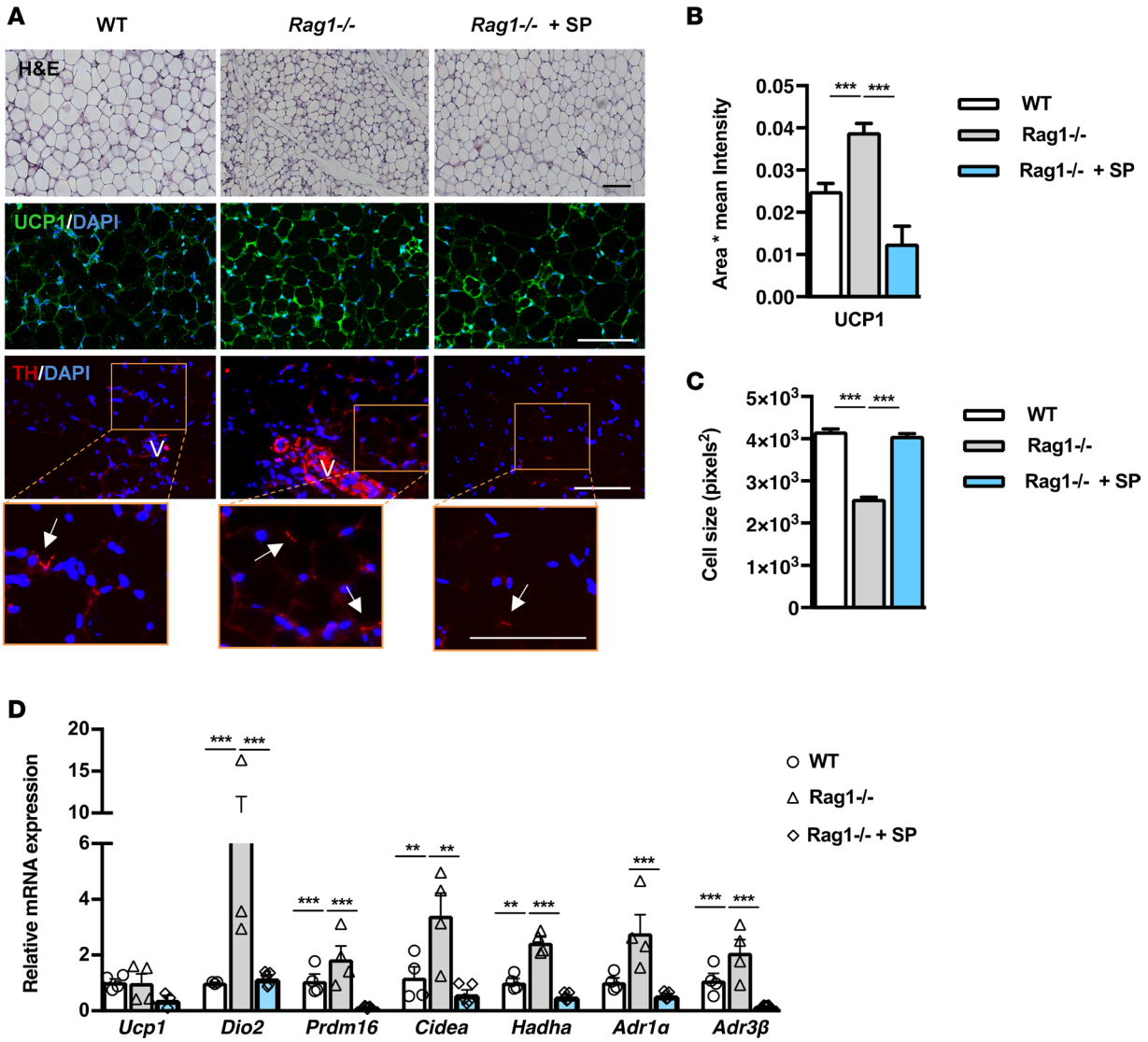

Figure 2. Adoptive transfer of whole splenocytes in Rag1$^{-/-}$ mice reverses the increased scWAT beiging. (**A**) Representative images of H&E and immunofluorescence (IF) staining for UCP1 or TH from WT, Rag1$^{-/-}$, or Rag1$^{-/-}$ mice reconstituted with 5×10^6 splenocytes, once a week for 2 weeks. Arrows represent the TH$^+$cells. V represents the vessels. Scale bar: 100 μm. (**B**) The relative UCP1 mean area and intensity in the above groups. Values represent the mean ± SD intensity of 15 patches for every image. $n = 3$ per group. (**C**) Relative scWAT adipocyte cell size of WT mice or Rag1$^{-/-}$ mice treated with PBS or adoptively transferred with splenocytes (5×10^6), once a week for 2 weeks. $n = 4$ per group. (**D**) Relative expression of beige, oxidation, and adrenergic receptors genes. Data are shown as mean expression normalized to actin ± SEM. $n = 5$ per group. Data are representative of 1 of 2 separate experiments. Data are presented as mean ± SEM. $^{**}P < 0.01$, $^{***}P < 0.001$. 1-way ANOVA with Bonferroni's post test.

pogenesis. Previous studies have described the contribution of the resident and/or infiltrated lymphocyte populations, including CD4$^+$ and CD8$^+$ T cells, to WAT biology (6, 7, 31). In particular, the CD8$^+$ T cells have been directly associated with lipid metabolism, as shown by their striking effects in promoting liver steatosis (32). We therefore assessed the effect of reconstitution of the Rag1$^{-/-}$ mice with CD8$^+$ T cells, on the beiging of their scWAT. CD8$^+$ T cells isolated from WT mouse splenocytes were transferred into Rag1$^{-/-}$ mice by retro-orbital administration. There was no difference in the weight of the scWAT between control Rag1$^{-/-}$ mice and those reconstituted with CD8$^+$ T cells (data not shown), while as expected, the abundance of CD8$^+$ T cells was substantially increased in the reconstituted scWAT (Supplemental Figure 2A). In line with the hypothesis attributing the increased beiging of the Rag1$^{-/-}$ scWAT to their lymphocyte deficiency, the reconstituted scWAT was characterized by attenuated beiging (Figure 3A). In line with this, reconstituted scWAT showed significantly compromised expression of AdR1α and AdRβ3 and of genes encoding proteins involved in thermogenesis, such as Ucp1, Cidea, Fgf21, and in lipid catabolism, such as Hadha and Lipe (Figure 3B). Upon reconstitution with CD8$^+$ T cells, the expression of UCP1 protein, the main protein

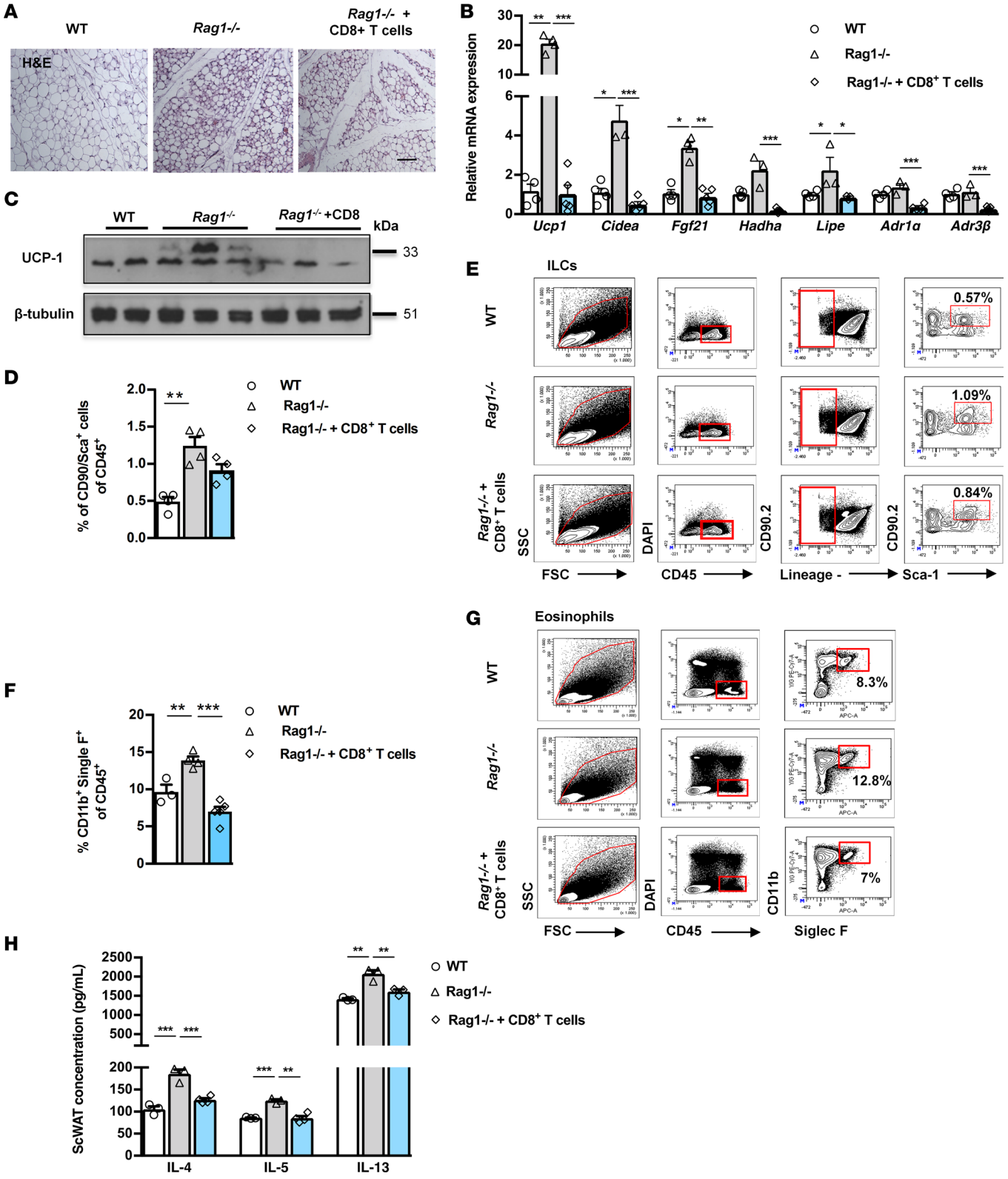

Figure 3. Adoptive transfer of CD8⁺ T cells in Rag1$^{-/-}$ mice reverses increased scWAT beiging in Rag1$^{-/-}$ mice and decreases ILCs and eosinophils. Data shown are from the scWAT of WT, Rag1$^{-/-}$, or Rag1$^{-/-}$ mice reconstituted with 5 × 10^6 CD8⁺ T cells, once a week for 2 weeks. (**A**) Representative H&E staining. Scale bar: 100 μm. n = 3 per group. (**B**) Expression of thermogenic, lipid metabolism, and adrenergic receptors genes. Data are shown as mean expression normalized to actin ± SEM. $n \geq 5$. Data shown are derived from 1 representative of 3 independent experiments (**C**) Protein expression of UCP1 and β-tubulin. (**D**) Percentage of ILCs (CD90.2⁺Sca-1⁺Lin⁻) gated on CD45⁺ cells. $n \geq 4$ per group. (**E**) Representative gating strategy for the identification of ILCs (CD90.2⁺ Sca-1⁺ Lin⁻). Percentage of CD90.2⁺Sca-1⁺Lin⁻ gated on the viable CD45⁺DAPI⁻ cells. Data shown are representative of 2 independent experiments. Flow cytometry was performed after pooling $n \geq 5$ mice per group. (**F**) Percentage of eosinophils gated (CD11b⁺Siglec F⁺) on the viable CD45⁺DAPI⁻ cells. $n \geq 4$ per group. (**G**) Representative gating strategy for identification of eosinophils (CD11b⁺Siglec F⁺). Percentage

of CD11b$^+$Siglec F$^+$ cells gated on the viable CD45$^+$DAPI$^-$ cells. Data shown are representative of 2 independent experiments. Flow cytometry was performed after pooling $n \geq 5$ mice per group. (**H**) Intra-scWAT levels of IL-4, IL-5, and IL-13. $n \geq 4$ per group. Data are presented as mean ± SEM. $^*P < 0.05$, $^{**}P < 0.01$, $^{***}P < 0.001$, 1-way ANOVA with Bonferroni's post test.

associated with beige adipogenesis, was dramatically reduced in the Rag1$^{-/-}$ scWAT (Figure 3C). The above findings argue for CD8$^+$ T cell deficiency as the potential driving mechanism behind the induction of energy dissipation in the Rag1$^{-/-}$ WAT.

Interaction between scWAT CD8$^+$ T cells and cells of innate immunity. As has been demonstrated in a number of studies, the relative abundance and the polarization of macrophages are both important determinants for the development of insulin resistance and the associated inflammatory features of obesity. The majority of adipose tissue macrophages in baseline conditions bear characteristics of "alternatively activated M2-like cells," while as obesity develops, "M1-like" proinflammatory macrophages become the predominant population (1). We detected no major differences in either the percentages or absolute numbers of CD11b$^+$ F4/80$^+$ cells expressed per gram of tissue of the scWAT between WT and Rag1$^{-/-}$ mice with or without reconstitution with CD8$^+$ T cells (Supplemental Figure 2, B and C). Further, we found no evidence for altered macrophage polarization in either of the experimental groups based on assessment of M1 and M2 markers (Supplemental Figure 2D). These data suggest that a shift or polarization in the scWAT macrophage content is unlikely to mediate the effects of lymphocyte deficiency on beige adipogenesis.

Emerging evidence demonstrates the specific contribution of particular components of type 2 immunity, like ILC2s and eosinophils, in the regulation of beige adipogenesis (3, 5). We sought to assess the potential link between these studies and our current findings by assessment of the effect of lymphocyte deficiency on the abundance of eosinophils and ILCs in the scWAT of WT, Rag1$^{-/-}$, and Rag1$^{-/-}$ mice reconstituted with CD8$^+$ T cells. Specifically, ILCs were defined as CD45$^+$, lineage$^-$ (CD3$^-$CD4$^-$CD8$^-$CD19$^-$B220$^-$ CD11b$^-$CD11c$^-$FceRI$^-$Gr-1$^-$Terr119$^-$), CD90.2$^+$Sca-1$^+$ cells. We found that the percentage of CD90$^+$Sca-1$^+$ cells gated on CD45$^+$ cells in Rag1$^{-/-}$ scWAT was significantly higher (1.244% ± 0.117%) than that of the WT scWAT (0.491% ± 0.061%) (Figure 3, D and E). Accordingly, the absolute numbers of ILCs (CD90.2$^+$Sca-1$^+$) per gram of tissue in the Rag1$^{-/-}$ scWAT were also significantly increased (Supplemental Figure 2E). A similar pattern was obtained in eosinophils, defined as CD45$^+$CD11b$^+$Siglec F$^+$ cells. Specifically, the percentage of eosinophils gated on CD45$^+$ cells (Figure 3, F and G) was higher in Rag1$^{-/-}$ scWAT (WT: 9.667% ± 0.953%; Rag1$^{-/-}$: 13.900% ± 0.521%), although the absolute numbers of eosinophils did not reach significantly different levels between the two genotypes (Supplemental Figure 2F).

Reconstitution of Rag1$^{-/-}$ mice with CD8$^+$ T cells reversed the expanded ILC (0.912% ± 0.081%) and eosinophil (7.000% ± 0.646%) populations to levels comparable to those detected in the WT scWAT (Figure 3, D–G, and Supplemental Figure 2, D and E). These findings indicate the dynamic relation between CD8$^+$ T and the cells of the innate immune system, further highlighted by the associated cytokines levels, such as IL-4 or IL-5 and IL-13, measured in the scWAT of the aforementioned experimental groups (Figure 3H). Along these lines, a recent report showed that the IL-33–induced ILC2s regulate energy homeostasis by increasing the energy expenditure via induction of beige adipogenesis (33), shown to be mediated by the intra-scWAT levels of IL-4, -5, and -13 (24, 33–35). Together, our findings provide evidence that in Rag1$^{-/-}$ scWAT enhanced activation of innate cells due to lack of CD8$^+$ T cells may account for their enhanced beige adipogenesis.

CD8$^+$ T cells block cold exposure–induced beige adipogenesis. Next, we asked if Rag1$^{-/-}$ mice retain their ability to respond to stimuli driving the beiging of scWAT, despite their already substantially expanded beige depot at baseline conditions (Figure 1). For this purpose, we exposed WT and Rag1$^{-/-}$ mice to cold via housing at 4°C, for a period of 2 days (16, 36). We found that Rag1$^{-/-}$ mice could adapt better to cold and thus resisted hypothermia more efficiently than WT mice, as depicted by the profiling of core body temperature over time (Figure 4A), while there were no differences between the WT and Rag1$^{-/-}$ scWAT weights (data not shown). Maintenance of homeostasis upon cold exposure is achieved by catecholamine-induced thermogenesis (16). Tyrosine hydroxylase (TH), the rate-limiting step in the biosynthesis of norepinephrine (37, 38) and a reliable routinely used marker for catecholaminergic neurons (19), was higher in the Rag1$^{-/-}$ scWAT upon exposure to cold (Figure 4B). We confirmed, by double immunofluorescent staining for TH and for the neuronal marker class III β-tubulin (Tuj1), that TH$^+$ cells in the scWAT are neuronal cells (39–43) by costaining with TH and the neuronal marker, Tuj1, of control (WT) scWAT sections (Supplemental Figure 3A). As expected, cold exposure led to significant induction of scWAT beiging and of corresponding Ucp1 expression in

both WT and Rag1$^{-/-}$ mice (Figure 4, B and C). The differences in the expression of other scWAT genes between WT and Rag1$^{-/-}$ mice were not as prominent as those detected in room temperature conditions (Figure 4C). Most importantly, the expression of UCP1 protein (Figure 4B and Supplemental Figure 3B) and TH remained substantially higher in the Rag1$^{-/-}$ scWAT (Figure 4B), highlighting the contribution of the lymphocyte deficiency to beige adipogenesis, even in states associated with excess beige fat development. All the above indicate that Rag1$^{-/-}$ mice retain their ability to respond to physiological challenges, such as cold, that drive beige adipogenesis, despite their constitutively increased beige adipogenesis.

The better adaptation of the Rag1$^{-/-}$ mice to cold exposure was attenuated by reconstitution with CD8^{+} T cells. Furthermore, this intervention reduced beige adipogenesis and decreased the expression of TH and the associated AdRs (Figure 4, A–C) in the scWAT of the Rag1$^{-/-}$ mice. However, the scWAT weight of reconstituted mice was not different compared with Rag1$^{-/-}$ mice (data not shown).

Next, we assessed the effect of cold exposure on the abundance of eosinophils and ILCs in the scWAT. Consistent with the above results, reconstitution of Rag1$^{-/-}$ mice with CD8^{+} T cells led to a significant reduction in the percentage of both eosinophils (11.150% ± 0.902%) and ILCs (1.265% ± 0.065%) gated on CD45^{+} cells, compared with those of the nontreated Rag1$^{-/-}$ mice (eosinophils: 17.150% ± 2.293%; ILCs:1.759% ± 0.189%) (Figure 4, D–G), while their absolute numbers did not display any significant difference (data not shown). At the same time, both eosinophils and ILCs were significantly higher in the cold-exposed Rag1$^{-/-}$ mice as compared with WT mice (eosinophils: 6.800% ± 2.491%; ILCs: 0.943% ± 0.044%) (Figure 4, D and F). This finding indicates that both eosinophils and the total ILCs may participate in the cold-induced beiging of Rag1$^{-/-}$ mice. The absolute numbers of eosinophils (WT: 34,082.84; Rag1$^{-/-}$: 35,087.72) and ILCs (WT: 3,393,272.00; Rag1$^{-/-}$: 3,810,893.00) per gram of tissue are relatively higher in Rag1$^{-/-}$ mice compared with WT mice.

CD8^{+} T cells, the main lymphocytes regulating beige adipogenesis. To strengthen our hypothesis that the absence of CD8^{+} T cells in Rag1$^{-/-}$ mice accounted for the increased beiging in their scWAT, we compared the phenotype of the scWAT in CD8^{+} T cell–deficient (CD8$^{-/-}$) and WT mice. Initially, we performed indirect calorimetry in age- and weight-matched CD8$^{-/-}$ and WT mice using CLAMS, and we found increased expenditure of energy in the CD8$^{-/-}$ mice compared with the WT mice (Figure 5A). This could be explained by the fact that CD8$^{-/-}$ mice showed increased total activity (Figure 5B), while they consumed the same amount of food as the WT mice (Figure 5C). Additionally, RER was found to be lower in the CD8$^{-/-}$ mice, suggesting that, in the absence of CD8^{+} T cells, mice shift to preferential usage of fatty acids, rather than carbohydrates, as energy substrate (Figure 5D). In line with their metabolic profile, we found that CD8$^{-/-}$ mice exhibited a significant expansion of the beige fat areas in scWAT; increased expression of beige-driving genes, such as Ucp1, Cidea, and Dio2 (Figure 5, E and F); and higher percentage of eosinophils content (Figure 5G) compared with the WT mice. However, we found no apparent differences between the scWAT and BAT weights between the two genotypes, despite the increase in the epiWAT weight in the CD8$^{-/-}$ mice (Supplemental Figure 4A), a finding of unknown significance as of now. We confirmed the above with complementary studies in WT mice treated either with anti-CD8 antibody or control IgG that supported the impact of CD8^{+} T cell depletion in the development of beige fat (Supplemental Figure 4B). Further, exposure to cold environment resulted in the anticipated activation of beige adipogenesis (Figure 5, H and I) and the associated increase in eosinophils in scWAT (Figure 5J). The absolute number of eosinophils per gram of tissue was 1,285,714 in CD8$^{-/-}$ mice versus 842,105 in WT mice. No changes were detected in the scWAT weights of age- and weight-matched WT and CD8$^{-/-}$ mice following cold exposure (data not shown).

IFN-γ negatively regulates beige adipogenesis. To further elucidate the specific factor(s) underlying the effects of CD8^{+} T cells in beige adipogenesis, we next measured the scWAT content in IFN-γ, a cytokine secreted in large amounts by activated CD8^{+} T cells and implicated in the regulation of resident innate immune cells within the scWAT (39, 40). Intra-scWAT IFN-γ showed a tendency to decrease levels in the Rag1$^{-/-}$ tissue; this difference was, however, abolished following reconstitution with CD8^{+} T cells (Supplemental Figure 5A). To confirm the specific role of CD8-derived IFN-γ in this process, we reconstituted Rag1$^{-/-}$ mice with CD8^{+} T cells isolated from IFN-γ–deficient (Ifnγ$^{-/-}$) mice. In contrast to reconstitution with WT CD8^{+} T cells that reduced the number of ILCs in the scWAT of Rag1$^{-/-}$ mice, reconstitution with Ifnγ$^{-/-}$ CD8^{+} T cells did not affect the number of ILCs in the scWAT of Rag1$^{-/-}$ mice (Supplemental Figure 5B). Additionally, reconstitution of Rag1$^{-/-}$ mice with CD8^{+} T cells derived from Ifnγ$^{-/-}$ mice did not alter the UCP1 expression in the scWAT, as opposed to its inhibition following reconstitution with WT CD8^{+} T cells (Figure 6, A and B), in further support of the contribution of IFN-γ in this process.

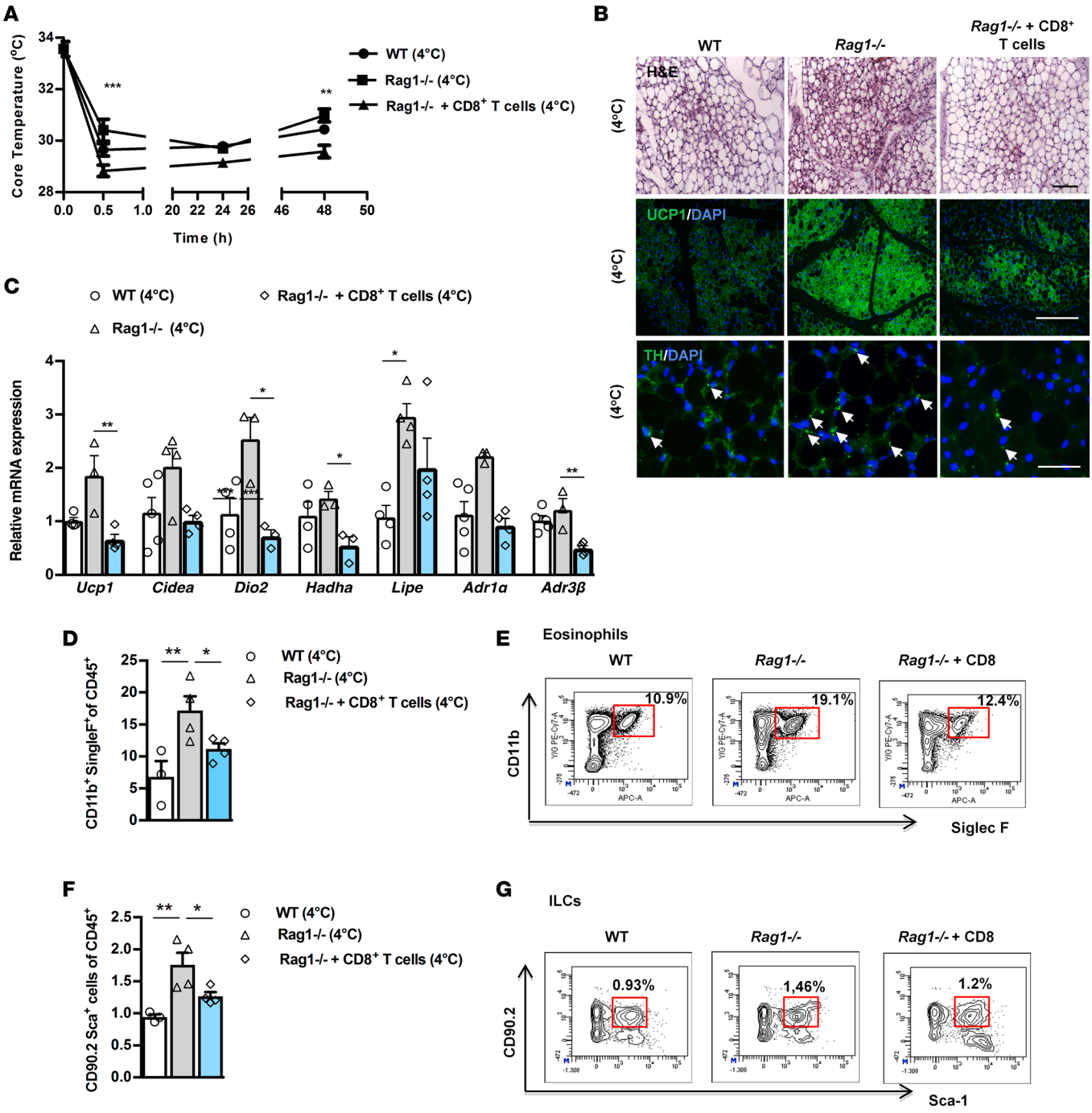

Figure 4. Adoptive transfer of CD8⁺ T cells inhibits increased scWAT beiging in Rag1$^{-/-}$ mice exposed to cold environment. Data shown are from the scWAT of WT, Rag1$^{-/-}$, or Rag1$^{-/-}$ mice reconstituted with 5×10^6 CD8⁺ T cells, once a week for 2 weeks. (**A**) Core temperature measurements. $n \geq 4$ per group. (**B**) Representative images of H&E and IF staining of UCP1 and TH. Arrows represent the TH⁺ cells. Scale bar: 100 μm. $n \geq 3$ per group. (**C**) Relative expression of thermogenic, lipid metabolism, and adrenergic receptors genes in the scWAT of age-matched mice, housed at 4°C for 2 days at the end of the second week. Data are shown as mean expression normalized to actin ± SEM. $n \geq 5$ per group. Data shown are derived from one representative of 2 independent experiments. (**D**) Representative percentages of eosinophils (CD11b⁺Siglec F⁺), housed at 4°C for 2 days. Data shown are representative of 2 independent experiments. Flow cytometry was performed after pooling $n \geq 4$ mice per group. (**E**) Results are expressed as percentages of CD11b⁺Siglec F⁺ eosinophils, gated on the viable CD45⁺DAPI⁻ cells. $n \geq 4$ per group. (**F**) Representative percentages of ILCs positive for CD90.2⁺ Sca-1⁺ Lin⁻ in WT mice or Rag1$^{-/-}$ mice treated with PBS or adoptively transferred with CD8⁺ T cells (5×10^6), once a week for 2 weeks, and housed at 4°C for 2 days are depicted on the flow cytometry plots. Data shown are representative of 2 independent experiments. Flow cytometry was performed after pooling $n \geq 4$ mice per group. (**G**) Results are expressed as percentages of CD90.2⁺Sca-1⁺ Lin⁻ gated on the viable CD45⁺DAPI⁻ cells. $n \geq 4$ per group. Data are presented as mean ± SEM. $^*P < 0.05$, $^{**}P < 0.01$, $^{***}P < 0.001$, 1-way ANOVA with Bonferroni's post test.

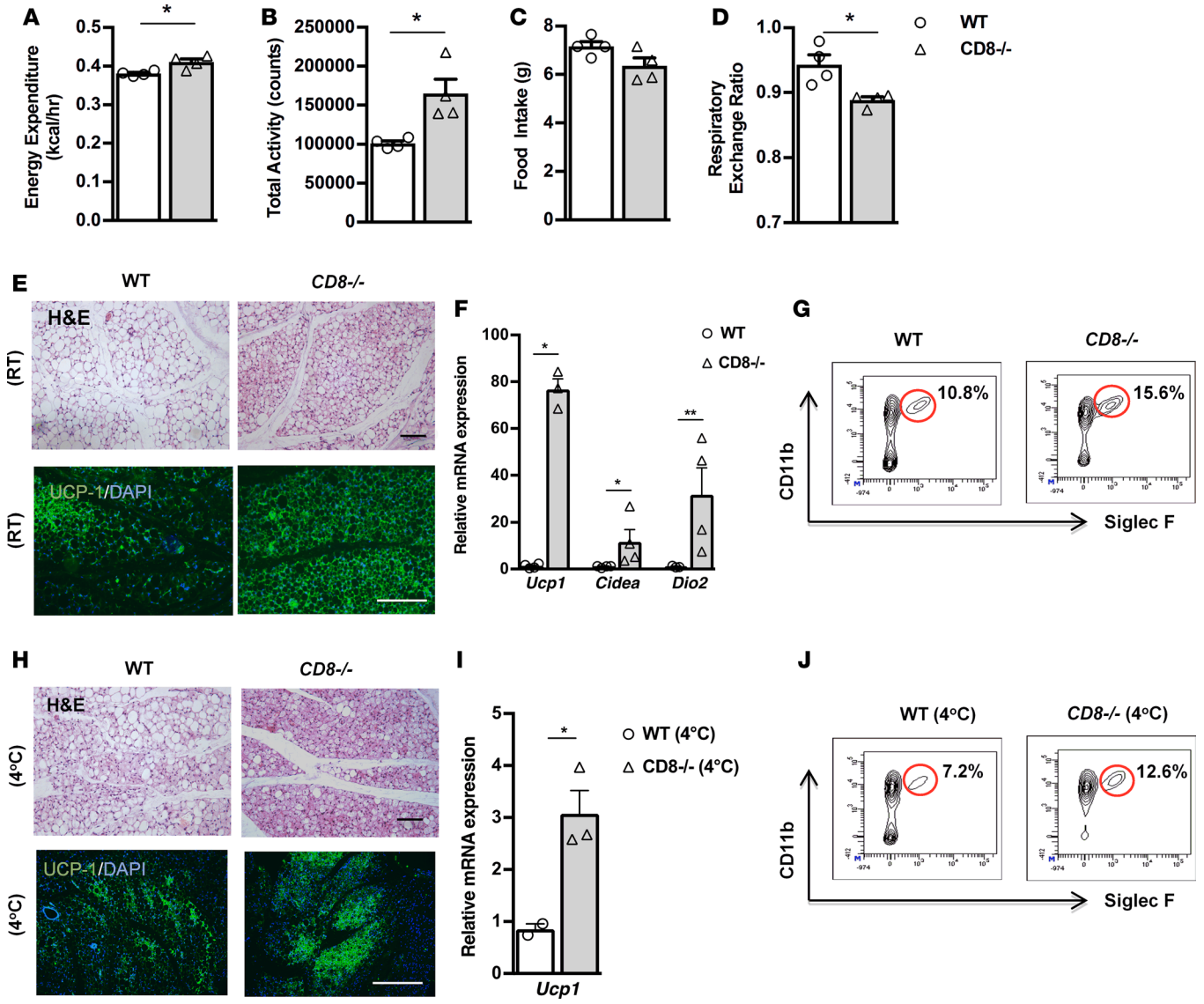

Figure 5. CD8$^{-/-}$ mice display increased beiging of scWAT and thermogenic capacity. (**A–D**) Assessment of metabolic behavior using indirect calorimetry, including energy expenditure adjusted to body weight (**A**), total activity (**B**), food intake (**C**), and respiratory exchange ratio (RER) (**D**). n = 4 per group. Data shown are derived from 1 experiment. (**E**) Representative H&E-stained images of scWAT of WT and CD8$^{-/-}$ mice. Scale bar: 100 μm. n = 3 per group. (**F**) Relative expression of beige genes, such as Ucp1, Cidea, and Dio2, in scWAT of CD8$^{-/-}$ mice versus WT mice. Data are shown as mean expression normalized to actin ± SEM. $n \geq 4$ per group. Data shown are derived from 1 representative of 2 independent experiments. (**G**) Single-cell suspensions prepared from scWAT, harvested from either WT or CD8$^{-/-}$ mice, were gated on the viable CD45^{+}DAPI^{-} cells and then depicted as percentages of Siglec F^{+} and CD11b^{+} cells to identify eosinophils. Flow cytometry was performed after pooling $n \geq 5$ mice per group. (**H**) Representative H&E-stained image of scWAT from WT and CD8$^{-/-}$ mice exposed to cold. Scale bar: 100 μm. n = 3 per group. (**I**) Relative expression of Ucp1 in scWAT from CD8$^{-/-}$ mice and WT mice. Data are shown as mean expression normalized to actin ± SEM. $n \geq 4$ per group. Data shown are derived from 1 experiment. (**J**) Single-cell suspensions from scWAT of WT and CD8$^{-/-}$ mice subjected to exposure at 4°C for 2 days were gated on the viable CD45^{+}DAPI^{-} cells and then analyzed for Siglec F and CD11b expression to measure eosinophils. Flow cytometry was performed after pooling $n \geq 5$ mice per group. Data are presented as mean ± SEM. $^{*}P < 0.05$, $^{**}P < 0.01$, Student's t test.

Next we sought to assess the importance of IFN-γ alone in beige adipogenesis by comparing the beiging of the scWAT in Ifn$\gamma^{-/-}$ and WT mice. In accordance with our previous findings, IFN-γ deficiency was associated with substantial expansion of the beige areas in the scWAT (Figure 6C), while there were no differences in the scWAT weights of the age- and weight-matched WT and Ifn$\gamma^{-/-}$ mice (Supplemental Figure 5C). Notably, the epiWAT weight of the Ifn$\gamma^{-/-}$ mice was significantly decreased compared with that of the WT epiWAT (Supplemental Figure 5C). Importantly, the Ifn$\gamma^{-/-}$ scWAT displayed increased numbers of eosinophils (Figure 6D) and of ILCs (Figure 6E) compared with WT scWAT, consistent with the mechanisms employed by CD8^{+} T cells to inhibit beige formation. Furthermore, a significant increase was noted

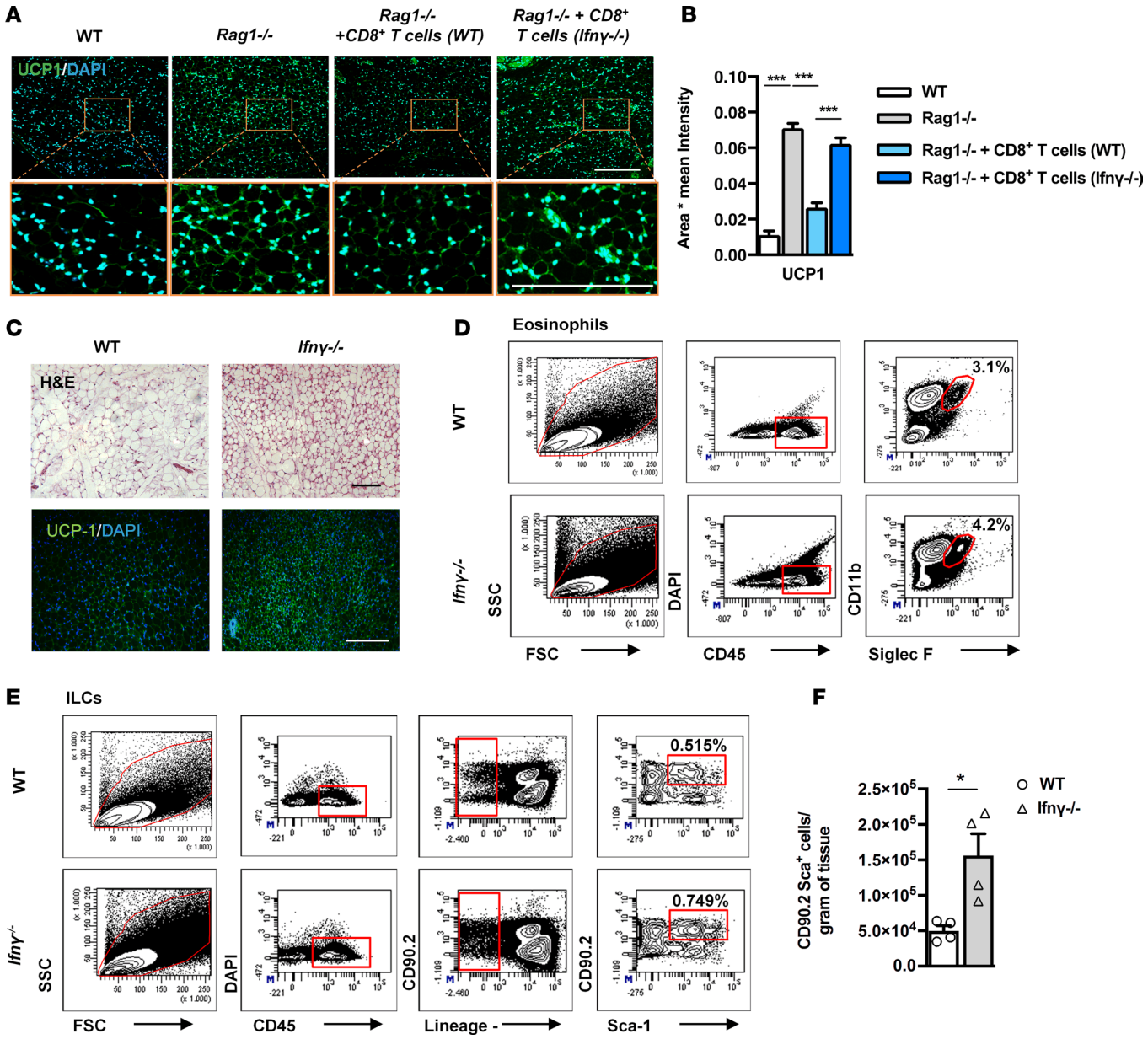

Figure 6. Increased beiging and eosinophils in the scWAT of Ifnγ$^{-/-}$ mice. (**A**) Representative images of UCP1 IF staining in the scWAT of WT or Rag1$^{-/-}$ mice treated with PBS or adoptively transferred with 5 × 10^6 WT-derived or Ifnγ$^{-/-}$-derived CD8$^+$ T cells, once a week for 2 weeks. Scale bar: 100 μm. (**B**) The relative UCP1 mean intensity in the above groups. Values represent mean ± SD intensity of 15 patches for every image. n = 3 per group. ***P < 0.001, 2-way ANOVA. (**C**) Representative images of H&E and UCP1 IF staining of scWAT from WT and Ifnγ$^{-/-}$ mice. Scale bar: 100 μm. n = 3 per group. Data shown are derived from 1 experiment. (**D**) Gating strategy for the identification of eosinophils gated on viable CD45$^+$DAPI$^-$ cells and further identified as CD11b$^+$Siglec F$^+$ cells. Data shown are depicted as percentages. Flow cytometry was performed after pooling n ≥ 4 mice per group. (**E**) Gating strategy for the identification of total ILCs in WT mice or Rag1$^{-/-}$ mice treated with PBS or adoptively transferred with 5 × 10^6 WT CD8$^+$ T cells or CD8$^+$ T cells derived from Ifnγ$^{-/-}$ mice, once a week for 2 weeks. Percentages of cells positive for CD90.2$^+$Sca-1$^+$Lin$^-$ gated on the viable CD45$^+$DAPI$^-$ cells are depicted on the flow cytometry plots. Flow cytometry was performed after pooling n ≥ 4 mice per group. (**F**) Absolute numbers of total ILCs (CD90.2$^+$ Sca-1$^+$Lin$^-$) per gram of tissue in scWAT of WT and Ifnγ$^{-/-}$ mice. n = 5 per group. Data are presented as mean ± SEM. *P < 0.05, Student's t test.

in the absolute numbers of eosinophils (WT: 810,000; Ifnγ$^{-/-}$: 1,100,000) and of ILCs per gram of tissue in Ifnγ$^{-/-}$ scWAT compared with WT scWAT (Figure 6F).

To summarize, our findings demonstrate that the inhibitory effects of CD8$^+$ T cells on the formation of beige fat are exerted at several levels, including regulation of the catecholaminergic input to the scWAT, targeting of specific adipocyte differentiation processes in an IFN-γ–dependent manner, and reduction of the abundance of cells of innate immunity (eosinophils, ILCs), and, thereby, a decrease of the levels of cytokines promoting beiging, such as IL-4, IL-5, and IL-13 (24) (Figure 7).

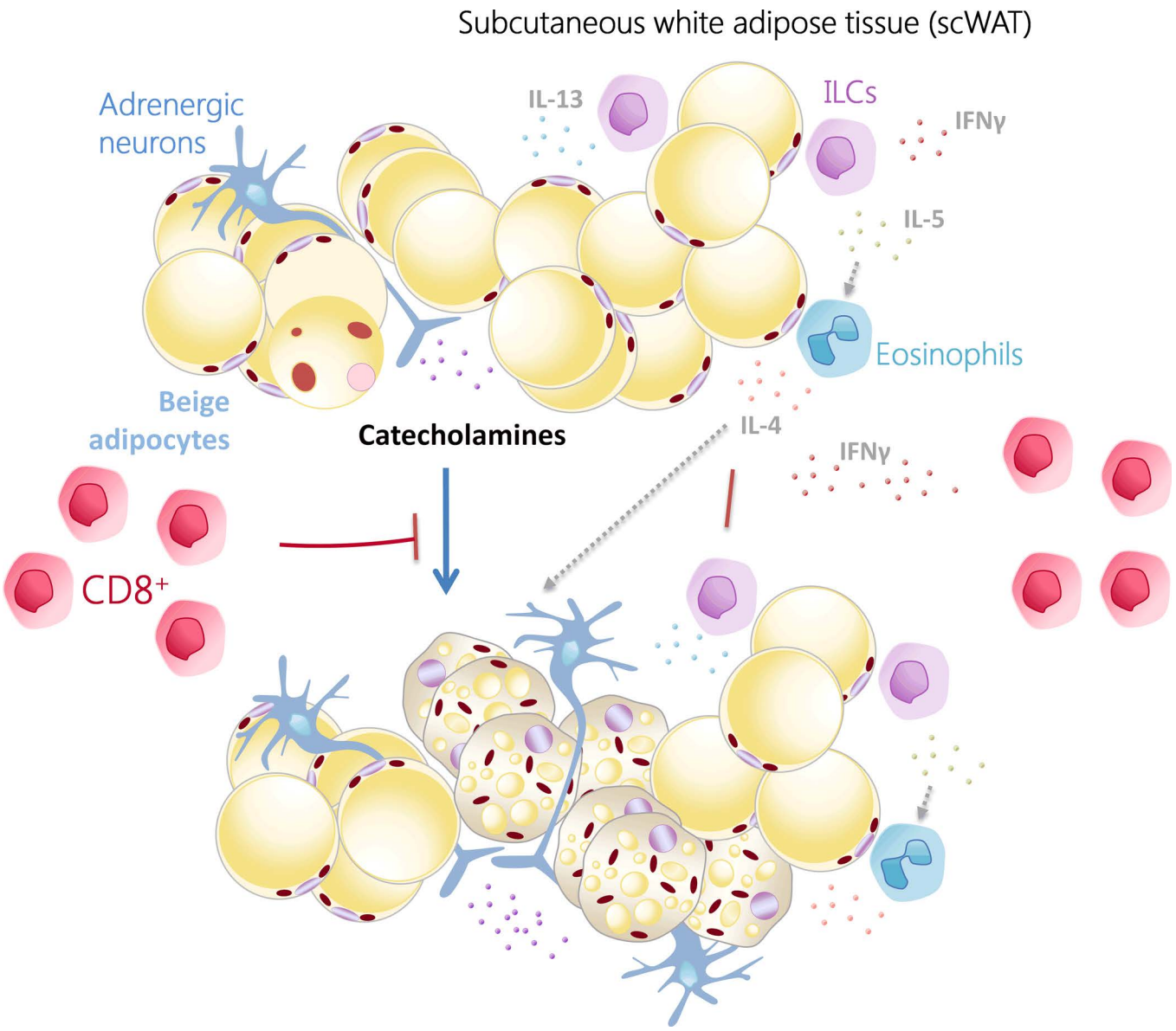

Figure 7. Schematic representation of the effects of the CD8⁺ T cells in the beiging of the scWAT. CD8⁺ T cells inhibit beige adipose tissue development in the scWAT by modulating the catecholaminergic input to scWAT and reducing the abundance of implicated innate immune cells and the associated cytokines, such as IL-4, IL-5, and IL-13, shown to induce beige fat formation (25). scWAT CD8⁺ T cells derived IFN-γ are a major mediator of these effects of the CD8⁺ T cells.

Discussion

In this paper, we describe a pathway in the regulation of beige adipogenesis, involving crosstalk of CD8⁺ T cells with catecholaminergic signaling and associated innate immune cells. In particular, we leveraged the Rag1$^{-/-}$ mouse model to unmask the significant contribution of T cells, particularly of CD8⁺ T cells, in energy homeostasis, as regulated at the level of the adipose tissue. We demonstrate that CD8⁺ T cell deficiency results in the induction of beige adipogenesis in the scWAT of Rag1$^{-/-}$ mice and corresponding changes in energy expenditure.

By employing several complementary approaches (CD8⁺ T cell reconstitution in Rag1-deficient, CD8⁺-deficient, or Ifn$\gamma^{-/-}$ mice), we can unequivocally demonstrate the inhibitory effect of CD8⁺ T cells on beige adipogenesis. Interestingly, we identified that several mechanisms involved in the immune plasticity and homeostatic functions of WAT likely cooperate with each other in mediating the inhibitory effect of CD8⁺ T cells on this process.

Our findings on increased expression in the scWAT of AdR(s) and TH, the rate-limiting enzyme for the synthesis of catecholamines, as well as drastic reduction of beiging upon treatment with the α-blocker prazosin hydrochloride, indicate the critical contribution of the increased catecholaminergic input in the beige adipogenesis in Rag1$^{-/-}$ mice. Although effects of α-adrenergic activation on lymphocytes have been reported (41–43), the potential effect of lymphopenia or lymphocytosis on catecholamine production and actions remains unknown (44). Notably, the catecholaminergic system in Rag1$^{-/-}$ mice retains its plasticity despite constitutive activation, as demonstrated by its sensitivity to temperature changes, including acclimatization or cold exposure, or even the reversal of catecholaminergic activity upon reconstitution of the missing CD8$^+$ T cells.

Interaction between adipocytes and cells of type 2 immunity was shown to regulate homeostasis and beige adipogenesis of the WAT in lean conditions. More specifically, it has been shown that beige fat development is dependent on ILC2s, eosinophils, and cytokines of type 2 immunity that act in concert to drive the differentiation of precursor cells to the smaller, multilocular beige adipocytes in specific WAT depots (24, 33). In agreement, Rag1$^{-/-}$ mice had increased ILCs in the scWAT that were dramatically decreased following reconstitution with CD8$^+$ T cells to levels resembling those in the WT tissue. We show that Rag1$^{-/-}$ mice, in addition to the increased ILCs and the associated cytokines, displayed increased IL-4 levels in the scWAT. On the other hand, both macrophage content and M2-specific markers were unaltered in the scWAT of Rag1$^{-/-}$ mice, suggesting that enhanced catecholaminergic signaling and beige adipogenesis in Rag1$^{-/-}$ mice do not necessarily involve alterations in macrophage numbers. These data indicate a CD8$^+$ T cell deficiency–mediated mechanism for beige adipogenesis that is not linked with alteration in M2 macrophage numbers, in further confirmation of the multifaceted regulation of this process (45). Reconstitution with CD8$^+$ T cells decreased the abundance of eosinophils and ILCs and blocked beige adipogenesis and the associated lipid oxidation in the scWAT of Rag1$^{-/-}$ mice, despite the deficiency in the other lymphocyte types. Furthermore, reversal of the Rag1$^{-/-}$ scWAT phenotype via replenishment of the missing CD8$^+$ T cells, led us to the hypothesis that CD8$^+$ T cells can counteract the effects of cells of innate immunity on beige adipogenesis. Our finding on increased beige adipogenesis in CD8$^{-/-}$ mice provided strong support for this hypothesis. Moreover, although this study has focused on the CD8$^+$ T cell–mediated regulation of beiging in the scWAT, the main fat depot with beiging capability, it is also conceivable that CD8$^+$ T cells might also act on other fat depots, such as epiWAT. Further, preliminary evidence from studies in CD4$^{-/-}$ mice suggested that CD4$^+$ T cells may also modulate beige adipogenesis, although in a less consistent manner, suggesting CD8$^+$ T cells as the predominant T cell group involved in beige adipogenesis. As the CD4$^+$ T cell pool is more diverse and more vulnerable to the experimental conditions applied, additional experiments are required to elucidate the exact positioning of this T cell subpopulation in the development of beige fat, which, however, needs to be addressed in a future study.

To further explore the mechanisms mediating the effects of CD8$^+$ T cells in beige adipogenesis, we assessed the effect of molecules secreted by CD8$^+$ T cells likely to effect on beige adipogenesis. According to the literature, obese Ifn$\gamma^{-/-}$ mice have been shown to have improved insulin sensitivity and decreased adipocyte size, suggesting the beneficial effects of IFN-γ deficiency for energy homeostasis (46). In line with this, we identified significant induction of beige fat generation and increased concentration of ILCs and eosinophils in the scWAT of Ifn$\gamma^{-/-}$ mice, all indicative of activation of mechanisms mediating utilization of energy. Finally, reconstitution of Rag1$^{-/-}$ mice with Ifn$\gamma^{-/-}$ CD8$^+$ T cells did not affect beige fat abundance in the scWAT, in contrast to the inhibitory (ablating) effect upon transfer of WT CD8$^+$ T cells. As established, CD8$^+$ T cells are not the only source of IFN-γ, as NK cells and ILC1 have been also shown as additional IFN-γ sources in the adipose tissue (47, 48). Assessment of the intra-scWAT levels of IFN-γ in Rag1$^{-/-}$ mice before and after reconstitution with CD8$^+$ T cells demonstrated that at least the contribution CD8$^+$ T cells to the total IFN-γ levels in this tissue is substantial (Supplemental Figure 5A) (49). Inhibition of beige adipogenesis upon reconstitution with CD8$^+$ T cells may be mediated by the increased intra-scWAT levels of IFN-γ, which might also exert dose-dependent effects on other inhibitors of beige adipogenesis. Notably, TH overexpression has been shown to decrease the production of IFN-γ (50), while challenge of PBMCs with IFN-γ decreased TH expression and the associated catecholamine production (43, 51). One other way to modulate IFN-γ levels and thus effect beige adipogenesis is to target upstream key pathways, such as IL-12 or STAT4 that lead to IFN-γ production or block IFN-γ itself (52). All of the above argue for operation of additional circuits among CD8$^+$ T cells, IFN-γ, and beige fat development.

Our findings raise the possibility for the potential benefits of targeted therapeutic interventions to leverage the effect of the $CD8^+$ T cells on the blockade of energy dissipation (15). Similar strategies targeting the inhibitory effect of $CD8^+$ T cells on the liver have been proposed for the treatment of diet-induced steatohepatitis and the associated hepatic carcinogenesis (32). Our findings also support the hypothesis that aggressive immunotherapies, for instance, employed in malignant and inflammatory disease, may substantially affect the regulation of energy homeostasis, which is already altered in these patients. This hypothesis raises the possibility that patients treated with immunomodulatory agents for cancer and other diseases may present with altered control of systemic metabolism, which, in a context-dependent manner, could also bear beneficial effects. Illuminating the specifics of the crosstalk between immunotherapeutic interventions and metabolism may provide a great benefit to patients, as these therapies extend to a number of diseases (14, 53, 54).

Methods

Animals and animal care. Age-matched (8–12 weeks) male mice, of $Rag1^{-/-}$, $CD8^{-/-}$, and IFN-$\gamma^{-/-}$ genotype, on C57BL/6J background were purchased from Jackson Laboratories and were bred in-house in a pathogen-free, temperature-controlled (22°C) environment, with a 12-hour-light/dark cycle, in accredited animal facilities at the Biomedical Research Foundation Academy Of Athens (BRFAA). Age- and weight-matched (22–25 g) WT mice with the above genotypes on C57BL/6J background were provided by the animal facilities at the BRFAA. All mice used for experimentation were provided by the colonies maintained in our facility for several generations in order to normalize facility-dependent changes in metabolic and other functions. Male mice 8–12 weeks of age were used at the start of each experiment. Mice were allocated randomly in experimental groups for each genotype.

Indirect calorimetry. Metabolic measurement was performed using an Oxymax indirect calorimetry system (Columbus Instruments). In short, preweighed mice were housed individually in specifically designed Oxymax calorimeter chambers with ad libitum access to diet and water for 72 hours, a 12-hour-light/dark cycle, and an ambient temperature of 22°C. Mice were singly housed for 2 days prior to transferring into the calorimeter chamber. VO_2, VCO_2, and rates were determined under Oxymax system settings as follows: air flow, 0.6 l/min; sample flow, 0.5 l/min. The system was calibrated against a standard gas mixture to measure O_2 consumed (VO_2, ml/kg/h) and CO_2 generated (VCO_2, ml/kg/h). Energy expenditure (kcal/h/kg), respiratory quotient (ratio of VCO_2/VO_2, RER), food intake (g), and activity (counts) were evaluated over a 48-hour period. The results were normalized and compared with the WT group per cohort, the results of which were set as 100%.

Tissue homogenization protocol for ELISA. scWAT from mice were weighed and homogenized with 600 μl cold HBSS (1×) supplemented with proteinase inhibitors (1:200) by using a tissue homogenizer. The homogenates were centrifuged at 400 *g* for 15 minutes at 4°C, and the supernatant was stored at –80C until analyzed. IL-4, IL-5, IL-13 (mouse IL-4, IL-5, IL-14 Elisa Ready-SET-Go!, eBioscience) and IFN-γ protein levels were determined by using ELISA (Biolegend ELISA Max).

Thermoneutrality experiment. Eight-week-old WT and $Rag1^{-/-}$ C57BL/6 mice were individually caged and housed at 28°C–30°C, with a 12-hour-light/dark cycle and free access to a standard chow diet for 20 days. Mice were housed in a controlled temperature room in the animal facilities at BRFAA.

Cold exposure experiment. Eight-week-old mice WT and $Rag1^{-/-}$ mice were housed in individual cages and acclimated at 18°C for 2 days followed by cold exposure at 4°C for another 2 days according to standard protocol. Core temperature was measured using an YSI Tele-Thermometer (Simpson Electric Co).

Histological analysis. Tissues were dissected, fixed in 4% paraformaldehyde solution overnight, and processed for routine paraffin histology. Paraffin-embedded tissues were sectioned at 5 μm and stained with H&E according to standard protocols. Adipocyte cell size was measured by automated software developed in our lab using Matlab. Images were obtained using a bright-field LEICA DMLS2 microscope. For immunohistochemistry, the tissues were incubated with 0.1% w/v Pronase (MilliporeSigma) at 37°C for 8 minutes and then washed again, blocked with PBS containing 10% normal goat serum and 0.1% Triton X-100 and incubated with the primary antibodies overnight at 4°C. UCP1 was detected using rabbit anti-Ucp1 antibody (ab10983, Abcam) at a concentration of 1:500, TH was detected by rabbit anti-TH (AB152; Millipore) at a concentration of 1:1,000, and β-tubulin was detected by mouse anti-Tuj1 (60052, STEMCELL Technologies Inc.). After several PBS washing steps, the tissue was incubated with the secondary antibody donkey anti-rabbit Alexa Fluor 488 (Thermo Fischer Scientific) or

donkey anti-mouse Alexa Fluor 568 (Thermo Fischer Scientific). Another washing step was followed by DAPI incubation and further washing steps before the sections were mounted using Vectashield mounting medium (Vector). For quantification of TH expression, parenchymal nerve fibers (Tuj1$^+$) were measured in 5 randomly selected area of the depot. Images were obtained using a confocal inverted LEICA TCS SP5 (DMI6000). For UCP1 quantification, patches (15 patches for every image, sized 128 × 128 pixels) of images were randomly selected, and the mean intensity of the staining was measured.

Adoptive transfer studies. To examine the effects of T cells in beige adipogenesis, 12-week-old Rag1$^{-/-}$ mice fed a chow diet were used for adoptive transfer of splenocytes, cells rich in B and T cells. Additionally, Rag1$^{-/-}$ mice, kept either at 24°C or 4°C, were adoptively transferred with CD8$^+$ T cells. Splenocytes were obtained from the spleens of lean C57BL/6 WT mice and dissociated into single-cell suspensions and red blood cells were removed. CD8$^+$ T cells were purified from the spleens of WT C57BL/6 male mice using mouse CD8α (Ly-2) microbeads (130-049-401, Miltenyi Biotec) according to the manufacturer's protocol. A total of 5 × 10^6 splenocytes containing 15%–20% CD8$^+$ T cells (around 8 × 10^5) or 5 × 10^6 CD8$^+$ T cells were injected retro-orbitally weekly and sacrificed after 2 weeks. Control groups received retro-orbital injections of PBS. Purity of CD8$^+$ T cells injected was measured by FACS analysis and was >85%. Homing of CD8$^+$ T cells in the scWAT was confirmed by flow cytometry analysis.

In vivo depletion of CD8$^+$ T cells. WT mice received 200 μg anti-CD8 antibody (BE0004-1, Bio X Cell) or normal rat IgG (control) (Bio X Cell) by the i.p. route at days 0, 2, and 6. Mice were euthanized at day 10 for further analysis. The depletion was assessed at days 24 hours after the treatment with mAbs by flow cytometric blood analysis.

scWAT preparation for flow cytometry analysis. scWAT was removed, weighed after careful removal of lymph nodes, and kept on ice in 3-cm dishes with Buffer I (PBS with 1 mM $CaCl_2$ and 0.5% BSA). The tissue was finely minced and washed with Buffer I at 500 *g* at 4°C for 10 minutes to remove erythrocytes and free leukocytes. The floating tissue (upper phase) was removed following centrifugation and was further dispersed by shaking into DMEM (high glucose) medium containing fresh collagenase D (2mg/ml) and 0.5% BSA (1 ml/ tissue g) at 37°C for 30–40 minutes with gentle agitation. Cell suspension was topped up to 10 ml by DMEM medium and then passed through 100-μm filters to generate single-cell suspensions, before being centrifuged at 300 *g* for 5 minutes to separate floating adipocytes from the SVF pellet. The cell pellet was resuspended in FACS buffer (PBS with 0.1% BSA and 2.5 mM EDTA) prior to staining with the indicated antibodies.

Flow cytometry. scWAT was processed and stained with fluorochrome-conjugated monoclonal antibody combinations for ILC staining. Monoclonal antibodies used for flow cytometry were as follows: allophycocyanin (APC) anti-CD45 (30-F11; Biolegend); phycoerythrin (PE) anti-CD3 (145-2C11; Biolegend); PE anti-CD4 (E121.19; Biolegend); PE anti-CD8 (53-6.7; Biolegend); PE anti-CD19 (6D5; Biolegend); PE anti-B220 (RA3-6B2; Biolegend); FITC CD11b (M1/70; Biolegend); PE anti-CD11c (N418; Biolegend); PE anti-FceRI (MAR-1; Biolegend); PE anti-Gr-1 (RB6-8C5; Biolegend); PE anti-Ter119 (Ter/119; Biolegend); peridinin-chlorophyll proteins (PercP) anti-CD90.2 (53-2.1; Biolegend); PE/Cy7 anti-Sca1 (D7; Biolegend) and Alexa Fluor 488–Gata3 (16E10A23; Biolegend). Representative gating schemes for each population are shown in Figure 3D. ILCs are identified as CD45$^+$, lineage$^-$ (CD3$^-$CD4$^-$CD8$^-$CD19$^-$B220$^-$CD11b$^-$CD11c$^-$FceRI$^-$Gr-1$^-$Terr119$^-$) CD90.2$^+$ Sca-1$^+$ cells. scWATs were processed and stained with fluorochrome-conjugated monoclonal antibody combinations for eosinophil staining. Eosinophils were identified as CD45$^+$, CD11b$^+$, and Siglec F$^+$ cells. Representative gating schemes are shown in Figure 3F. Trafficking of CD45$^+$CD3$^+$CD8$^+$ in the scWAT was assessed using the following monoclonal antibodies: APC anti-CD45 (30-F11; Biolegend); FITC anti-CD3 (145-2C11; Biolegend), and PeCy7 anti-CD8 (53-6.7; Biolegend). Representative gating schemes are shown in Supplemental Figure 2A. Macrophage assessment of the subcutaneous adipose tissue was assessed by staining with the following fluorochrome-conjugated monoclonal antibodies: APC anti-CD45 (30-F11; Biolegend); FITC anti-CD11b$^+$ (M1/70; Biolegend); and PE F480$^+$ (BM8; eBioscience). Representative gating schemes are shown in Supplemental Figure 2B. Samples were analyzed on a FACSAria III (Becton Dickinson). As indicated, data are expressed as percentages of CD45$^+$ hematopoietic cells. Live lymphocytes were gated by DAPI exclusion, size, and granularity based on forward- and side-scatter. Data were analyzed using BD FACSDiVa software. Appropriate isotype-matched controls for all antibodies were used to determine positive staining.

Western blot. Tissues were harvested in RIPA buffer (ThermoFisher Scientific) with 1% protease and 1% phosphatase inhibitors (ThermoFisher Scientific). 20 ng protein was loaded into each well of a 4%–12% Bis-Tris polyacrylamide gel (ThermoFischer Scientific) and transferred to nitrocellulose membrane (ThermoFischer Scientific). Protein-bound membranes were blocked for 30 minutes with 5% nonfat dry milk in 0.1% Tris-buffered saline with Tween and incubated with rabbit anti-Ucp1 antibody (ab10983, Abcam) or anti-tubulin (ab15568, Abcam) in blocking buffer overnight at 4°C. Membranes were treated with HRP-conjugated secondary antibodies diluted 1:5,000 in blocking buffer for 2 hours and rinsed with Pierce ECL chemiluminescent solution (Thermo Fischer Scientific). Membranes were immediately read in a Kodak Image Station 4000 mm PRO, and protein levels were quantified using ImageJ (NIH) free, open-source software.

Quantitative real-time RT-PCR. Total RNA was isolated from tissues using TRI reagent (MilliporeSigma) and treated with DNase using the DNA-free kit (Ambion). Complementary DNA was made from 2 μg total RNA by MMLV reverse transcriptase (Invitrogen) and initiated from random hexamer primers (Life Technologies Inc). Quantitative real-time PCR analysis was performed using RT² SYBR Green qPCR Master Mix (SA biosciences) in a ABI PRISM 7000 Sequence Detection System (Applied Biosystems). Primers used for real-time PCR are shown in Supplemental Table 1. Gene expression levels were normalized to actin in vivo and calculated according to the $2^{-\Delta\Delta Ct}$ method.

Adrenergic blockade. For α-adrenergic blockade, prazosin hydrochloride (MilliporeSigma), a selective α1-adrenergic antagonist, was administered via the drinking water (8 mg/kg) for 5 days.

Statistics. Data are presented as mean ± SEM. All statistical analysis was performed using GraphPad Prism software version 5.0. The statistical significance of the differences between various treatments was measured by either the 2-tailed Student's *t* test or 1-way ANOVA with Bonferroni's post-test. A *P* value of less than 0.05 was considered statistically significant. Sample size, number of replicates, and statistical tests are reported in figure legends.

Study approval. All experimental procedures reported here were approved by the competent veterinary authority of the prefectures of Athens, Greece, in accordance with the National Registration (Presidential Decree 56/2013) and with European Directive 63/2010.

Author contributions

MM, SK, EK, YK, and KK designed and performed experiments and analyzed and interpreted the data. SO and AK were involved with some of the in vivo experiments. PT analyzed data. MS and EA designed and performed flow cytometry studies and provided the Ifnγ-knockout mice. NK is the veterinarian and reviewed all experimental protocols and supervised all animal studies. AC, SK, KJC, DS, SB, MWS, and TC were involved in experimental design and data interpretation. TC was involved in editing of the manuscript. KPK planned and designed the experiments; supervised all experiments and interpretation of results with SK; coordinated the writing of the manuscript by SK, MM, and EK; and edited the final manuscript.

Acknowledgments

This work was supported by the European Union 7th Framework Programme, Regpot activity grant 245928 (TRANSMED), and Cooperation Programme 305739 (RISKYCAD), and Greek national funds through the Operational Program "Education and Lifelong Learning" of the National Strategic Reference Framework–Research Funding Program: Herakletus II. This work was cofinanced by the European Union (European Social Fund). SK was funded by NIH grant R21EB019079, the National Strategic Reference Framework 2007-2013 Programme for Development (EU Regional Development Fund), and the Greek Ministry of Education and Religious Affairs, Culture & Sports.

Address correspondence to: Katia Karalis, Emulate Inc., 27 Drydock Ave., Boston, Massachusetts 02210, USA. Phone: 508.843.5324; Email: katia.karalis@childrens.harvard.edu or katia.karalis@eulatebio.com. Or to: Sevasti Karaliota, Biomedical Research Foundation Academy of Athens, Soranou Efesiou 4, Athens 11527, Greece. Phone: 30.2106597240; Email: skaral@bioacademy.gr.

KPK's present address is: Emulate Inc., Boston, Massachusetts, USA.

1. Lumeng CN, Bodzin JL, Saltiel AR. Obesity induces a phenotypic switch in adipose tissue macrophage polarization. *J Clin Invest*. 2007;117(1):175–184.
2. Shi MA, Shi GP. Different roles of mast cells in obesity and diabetes: lessons from experimental animals and humans. *Front Immunol*. 2012;3:7.
3. Wu D, et al. Eosinophils sustain adipose alternatively activated macrophages associated with glucose homeostasis. *Science*. 2011;332(6026):243–247.
4. Talukdar S, et al. Neutrophils mediate insulin resistance in mice fed a high-fat diet through secreted elastase. *Nat Med*. 2012;18(9):1407–1412.
5. Molofsky AB, et al. Innate lymphoid type 2 cells sustain visceral adipose tissue eosinophils and alternatively activated macrophages. *J Exp Med*. 2013;210(3):535–549.
6. Winer S, et al. Normalization of obesity-associated insulin resistance through immunotherapy. *Nat Med*. 2009;15(8):921–929.
7. Nishimura S, et al. CD8+ effector T cells contribute to macrophage recruitment and adipose tissue inflammation in obesity. *Nat Med*. 2009;15(8):914–920.
8. Feuerer M, et al. Lean, but not obese, fat is enriched for a unique population of regulatory T cells that affect metabolic parameters. *Nat Med*. 2009;15(8):930–939.
9. Cipolletta D, et al. PPAR-γ is a major driver of the accumulation and phenotype of adipose tissue Treg cells. *Nature*. 2012;486(7404):549–553.
10. Scherer PE. Adipose tissue: from lipid storage compartment to endocrine organ. *Diabetes*. 2006;55(6):1537–1545.
11. Vosselman MJ, van Marken Lichtenbelt WD, Schrauwen P. Energy dissipation in brown adipose tissue: from mice to men. *Mol Cell Endocrinol*. 2013;379(1-2):43–50.
12. Fedorenko A, Lishko PV, Kirichok Y. Mechanism of fatty-acid-dependent UCP1 uncoupling in brown fat mitochondria. *Cell*. 2012;151(2):400–413.
13. Cohen P, et al. Ablation of PRDM16 and beige adipose causes metabolic dysfunction and a subcutaneous to visceral fat switch. *Cell*. 2014;156(1-2):304–316.
14. Ishibashi J, Seale P. Medicine. Beige can be slimming. *Science*. 2010;328(5982):1113–1114.
15. Harms M, Seale P. Brown and beige fat: development, function and therapeutic potential. *Nat Med*. 2013;19(10):1252–1263.
16. Wu J, et al. Beige adipocytes are a distinct type of thermogenic fat cell in mouse and human. *Cell*. 2012;150(2):366–376.
17. Lee YH, Petkova AP, Mottillo EP, Granneman JG. In vivo identification of bipotential adipocyte progenitors recruited by β3-adrenoceptor activation and high-fat feeding. *Cell Metab*. 2012;15(4):480–491.
18. Petrovic N, Walden TB, Shabalina IG, Timmons JA, Cannon B, Nedergaard J. Chronic peroxisome proliferator-activated receptor gamma (PPARgamma) activation of epididymally derived white adipocyte cultures reveals a population of thermogenically competent, UCP1-containing adipocytes molecularly distinct from classic brown adipocytes. *J Biol Chem*. 2010;285(10):7153–7164.
19. Schulz TJ, et al. Brown-fat paucity due to impaired BMP signalling induces compensatory browning of white fat. *Nature*. 2013;495(7441):379–383.
20. Shabalina IG, Petrovic N, de Jong JM, Kalinovich AV, Cannon B, Nedergaard J. UCP1 in brite/beige adipose tissue mitochondria is functionally thermogenic. *Cell Rep*. 2013;5(5):1196–1203.
21. Boström P, et al. A PGC1-α-dependent myokine that drives brown-fat-like development of white fat and thermogenesis. *Nature*. 2012;481(7382):463–468.
22. Qiu Y, et al. Eosinophils and type 2 cytokine signaling in macrophages orchestrate development of functional beige fat. *Cell*. 2014;157(6):1292–1308.
23. Ye L, et al. Fat cells directly sense temperature to activate thermogenesis. *Proc Natl Acad Sci USA*. 2013;110(30):12480–12485.
24. Lee MW, et al. Activated type 2 innate lymphoid cells regulate beige fat biogenesis. *Cell*. 2015;160(1-2):74–87.
25. Chung KJ, et al. A self-sustained loop of inflammation-driven inhibition of beige adipogenesis in obesity. *Nat Immunol*. 2017;18(6):654–664.
26. Shan B, et al. The metabolic ER stress sensor IRE1α suppresses alternative activation of macrophages and impairs energy expenditure in obesity. *Nat Immunol*. 2017;18(5):519–529.
27. Seale P, et al. Prdm16 determines the thermogenic program of subcutaneous white adipose tissue in mice. *J Clin Invest*. 2011;121(1):96–105.
28. Feldmann HM, Golozoubova V, Cannon B, Nedergaard J. UCP1 ablation induces obesity and abolishes diet-induced thermogenesis in mice exempt from thermal stress by living at thermoneutrality. *Cell Metab*. 2009;9(2):203–209.
29. Cui X, et al. Thermoneutrality decreases thermogenic program and promotes adiposity in high-fat diet-fed mice. *Physiol Rep*. 2016;4(10):e12799.
30. Gospodarska E, Nowialis P, Kozak LP. Mitochondrial turnover: a phenotype distinguishing brown adipocytes from interscapular brown adipose tissue and white adipose tissue. *J Biol Chem*. 2015;290(13):8243–8255.
31. Mathis D. Immunological goings-on in visceral adipose tissue. *Cell Metab*. 2013;17(6):851–859.
32. Wolf MJ, et al. Metabolic activation of intrahepatic CD8+ T cells and NKT cells causes nonalcoholic steatohepatitis and liver cancer via cross-talk with hepatocytes. *Cancer Cell*. 2014;26(4):549–564.
33. Brestoff JR, et al. Group 2 innate lymphoid cells promote beiging of white adipose tissue and limit obesity. *Nature*. 2015;519(7542):242–246.
34. Lee MW, et al. Activated type 2 innate lymphoid cells regulate beige fat biogenesis. *Cell*. 2015;160(1-2):74–87.
35. Nguyen KD, et al. Alternatively activated macrophages produce catecholamines to sustain adaptive thermogenesis. *Nature*. 2011;480(7375):104–108.
36. Nedergaard J, Cannon B. UCP1 mRNA does not produce heat. *Biochim Biophys Acta*. 2013;1831(5):943–949.
37. Thomas SA, Palmiter RD. Thermoregulatory and metabolic phenotypes of mice lacking noradrenaline and adrenaline. *Nature*. 1997;387(6628):94–97.
38. Zhou QY, Quaife CJ, Palmiter RD. Targeted disruption of the tyrosine hydroxylase gene reveals that catecholamines are required for mouse fetal development. *Nature*. 1995;374(6523):640–643.
39. Huh JY, Park YJ, Ham M, Kim JB. Crosstalk between adipocytes and immune cells in adipose tissue inflammation and meta-

bolic dysregulation in obesity. *Mol Cells*. 2014;37(5):365–371.
40. Huh JY, Park YJ, Ham M, Kim JB. Crosstalk between adipocytes and immune cells in adipose tissue inflammation and metabolic dysregulation in obesity. *Mol Cells*. 2014;37(5):365–371.
41. Pesić V, et al. Expression of alpha1-adrenoceptors on thymic cells and their role in fine tuning of thymopoiesis. *J Neuroimmunol*. 2009;214(1-2):55–66.
42. Krüger K, Lechtermann A, Fobker M, Völker K, Mooren FC. Exercise-induced redistribution of T lymphocytes is regulated by adrenergic mechanisms. *Brain Behav Immun*. 2008;22(3):324–338.
43. Qiu YH, Cheng C, Dai L, Peng YP. Effect of endogenous catecholamines in lymphocytes on lymphocyte function. *J Neuroimmunol*. 2005;167(1-2):45–52.
44. Wolf Y, et al. Brown-adipose-tissue macrophages control tissue innervation and homeostatic energy expenditure. *Nat Immunol*. 2017;18(6):665–674.
45. Fischer K, et al. Alternatively activated macrophages do not synthesize catecholamines or contribute to adipose tissue adaptive thermogenesis. *Nat Med*. 2017;23(5):623–630.
46. O'Rourke RW, et al. Systemic inflammation and insulin sensitivity in obese IFN-γ knockout mice. *Metab Clin Exp*. 2012;61(8):1152–1161.
47. Arase H, Arase N, Saito T. Interferon gamma production by natural killer (NK) cells and NK1.1+ T cells upon NKR-P1 cross-linking. *J Exp Med*. 1996;183(5):2391–2396.
48. Jiao Y, Huntington ND, Belz GT, Seillet C. Type 1 innate lymphoid cell biology: Lessons learnt from natural killer cells. *Front Immunol*. 2016;7:426.
49. Vielma SA, Klein RL, Levingston CA, Young MR. Adipocytes as immune regulatory cells. *Int Immunopharmacol*. 2013;16(2):224–231.
50. Huang HW, Zuo C, Chen X, Peng YP, Qiu YH. Effect of tyrosine hydroxylase overexpression in lymphocytes on the differentiation and function of T helper cells. *Int J Mol Med*. 2016;38(2):635–642.
51. Cosentino M, et al. Interferon-gamma and interferon-beta affect endogenous catecholamines in human peripheral blood mononuclear cells: implications for multiple sclerosis. *J Neuroimmunol*. 2005;162(1-2):112–121.
52. Lund RJ, Chen Z, Scheinin J, Lahesmaa R. Early target genes of IL-12 and STAT4 signaling in th cells. *J Immunol*. 2004;172(11):6775–6782.
53. McPhee JB, Schertzer JD. Immunometabolism of obesity and diabetes: microbiota link compartmentalized immunity in the gut to metabolic tissue inflammation. *Clin Sci*. 2015;129(12):1083–1096.
54. Jones L, et al. Genetic evidence implicates the immune system and cholesterol metabolism in the aetiology of Alzheimer's disease. *PLoS One*. 2010;5(11):e13950.